Fatigue Performance Comparison and Life Predictions of Forged Steel and Ductile Cast Iron Crankshafts

Jonathan R. Williams and Ali Fatemi
Graduate Research Assistant and Professor, Respectively

A Final Project Report Submitted to the

Forging Industry Educational Research Foundation (FIERF)
and
American Iron and Steel Institute (AISI)

The University of Toledo

August 2007

FORWARD

The overall objective of this study was to evaluate and compare the fatigue performance of two competing manufacturing technologies for automotive crankshafts, namely forged steel and ductile cast iron. In addition, weight and cost reduction opportunities for optimization of the forged steel crankshaft were also investigated. The detailed results are presented in two reports. **This first report** deals with the fatigue performance and comparison of forged steel and ductile cast iron crankshafts. The second report deals with analyses of weight and cost reduction for optimization of the forged steel crankshaft.

ABSTRACT

Fatigue Performance Comparison and Life Predictions of Forged Steel and Ductile Cast Iron Crankshafts

The primary objective of this study was to evaluate and compare the fatigue performance of forged steel and ductile cast iron crankshafts. Fatigue is the primary cause of failure of crankshafts due to the cyclic loading and presence of stress concentrations at the fillets. The crankshafts used in this study were from one-cylinder engines typically used in lawnmowers. Recent publications relevant to this work are presented. The experimental program included monotonic tensile tests, strain-controlled fatigue tests, Charpy V-notch impact tests, as well as load-controlled component fatigue tests on both crankshafts. Monotonic and cyclic properties of the two materials were obtained and compared, which showed a higher tensile strength and better fatigue performance for the forged steel compared to the ductile cast iron. The results from the Charpy V-notch tests showed that the forged steel material has higher impact toughness than the ductile cast iron material. The results of the component fatigue tests are presented as S-N curves for the two crankshafts and show a superior fatigue performance for the forged steel crankshafts. In addition to the experimental program, life predictions were performed for the two crankshafts using the properties obtained from the strain-controlled specimen tests. Results from FEA were used to determine the stress concentrations in the crankshafts along with the stress distributions. S-N life predictions were performed using the modified Goodman equation to account for the mean stress

effects caused by the R = -0.2 loading. Strain-life predictions were also performed using Neuber's rule to determine the notch stresses and strains and the SWT parameter for accounting for mean stress effects. Both the S-N and strain-life predictions provided reasonable estimates to the fatigue lives of the crankshafts, although the S-N predictions were in better agreement with the experimental data than the strain-life predictions.

ACKNOWLEDGEMENTS

Financial support for this research project was provided by the Forging Industry Educational Research Foundation (FIERF) and the American Iron and Steel Institute (AISI). We would like to thank Karen Lewis (Executive Director of FIERF), David Anderson (Director of Bar and Rod Products at AISI), Michael Wicklund (President of FIERF) for providing technical support and information, and George Mochnal from the Forging Industry Association. In addition we would like to acknowledge Bill Heitmann and Louie Laus of Arcelor Mittal Steel for there generous help and assistance with the chemical analyses and microstructure imaging.

TABLE OF CONTENTS

LIST OF TABLES

LIST OF FIGURES

CHAPTER 1

INTRODUCTION

1.1 Background

A crankshaft, in general, converts linear motion into rotary motion. In an internal combustion engine, the reciprocating motion of the piston is linear and is converted into rotary motion through the crankshaft. The most common application of a crankshaft is in an automobile engine. However, there are many other applications of a crankshaft which range from small one cylinder lawnmower engines to very large multi cylinder marine crankshafts and everything in between.

1.1.1 Crankshaft description

A crankshaft consists of main journals, webs, and connecting rod journals, commonly known as “crank-pins”. The main components of a crankshaft are shown in Figure 1.1. The crankshaft rotates on bearings inside the engine. The bearings supporting the crankshaft are the main bearings of an engine and the part of the crankshaft that rides on the bearings are called the main bearing journals. The number of main bearings and main journals in an engine depend on its size. Small one cylinder engines have only two main bearings, one at each end of the crankshaft. Larger multi-cylinder engines usually have more than two main bearings at the ends and include some in the center part of the crankshaft for more support. The piston connects to the

crankshaft on a bearing journal, referred to as a crank-pin. The crank-pins are offset from the central rotating axis of the crankshaft causing the pistons to move when the crankshaft rotates. The webs create the offset between the central axis and the crank-pins. The number of crank-pins depends on the type of engine and number of cylinders. A single –cylinder engine will have only one crank-pin and two webs. Multi-cylinder engines will have one crank-pin per piston if the engine is a straight engine, meaning that all cylinders are in a line. If the engine is a V-engine, one bank of cylinders on each side of the crankshaft, two pistons will attach to the same crank-pin. Commonly a crankshaft will be classified by the number of "crank throws" or simply "throws", which simply refers to the combination of the two webs and crank-pin. Therefore, a straight four cylinder engine will have four crank-pins as will a V-8 engine and both will be classified as four throw crankshafts.

The high speed rotation of a crankshaft requires a very balanced component. If the crankshaft is not balanced damage to the engine can result or at the very least there will be a heavy vibration. Balancing of a crankshaft is partly achieved by using counter balance weights on the crankshaft. The webs usually extend past the central axis of the crankshaft to form the counterweights. Fine balancing is usually done by drilling holes in the underside of the counterweights to remove material. The locations of the holes are such that when the material is removed the crankshaft will be in balance.

There are several different material options available for manufacturing crankshafts, with the two most popular being steel and iron. Crankshafts can be machined from a billet, forged, or cast. Machining a crankshaft from a billet is not typically done due to the prohibitively long machining times, however for low production

custom pieces it is still done. The steel crankshaft is usually forged to near net shape and then finished by machining processes. The iron crankshafts are typically cast and then machined. Generally a crankshaft can be classified as forged steel or cast iron, however, within these two categories there are many options. A forged steel crankshaft, for example, may be manufactured from microalloyed steel which can eliminate the need for heat treatment. A cast iron crankshaft, which is typically ductile cast iron, has more ductility and therefore higher fatigue resistance than ordinary gray iron. The cast iron crankshaft could also be made from austempered ductile iron or ADI, which is a higher strength iron and has been shown to have longer fatigue life than ordinary ductile cast iron [Chatterley and Murrell, 1998].

Crankshaft design is not limited to selecting a material, such as steel or iron, a process, such as forging or casting, and geometry. Surface treatments also play a major role in the performance of the crankshaft. The fillets in a crankshaft are often rolled in order to induce compressive residual stresses, thus increasing the fatigue performance of the crankshaft. Case hardening, or hardening on the surface of the material, is often done to increase the hardness in the main journals and crank-pins of the crankshaft, resulting in better wear. Not only does the surface hardening improve wear resistance, it also can induce compressive residual stresses, which results in increased fatigue performance of the crankshaft [Grum, 2003]. Ion nitriding is also used and has been shown to increase the fatigue strength of crankshafts [Park et al., 2001; Pichard et al, 1993].

1.1.2 Function of a crankshaft

As mentioned previously, the function of a crankshaft in an internal combustion engine is to translate the linear motion of the pistons into a rotary motion. The rotary motion can then be used to power the device, such as propel an automobile or turn the blade of a lawnmower engine. The most common application is the automobile engine. The function of the crankshaft in an automobile engine can easily be extended to a crankshaft in another type of engine since their functions are the same. Since the crankshafts used in this study are from a four-cycle engine, the four-cycle engine process is discussed. Crankshafts, however, perform similar functions in the two-cycle engine which is common in small garden equipment.

The most common type of engine is the four-cycle (or four-stroke) engine which uses the Otto cycle (if gasoline powered) or Diesel cycle (if diesel powered). The four cycles are the intake, compression, power, and exhaust, which are shown in Figure 1.2. The cycle starts at top dead center (TDC) where the piston is furthest away from the crankshaft. In the first cycle, the intake cycle, the piston moves down and an air-fuel mixture is drawn into the cylinder through the intake valves. Next the valves close and the piston moves up, compressing the air-fuel mixture in the compression cycle. The compressed air-fuel mixture is ignited (by a sparkplug in a gasoline engine) at the top of the compression stroke. The power cycle occurs when the gases in the combustion chamber ignite, resulting in expansion and a large force on the piston. The force pushes the piston down resulting in a rotation of the crankshaft. Finally, in the exhaust cycle, the exhaust valves open and the gases in the cylinder are forced out during the upward

motion of the piston as the crankshaft rotates. The entire process results in a 720 degree rotation of the crankshaft, as each cycle takes approximately 180 degrees to complete.

1.1.3 Failure of a crankshaft

The crankshaft is the central part of the engine and its failure would render the engine useless until costly repairs could be made or a replacement engine could be installed. The failure of a crankshaft can damage other engine components including the connecting rods or even the engine block itself. Therefore, when the failure of a crankshaft does occur it often results in replacing the engine or even scrapping the equipment the engine was used in. Considering the ramifications of a crankshaft failure, a crankshaft must be designed to last the lifetime of an engine.

The engine of a typical gasoline powered automobile has an engine speed that varies from 500 to 6,500 rpm and while traveling at highway speeds may be 2,500 rpm. It can easily be shown that a crankshaft has a desired life of many millions or even billions of cycles. For example if the life of an automobile is 120,000 miles and has an average speed of 50 mph and engine speed of 2,500 rpm, the engine, and crankshaft, would need to have a life of at 360 million cycles. Crankshafts used in lawnmower engines, such as those in this study, would not see as many cycles as the automobile engine with considerably higher usage, but a long life situation still exists. With such a long life situation, a design for infinite life is necessary.

The gas and inertial loads in an engine create a multiaxial loading condition on a crankshaft as was shown by Jensen [1970]. In the study strain gages were mounted to a crankshaft from a V-8 engine and installed back in the engine. By running the engine

and acquiring data, he was able to show that there was bending and torsion on the crankshaft. The study by Jensen and subsequent studies show that the torsion is small compared to the bending stress, therefore, the torsion is often neglected.

The fillets in crankshafts have been identified as the highest stressed, or critical, location of a crankshaft and are often the sight of fatigue crack initiation as was shown in the previously mentioned study by Jensen and other studies, including this one. The presence of a fillet or notch in a crankshaft is virtually unavoidable. Any change of diameter results in a stress concentration. While sharp corners can be avoided with the use of fillets, other measures are often necessary in order to increase the fatigue performance of crankshafts. Compressive residual stresses have been shown to increase the fatigue performance of components, not just limited to crankshafts. Often in an attempt to induce compressive residual stresses at notches, the fillets are rolled. This compressive residual stress increases the fatigue strength at long life.

Silva [2003] classified the failure of crankshafts into three categories: operating sources, mechanical sources, and repairing sources. Operating sources include things such as misuse of an engine and a lack of lubrication. Mechanical sources of failure can include misalignment or vibration of the crankshaft due to balance issues. Repairing sources are those that are caused by repair to an engine or finishing of a crankshaft, such as improper grinding, incorrect bearings, or misalignment.

1.2 Literature Review

The literature review for this project by Zoroufi and Fatemi [2005] was completed previously. Therefore the literature review included in this chapter only contains

additional information that was published after the previous literature review was completed and information that is mentioned again due to specific application to this study.

1.2.1 Failure analysis

The analysis of failed in service crankshafts is vital to laboratory crankshaft studies, as it allows the researcher to better adapt experiments to real life situations as well as validates results. Crankshaft studies, including this one, suggest that crankshaft failures often occur in the crank-pin fillet areas, which is also supported by the analysis of failed in service crankshafts.

Bayrakçeken et al. [2006] investigated the failure of a small one-cylinder diesel engine used in agricultural applications. The analysis was performed on two crankshafts made of AISI 4140 steel, one of which was case hardened. The basic crankshaft geometry used in the study is shown in Figure 1.3. Both failures were attributed to fatigue crack propagation in the fillet of the crankshafts. Fracture surfaces which show typical fatigue fractures, as indicated by beach marks, from both crankshafts are shown in Figure 1.4. The premature failure was suspected to be caused by the larger than normal carbide inclusions present in the material as shown by the scanning electron microscope (SEM) images in Figure 1.5.

Asi [2006] investigated the failure of a diesel crankshaft made of ductile cast iron. The crankshaft was taken from a 6 cylinder 115 HP engine which is shown in Figures 1.6 and 1.7. The failure of the crankshaft resulted in "catastrophic failure of the engine" after only 400 hours of service. Circumferential cracks were found by visual inspection in the

crankpin fillet region as shown in Figure 1.8. From high magnification analysis of the fracture surfaces using SEM, the initiation of the cracks was at the surface in the region of the fillet as shown in Figure 1.9. The free graphite and nonspheroidal graphite in ductile cast iron act as notches, and therefore stress concentrations, and are often the source of fatigue crack initiation. The initiation site of the cracks in the analyzed crankshaft is in the periphery of graphite. The analysis showed that the failure occurred due to rotating bending fatigue. The initiation of cracks which ultimately led to the fracture of the crankshaft occurred in the crankpin fillet region.

1.2.2 Testing and comparison of fatigue performance of crankshafts

Fatigue testing typically requires destructive testing of both specimens and components in order to characterize the fatigue performance of a material or compare two materials. Damir et al. [2007], however, describe a process for nondestructive comparisons of fatigue behavior using modal analysis. Dynamic impact testing on simple, cylindrical geometry, was performed along with rotating bending fatigue tests on the same material using standard specimen geometry. An impact hammer equipped with a force transducer was used to excite the specimen, while an accelerometer was used to measure the response. The test set-up used is shown in Figure 1.10. Ductile cast iron and gray cast iron were used in the study. The damping ratio and fatigue life were affected by the microstructure of the material. Within a family of materials, a trend was observed between the damping ratio and fatigue life as shown in Figure 1.11. A higher damping ratio indicated a higher fatigue life. Ductile (nodular) cast iron specimens having a higher damping ratio also had a higher fatigue life than the gray cast iron

specimens. There was no trend observed between natural frequency or magnitude of the frequency response function (FRF) and fatigue life. Using austempered ductile iron (ADI) a quadratic relationship between damping ratio was developed as shown in Figure 1.12. The equation of the curve shown in Figure 1.12 can be used to predict the fatigue life based on the damping ratio for ADI at a stress of 500 MPa.

Spiteri et al. [2007] experimentally and analytically investigated the fatigue performance of a ductile cast iron crankshaft subjected to bending loads. The objective of the study was to compare different failure criteria. Tests were performed on a sample cut from the crankshafts that consisted of two main bearings, one crankpin, and two webs, as shown in Figure 1.13. Resonant bending fatigue tests were performed on the test samples such that the crankpin fillet area was the highest stressed location. The test fixture and setup is shown in Figure 1.14 and was the same fixture used by Chien et al. [2005]. The data for the surface crack initiation failure criterion was taken from the study by Chien et al. and the fatigue limit using this criterion was found to be 414 N-m. Testing was done to compare the resonant frequency drop with the size of the crack. Using a frequency drop failure criterion, the fatigue limit was found to be 642 N-m. Therefore, the surface crack failure criterion was lower than the fracture criterion.

Papers by Park et al. [2001], Chatterley and Murrell [1998], and Pichard et al. [1993] are included in the previous literature review [Zoroufi and Fatemi, 2005], however, due to their direct relevance to this study they are mentioned here again.

In a study by Park et al. [2001] the effect of surface modifications was studied on microalloyed CrMo crankshafts. The effect of fillet rolling using different forces as well as nitriding was investigated. The results from component fatigue tests on the materials

and treatments are shown in Figure 1.15. It can be seen that many of the tests were conducted to yield lives between 10^5 and 10^6 cycles, which compare to the types of tests conducted in this study. The results show that a higher fillet rolling force induces higher compressive residual stresses and in turn, produces better fatigue strength. However, forces too high can be detrimental to the fatigue performance. Fillet rolling and nitrided samples both produced approximately a factor of 1.8 increase in fatigue limit when compared to untreated samples.

Chatterley and Murrell [1998] compared the fatigue performance of several materials for use in a four-cylinder turbo charged diesel engine. The materials tested in the study were nitrided 1% CrMo, fillet rolled ductile iron (S_u = 700MPa), and fillet rolled austempered ductile iron (ADI). Constant amplitude bending fatigue tests were conducted on the crankshafts to 10^7 cycles or failure, whichever occurred first. The results from the study are summarized in Table 1.1. The results indicate that nitrided forged steel had a higher fatigue strength (10^7 cycles) than ductile iron or ADI regardless of their surface treatments. The results also showed that ADI with higher rolling forces had higher fatigue strength than the rolled ductile iron.

The study by Pichard et al. [1993] explored the possibility of replacing forged steel or cast iron with a mircoalloyed steel in order to eliminate the need for additional heat treatments. Tests on ductile cast iron, 1042 steel, 35MV7 microalloyed steel, and 32CDV13 high alloyed steel crankshafts were conducted. The results from the component tests are shown in Table 1.2. The results showed that the control cooled microalloyed steel had a higher fatigue strength than the 1042 steel and the ductile iron for short nitriding treatments. The quenched and tempered 1042 steel did show

significantly higher fatigue strength than the ductile iron with the same surface treatment. The microalloyed 35MV7 nitrided for 4 hours had only 10% lower fatigue strength than the high alloyed 32CDV13 steel nitrided for 7 hours. This slightly lower fatigue strength was combined with a significant cost savings, making the microalloyed steel a significant contender.

1.2.3 Crankshaft manufacturing

As mentioned previously, there are several options available for manufacturing crankshafts, most commonly casting and forging. While casting and forging are generally used for high volume, ordinary sized crankshafts, alternative processes have been investigated for low volume very large scale crankshafts. Wang et al. [2007] discuss the fabrication of a large scale locomotive crankshaft using the electro-slag casting (ESC) process which is shown schematically in Figure 1.16. Each manufacturing process has its positive and negative attributes. These processes compete against one another for strength, cost, efficiency, and production time motivations.

In order to decrease the amount of machining time, a precision forging technique is used to produce forgings that are near net shape. Precision forging is a flashless forging operation and has been used to produce small pieces such as connecting rods or hand tools. Behrens et al. [2005] discuss the process of extending the precision forging technique to larger, more complex shapes such as the crankshaft. Precision forging is a hot forging process that uses closed dies. The process consists of an upper and lower die and one or more punches. In order to develop a process for the complex crankshaft shape, a series of steps were used. First the elementary cell, consisting of one main

bearing, one web, and one crankpin, was developed and verified which is shown in Figure 1.17. After successful results with the elementary cell, the process was extended to the one-cylinder crankshaft, consisting of one crankpin, two webs, and two half main bearings (one on each side). The forging sequence for the one-cylinder crankshaft is shown in Figure 1.18 with the final stage tool setup shown in Figure 1.19. Finally the procedure for a three-cylinder crankshaft was developed. The forging sequence for the three-cylinder crankshaft is shown in Figure 1.20. In the first process the main bearings and the crankpins are formed. In the second process the webs are compressed and the crankpins are translated to their eccentric position. The final step involves a tool with punches integrated into the top and bottom dies. The dies in the final step represent the shape of the main bearings and the crankpins that were formed in previous steps. The punches in the final step form the geometry of the web sections.

1.3 Motivation and Objectives

In many industries, especially the automotive industry, there is a constant demand for components that have less mass, are stronger, and cost less to produce. The automotive industry, in particular, often seeks to improve gas mileage by using lighter components, including optimized geometry and materials, all while reducing the cost of manufacturing. Because of this, there is a constant debate over which material and manufacturing process can be the most cost effective and lightest weight without sacrificing performance.

The objective of this study was to assess and compare the fatigue performance of forged steel and ductile cast iron crankshafts from a one-cylinder engine typical to that

used in a riding lawnmower. The forged steel crankshaft was designed to be used in a 460cc engine which produces approximately 9.3 kW. The ductile cast iron crankshaft was from a similar engine size and type. The masses of both crankshafts were similar with the forged steel at 3.9 kg and the ductile cast iron at 3.7 kg. Fatigue and monotonic tests were conducted on standard specimens machined from the forged steel and ductile cast iron crankshafts to compare the two materials. Component tests on both crankshafts were conducted to obtain the fatigue properties and compare the two crankshafts. Finite element analysis was used to determine the critical location of the crankshafts and to determine the stress concentration factors. Life predictions were performed using both the S-N approach and the strain-life approach, results of which were compared with the component test data.

Dynamic load and stress analysis on the forged steel and ductile cast iron crankshafts used in this study, as well as optimization of the forged steel crankshaft was performed in another study, details of which can be found in Montazersadgh [2007]. Other details of the crankshaft study presented in this work can also be found in Zoroufi and Fatemi [2005], Williams and Fatemi [2007], Montazersadgh and Fatemi, [2007], and Williams et al. [2007].

The crankshafts used, being from a one-cylinder engine, were single throw crankshaft consisting of two web sections and a one crankpin. Typically in automotive crankshaft analysis a single throw is analyzed regardless of the size of the crankshaft. Literature shows that for automotive crankshaft component fatigue tests, the crankshafts are often sectioned so that a single throw can be tested [Chien et al., 2005; Spiteri et al., 2007]. Therefore, the analyzed section in automotive crankshafts closely resembles the

analyzed section in this study, allowing the procedures and information to be easily applied to automotive applications. Also, the failure location of the crankshafts used in this study was in the crank-pin fillet, which agrees with the typical failure location for an automotive crankshaft [Jensen, 1970].

Chapter 2 provides detailed description of the test procedures, results, and comparisons of the specimen monotonic and fatigue tests as well as Charpy V-notch impact tests. The Charpy V-notch tests were conducted due to the possibility that the lawnmower contacts a hard object causing the engine to stop suddenly, thus resulting in an impact loading condition in the engine. Chapter 3 describes the component fatigue test procedures, results, and comparisons. The results of the stress analysis and FEA performed are then discussed in Chapter 4. Chapter 4 also describes the life predictions used and compares the results of the component tests with the life predictions. Finally, Chapter 5 summarizes the conclusions made from the study.

Table 1.1: Results from component fatigue tests on forged steel, ductile iron and ADI crankshafts with various surface treatments from the study by Chatterley and Murrell [1998].

Crankshaft Material	Fatigue Limit at 10×10^6	
	Applied Bending Moment ± Nm	Approximate Applied Stress**, ± N/mm^2
Forged Steel	1050	660
Un-rolled Solid ADI	500	280
Rolled* Solid ADI	750	420
Rolled* Hollow ADI	650	360
Rolled* Solid 700/2 Iron	800	450
Solid ADI Rolled at + 25% Rolling Force	850	475
Solid ADI Rolled at + 50% Rolling Force	1000	560

*Rolling force calculated according to MIRA formula
**Based on average stress measurements taken by engine manufacturer under static load/deflection conditions

Table 1.2: Results from component fatigue tests on forged steel, ductile iron, and microalloyed steel crankshafts from the study by Pichard et al. [1993].

MATERIAL	STATE	SURFACE HARDENING TREATMENT	BENDING MOMENT (N.m)
Ductile iron	As cast	Without	± 1500
Alloyed ductile iron	Q. + Temp.	Ion nitriding : 4 h	± 2230
Ductile iron	As cast	Fillet rolling. P (*) : 8000 N	± 2935
1042 steel	Q. + Temp.	Ion nitriding : 4 h	± 3480
35 MV7 steel	Cont. Cooled	Fillet rolling. P(°) : 9000 N	± 3715
35 MV7 steel	Cont.Cooled	Fillet rolling. P(°): 12000 N	± 4472
35 MV7 steel	Cont.Cooled	Ion nitriding : 4 h	± 4660
32 CDV13 steel	Q. + Temp.	Ion nitriding : 7 h	± 5170

(°) P = Pressure

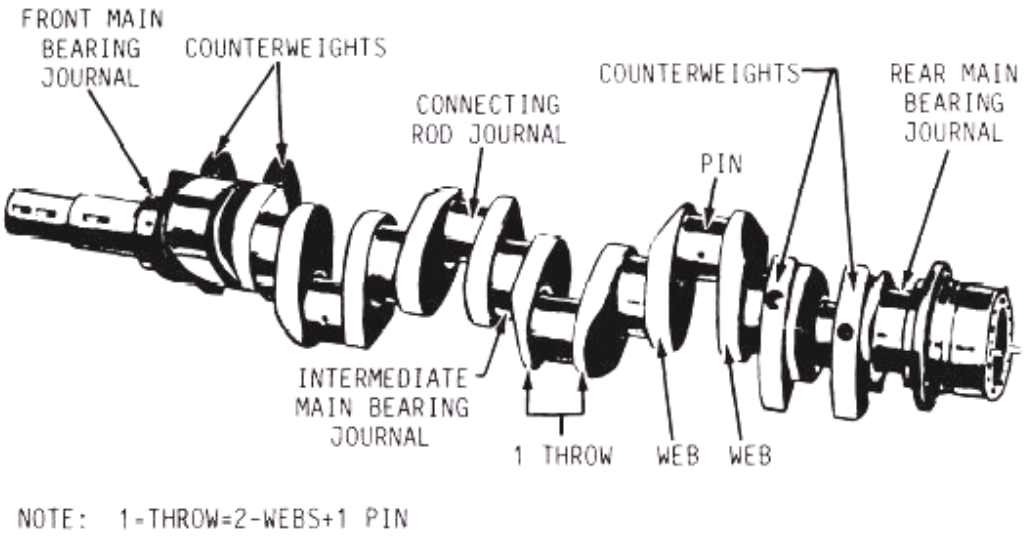

Figure 1.1: Crankshaft terminology [www.tpub.com].

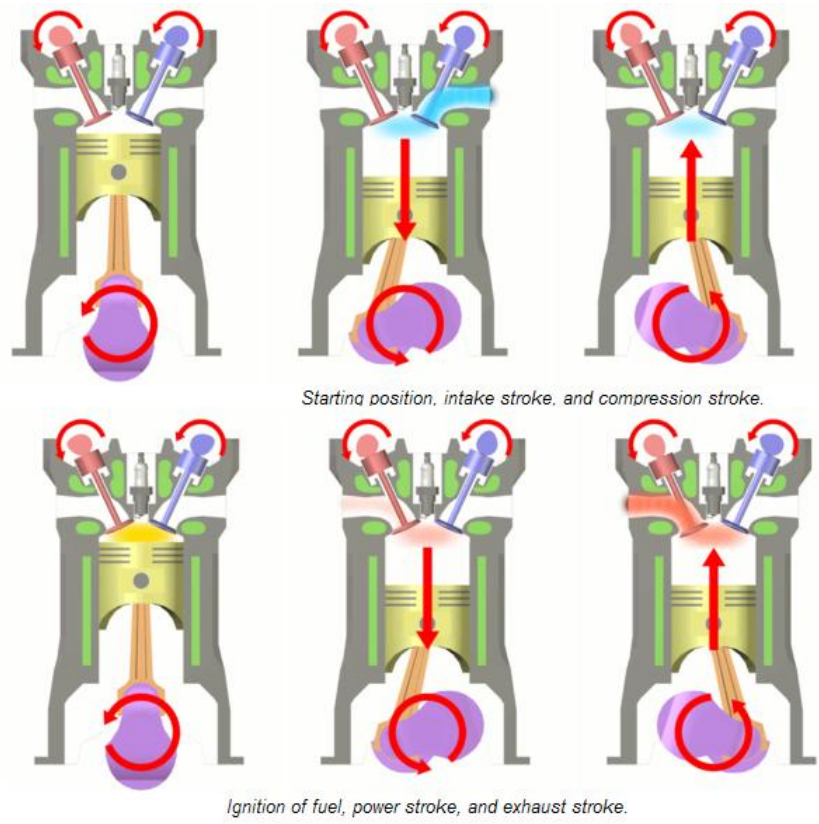

Figure 1.2: The cycles of a four-stroke engine [en.wikipedia.org].

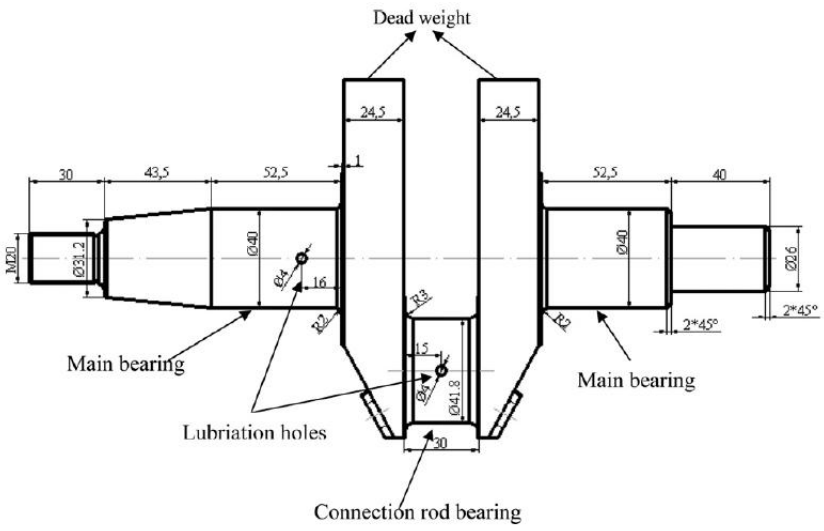

Figure 1.3: Geometry of one cylinder diesel crankshaft used in the study by Bayrakçeken et al. [2006].

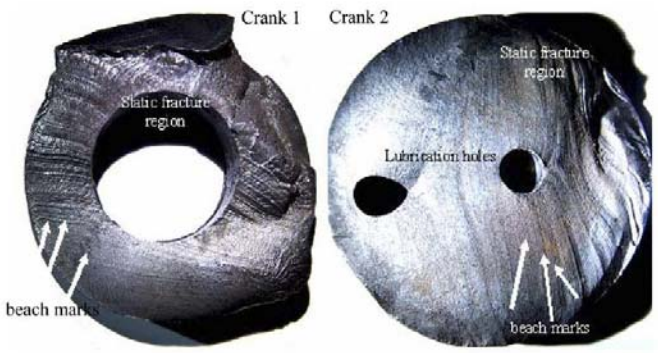

Figure 1.4: Fracture surfaces from failed one-cylinder diesel crankshafts from the study by Bayrakçeken et al. [2006].

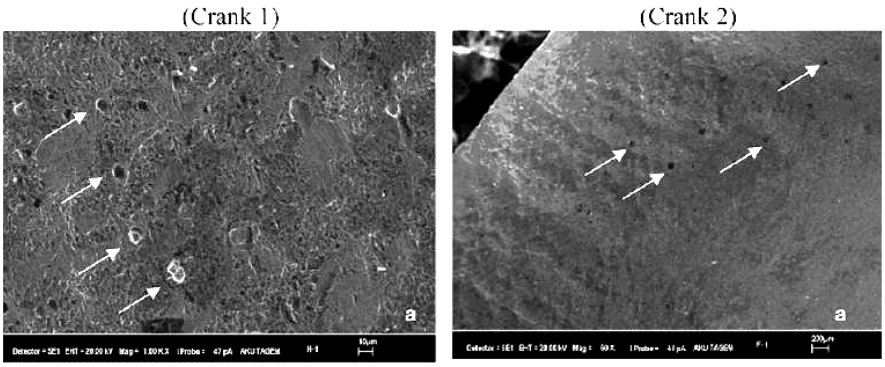

Figure 1.5: SEM photographs of failed crankshafts showing carbide inclusions indicated with arrows from the study by Bayrakçeken et al. [2006].

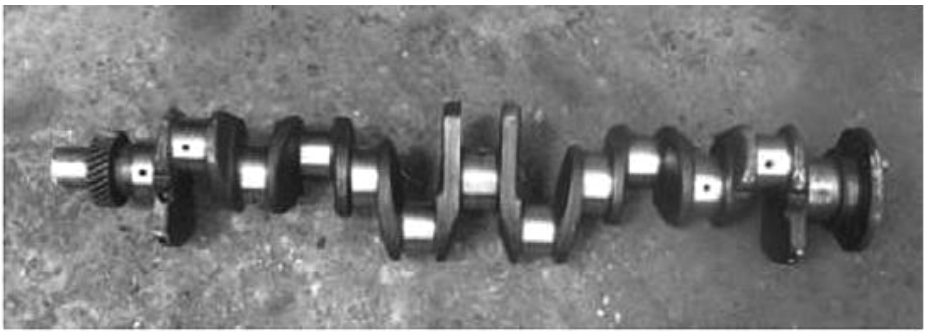

Figure 1.6: Failed crankshaft from a 6-cylinder diesel engine from the study by Asi [2006].

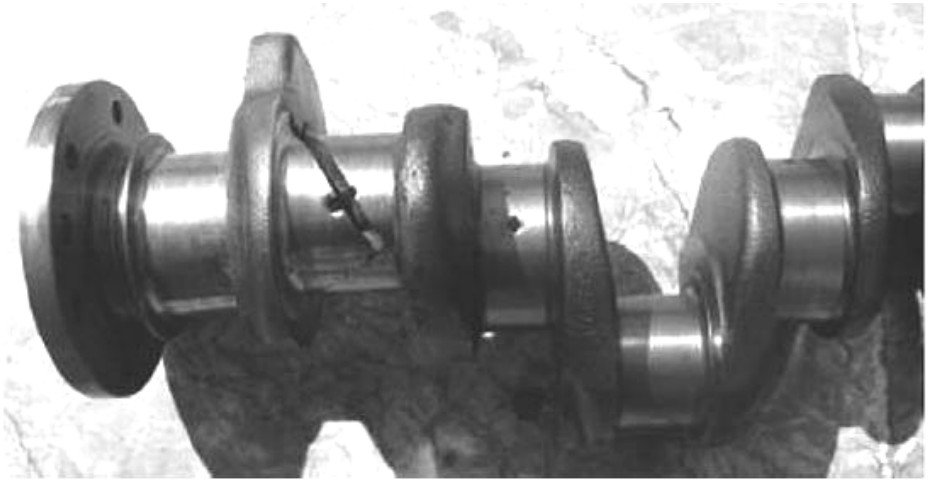

Figure 1.7: Close up of crack in failed crankshaft from the study by Asi [2006].

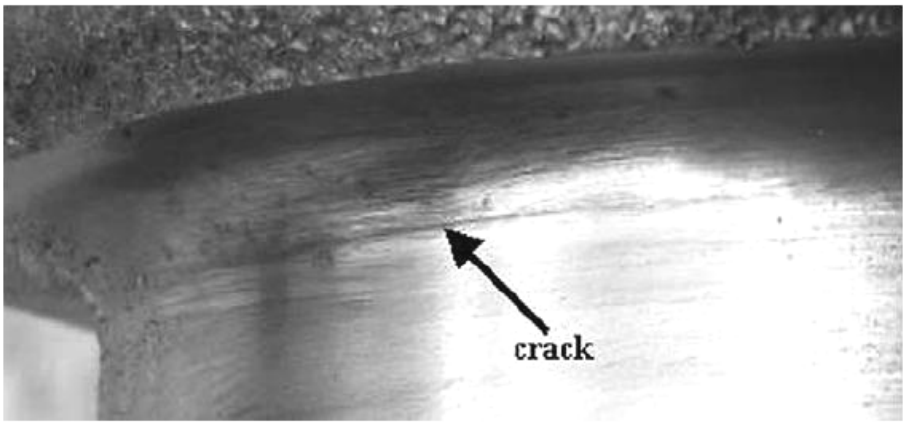

Figure 1.8: Circumferential crack in failed crankshaft from the study by Asi [2006].

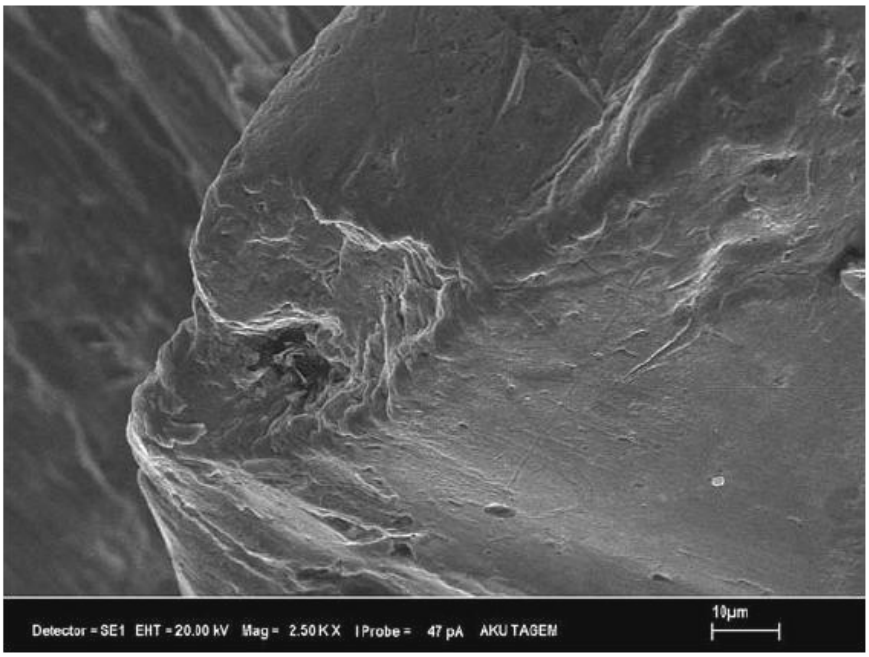

Figure 1.9: SEM photograph of crack initiation site in the fillet region from the study by Asi [2006].

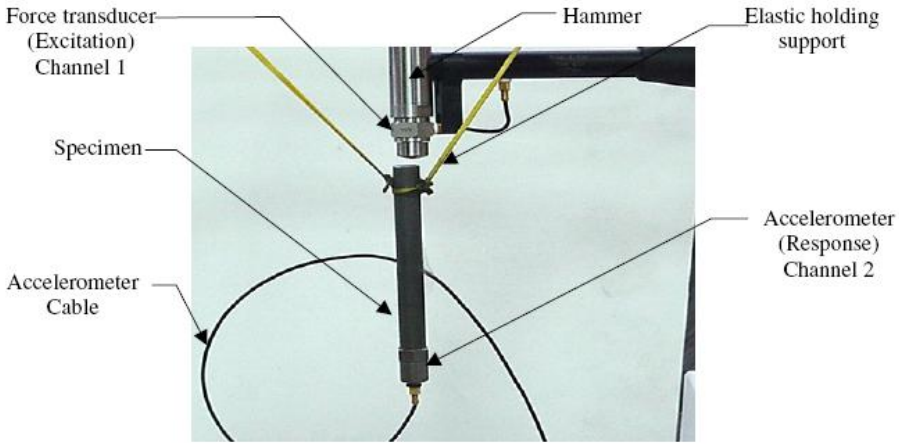

Figure 1.10: Test set-up to determine the modal response of specimens from the study by Damir et al. [2007].

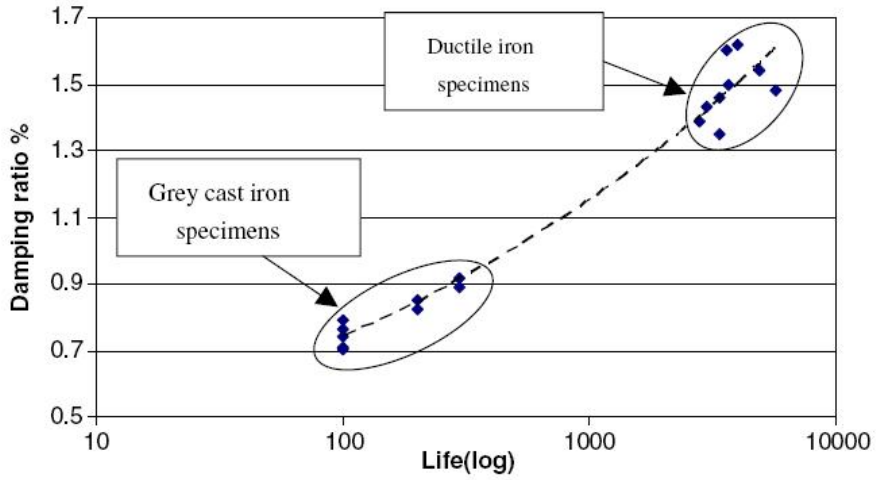

Figure 1.11: Damping ratio versus life to failure for grey cast iron and ductile cast iron specimens from the study by Damir et al. [2007].

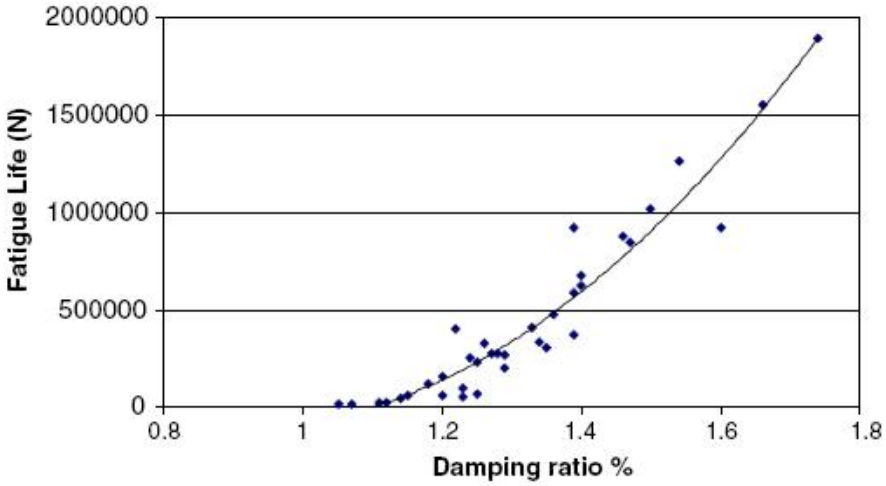

Figure 1.12: Life to failure versus damping ratio for ADI specimens showing a quadratic correlation from the study by Damir et al. [2007].

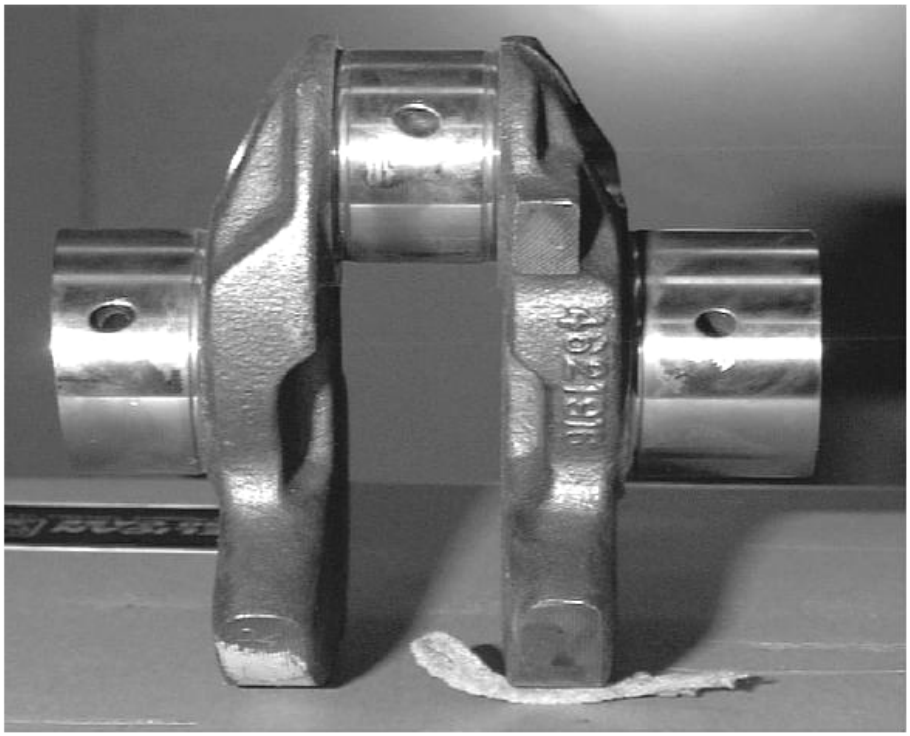

Figure 1.13: Test section for resonant bending test from the study by Spiteri et al. [2007].

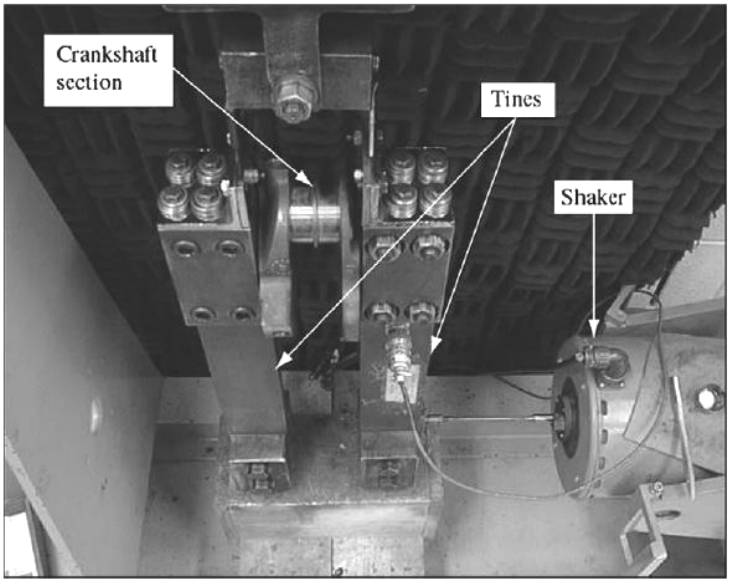

Figure 1.14: Test apparatus for resonant bending fatigue test from the study by Spiteri et al [2007].

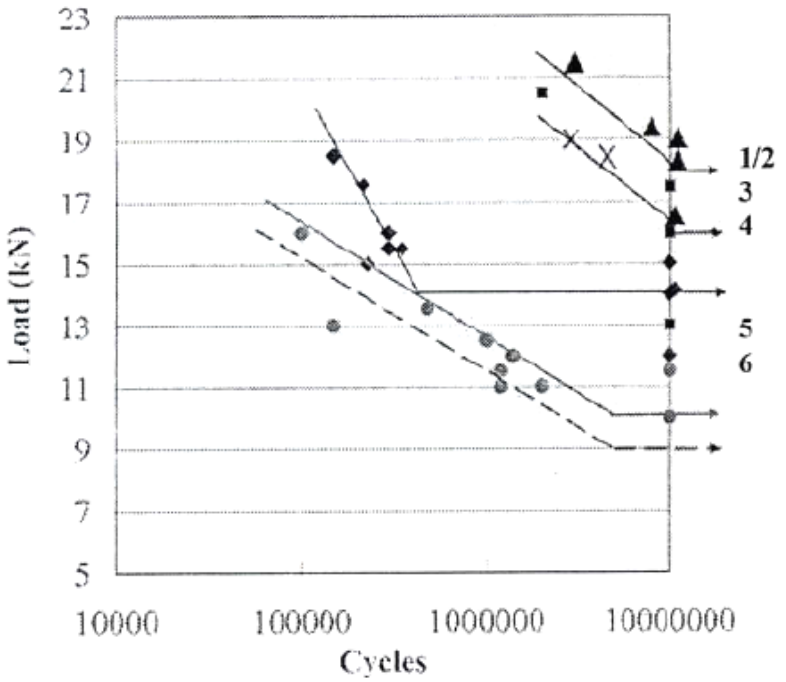

No.	Specimens	Fatigue limit (kN)
1	Fillet rolling (900kgf)	18↑
2	Nitriding	
3	Nitriding (Low hardness)	16
4	Fillet rolling (500kgf)	14
5	Bare sample	10
6	Bare sample (Low hardness)	9

Figure 1.15: Results from component tests on ductile cast iron crankshafts with various surface treatments from the study by Park et al. [2001].

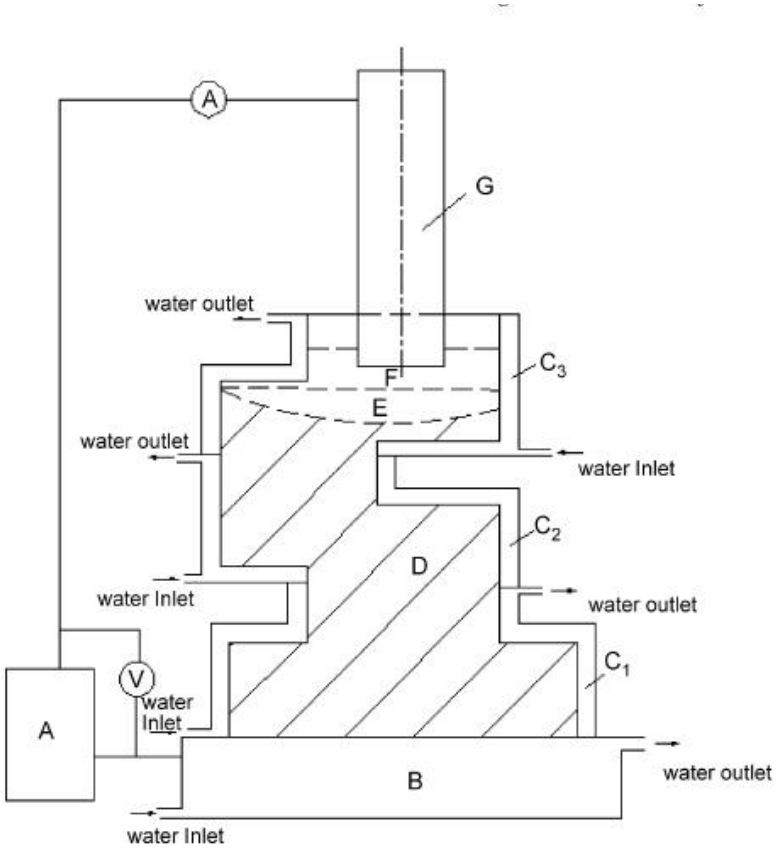

Figure 1.16: Electroslag casting (ESC) process shown schematically where A: transformer; B: Bottom mould; C1, C2, C3: mould; D: casting; E: molten metal pool; F: slag pool; G: electrode [Wang et al. 2007].

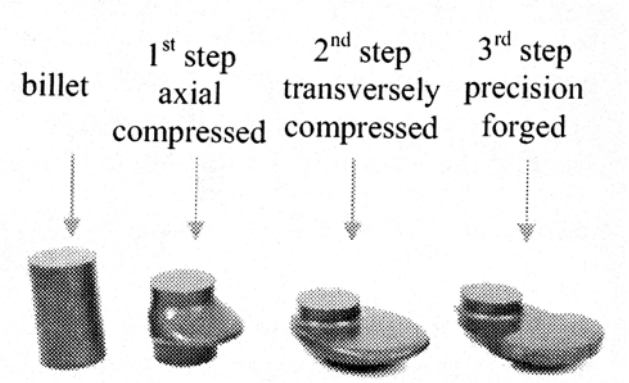

Figure 1.17: Forging sequence of the elementary cell for a precision forged crankshaft from the study by Behrens et al. [2005].

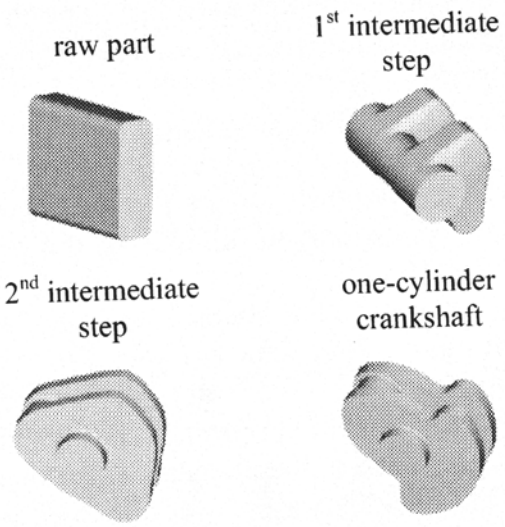

Figure 1.18: Sequence for precision forging of a one-cylinder crankshaft from the study by Behrens et al. [2005].

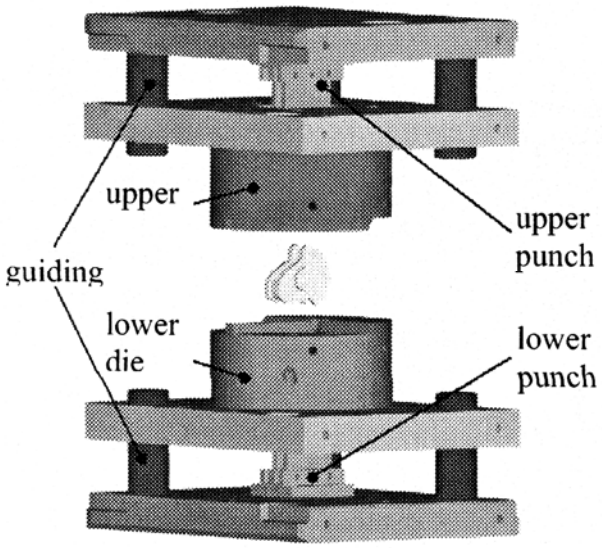

Figure 1.19: Tool layout for the final forming stage of a one-cylinder crankshaft from the study by Behrens et al. [2005].

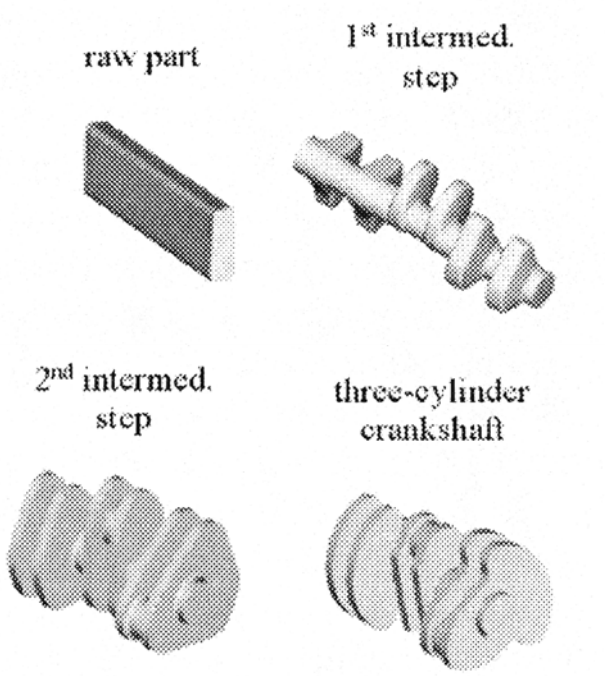

Figure 1.20: Forging sequence for the precision forging of a three-cylinder crankshaft from the study by Behrens et al. [2005].

CHAPTER 2

SPECIMEN TESTING PROCEDURES AND RESULTS

2.1 Monotonic and Fatigue Tests and Results

2.1.1 Materials, specimen, and test equipment

Ductile cast iron crankshafts and 1045 forged steel crankshafts were used in this study. Both crankshafts were designed to be used in a one-cylinder small engine typical to those found in riding lawn mowers. The crankshafts used for obtaining test specimens were in the as cast and as forged condition when received and had not yet been through the final machining process. The ductile iron and forged steel crankshafts in their unmachined state are shown in Figure 2.1.

While limited information was available to identify the exact materials used in the crankshaft, chemical analysis confirmed that the forged steel crankshaft was AISI 1045 steel. The chemical analysis along with microstructure analysis also confirmed that the cast iron crankshaft was in fact a ductile cast iron. The chemical composition was obtained from small sections removed from the as cast and as forged crankshafts. The results from the chemical analyses of samples taken from the forged steel and ductile cast iron are given in Table 2.1.

The microstructure of the ductile cast iron material consisted of spheriodal graphite particles surrounded by patches of ferrite in a pearlite matrix. The optical photomicrograph at 500X is shown for the ductile cast iron in Figure 2.2a. The scanning electron microscope (SEM) photomicrograph at 1000X for the ductile cast iron is shown in Figure 2.2b. The microstructure of the forged steel material was ferrite-pearlite. An optical photomicrograph at 500X is shown in Figure 2.3.

Round specimens having the dimensions shown in Figure 2.4 were machined from the two materials. Two specimens were machined from each crankshaft. The longitudinal axis of the specimens coincided with the longitudinal axis of the crankshafts. The locations where the specimens were taken from are shown in Figure 2.5. The specimen geometry was slightly modified from the ASTM Standard E606 [2004]. The standard specifies uniform, or hourglass specimens, while the specimen geometry used in this study has a large secondary radius in the test section. The length of the grip section was also shortened such that the specimens could be taken from the crankshafts, which had limited usable length. Machining was performed by The University of Toledo Mechanical, Industrial, and Manufacturing Engineering Machine Shop. The specimens were rough cut to an approximate length from the indicated locations and then turned down on a lathe to the desired diameter of the grip section. They were then cut to length and center drilled. The final dimensions were machined using a CNC lathe.

The gauge section of each specimen was polished to remove all machining marks by fixing one end of the specimen in the lathe and running the machine with a speed of 720 rpm. The polishing was done in five steps starting with the coarsest and ending with the finest. Four of the steps were accomplished with small strips of sandpaper with grits

of 400, 600, 800, and 1000. The paper was kept wet by dipping it in water repeatedly during the polishing process. The 400 grit paper was used until all machining marks were removed. The subsequent steps were performed to remove the marks left by the previous polishing process. The final of the five steps was a high speed rotating die grinder with a buffing wheel attached. A polishing compound was applied to the wheel and then the wheel was placed on the rotating specimen such that the direction of the wheel was along the longitudinal axis of the specimen so that any marks from the final step would be in the direction of the applied load during testing, minimizing their effect. The specimens were carefully examined prior to testing to ensure that all marks were removed from the test section.

Testing was performed on an Instron 8801 closed loop servo-hydraulic axial load frame in combination with a Fast Track 8800 digital servo-controller. The load frame was fitted with a 50 kN capacity load cell. The calibration of the system was verified prior to testing. Collet type hydraulic grips were used in the test program. To insure that the grips would maintain proper gripping of the specimen that had a grip section shorter than the standard type specimen, spacer blocks were machined to fit in the collets of the grip at each end of the specimen.

For the tests conducted in strain control an Epsilon Extensometer Model 3442 was used to control the total strain. The extensometer conformed to ASTM Standard E83 [2004]. A verification procedure was performed on the extensometer to ensure proper calibration. A displacement apparatus with a micrometer head (smallest increment of measure 0.0001 inch) was used for the verification. The gauge length of the extensometer was 6 mm (0.02362 in) and had a range of -6% to 10%. Each specimen was coated with

M-coat D at the locations of the extensometer edges prior to each test. This coating was applied in order to prevent the knife edges of the extensometer from causing damage to the specimen in the form of a stress concentration that could lead to fatigue failure at that point. Prior to testing the extensometer was installed at the center of the specimens gauge section and special care was taken to ensure that the extensometer was oriented parallel to the load direction. Prior to performing a test the extensometer was allowed to reach a state of stability by allowing it to be attached to the specimen for approximately one hour (or until the changes in extensometer readout had stabilized). The tests were not conducted until the reading of the extensometer was stable.

The environment in which the tests were carried out was carefully monitored and maintained in order to minimize the effects on the extensometer and load cell due to temperature. The ambient temperature was monitored during testing. The relative humidity was also monitored using a hydrometer.

Due to the fact that any misalignment in the load train can result in inaccurate tests caused by bending in the specimen, particular care was used in achieving proper alignment. A precision round bar was fitted with eight strain gauges and placed in the grips. The fine alignment adjustments were made with the Instron alignment fixture. This fixture allows alignment adjustment that can result from tilt and/or eccentricity between the central axis of the load train. Satisfactory alignment was achieved when the bending was less than 5% of the axial load throughout the entire loading range used for the testing. This is in accordance with the ASTM Standard E606 [2004] which prohibits bending strains greater than 5% of the minimum axial strain range used for any fatigue test.

2.1.2 Test procedures

2.1.2.1 Monotonic tension tests

A monotonic tension test was performed on each of the two materials. The test was conducted in accordance with ASTM Standard E8 [2004]. Prior to testing the location of the extensometer edges was marked on the specimen and the diameter of the gauge section was measured using a 10X magnification optical comparator. The software recorded the stress and strain data during the test in order to generate a stress-strain curve. The extensometer has a maximum strain of 10% and the forged steel test would have exceeded this value. The forged steel test was stopped prior to reaching 10% strain and continued in displacement control until fracture. The cast iron specimen did not approach the maximum range of the extensometer.

A strain rate of 0.0025 mm/mm/min was used from 0% to 0.5% strain. This region represents the elastic and initial yield portion of the curve. This strain rate was chosen because it is 75% of the maximum allowable strain rate specified by ASTM Standard E8 [2004] for the initial yield region. After the specimen yielded, from 0.5% to 10% strain, the strain rate was increased by a factor of three to 0.0075 mm/mm/min. For the forged steel test, once it reached near 10% strain (maximum permissible due to the limitations of the extensometer) the test was switched to displacement control and a rate of 0.152 mm/min was used. The rate of displacement was chosen to approximate the rate of strain that the material experienced when the extensometer was attached.

Following the conclusion of the tests, the specimens were reassembled to their prior to tested state. The final gauge length of the specimen was measured using a digital caliper with a resolution of 0.025 mm. A 10X magnification optical comparator was used

to measure the final cross section diameter and the neck radius at the fracture location of the forged steel specimens. The use of these measurements is further explained in subsequent sections.

2.1.2.2 Constant amplitude fatigue tests

The uniaxial fatigue tests were performed according to ASTM Standard E606 [2004]. A total of 13 specimens of forged steel and 15 specimens of cast iron were tested. The standard specifies using a minimum of 10 specimens, so the requirement was met for both materials. Instron LCF (low cycle fatigue) software was used primarily with the exception of some of the longer life tests, in which Instron SAX software was used after switching to load control. During the test the software recorded the total strain along with the test load at an interval of 2^n cycles automatically. Manual data saves were performed periodically around the expected mid life of the test. A total of seven strain amplitudes were chosen which included 2%, 1%, 0.5%, 0.35%, 0.25%, 0.2%, and 0.16%. A minimum of two tests (for each material) were conducted at each strain amplitude with the exception of 2%, where there was only 1 test for each material. The reason for this was because the primary interest was the long life region of the curve due to the application of the material. More specimens were desired for longer life tests.

Strain control was primarily used for the testing with a few exceptions. During several of the longer life specimens with relatively small strain amplitudes (0.25% or less) there was a mean stress that built up as the specimen cycled. The tests were conducted in strain control until the load amplitude became stable and then the test was conducted in load control at the stable load determined from the strain-controlled test. For these tests where there was some plastic deformation, the test frequency in load

control remained the same as the strain-controlled tests. Load control was also used for longer life tests where the strain was all or almost all elastic. For these tests the test was first conducted in strain control to determine if there was any plastic deformation and to determine the stabilized load. The reason for switching these tests to load control was due to the frequency limitations of the extensometer. For strain-controlled tests the test frequencies ranged from 0.1 Hz to 1.0 Hz. For load-controlled tests with little or no plastic deformation present, the test frequency was increased to 25 Hz to minimize the time required for each test. A triangular waveform was used in each test.

After each fatigue test, the test specimen was sectioned in the grip section in order to measure hardness. The specimens were cut using an abrasive cutoff tool with cutting fluid. The hardness was measured using an Accupro AR-10 Hardness Tester. The hardness was measured at three locations in the specimen. The hardness values in HRC were averaged for each specimen. The hardness measured using the Rockwell B and Rockwell C scales along with the averages for the fatigue specimens are shown in Table 2.2. Both hardness scales were used due to the values measured being at the limits of both scales. The hardness measurements revealed a hardness value for two forged steel specimens, listed as FS-2 and FS-11, and one cast iron specimen, CI-12, that were much lower than the average hardness for the other specimens. The data from these tests also indicated a higher amount of plastic strain which resulted in a lower stress. This higher plastic deformation was connected to the lower hardness values. Therefore, these data points were not used in the determination of any fatigue properties of the forged steel or cast iron materials. In Table 2.2, the specimens that were not included due to low hardness values are shown with an asterisk. It should be noted that the forged steel

specimen labeled FS-8 also showed a lower hardness value. However the plastic strain observed during the test was as expected as evidence by the true stress amplitude versus true plastic strain amplitude plot presented in Section 2.1.3.2.

2.1.3 Experimental results and comparisons

2.1.3.1 Monotonic properties

Properties obtained from the monotonic tensile tests include: modulus of elasticity (E), yield strength (YS), ultimate strength (Su), percent elongation (%EL), percent reduction in area (%RA), strength coefficient (K), strain hardening exponent (n), true fracture strength (σ_f), and true fracture ductility (ε_f).

Engineering strain (e) and engineering stress (S) were recorded during the test. From the engineering stress and strain, the true stress (σ) and true strain (ε), were calculated using the constant volume assumption which results in the following relationships:

$$\sigma = S(1+e) \tag{2.1}$$

$$\varepsilon = \ln(1+e) \tag{2.2}$$

True plastic strain (ε_p) was calculated from:

$$\varepsilon_p = \varepsilon - \varepsilon_e = \varepsilon - \frac{\sigma}{\varepsilon} \tag{2.3}$$

The Ramberg-Osgood equation is often used to represent the true stress (σ)-true strain (ε) plot. The Ramberg-Osgood equation is given by:

$$\varepsilon = \varepsilon_e + \varepsilon_p = \frac{\sigma}{E} + \left(\frac{\sigma}{K}\right)^{1/n} \tag{2.4}$$

The strength coefficient (K) and strain hardening exponent (n) are the stress intercept at a plastic strain of 1 and slope, respectively, to the best fit line of the true stress (σ) versus true plastic strain (ε_p) data when plotted in a log-log scale. The equation of the best fit line is therefore:

$$\sigma = K\left(\varepsilon_p\right)^n \tag{2.5}$$

The strength coefficient (K) and strain hardening exponent (n) were obtained by performing a least squares fit of the true stress (σ) versus true plastic strain (ε_p) data. The data used in this fit were between the yield stress and the ultimate strength of the material. This was chosen because of the discontinuous yielding definition in the ASTM Standard E646 [2004]. The true plastic strain (ε_p) was the independent variable and the true stress (σ) was the dependent variable as specified by the ASTM Standard E739 [2004]. The true stress versus true plastic strain plot of both materials is shown in Figure 2.6. It can be seen from the figure that the strength coefficient (K) is slightly higher for forged steel than for cast iron and the strain hardening exponent is lower for forged steel than for cast iron.

True fracture strength (σ_f) can be calculated using the load at fracture, P_f, and the area at fracture, A_f, but when there is necking present there exists a biaxial state of stress on the cylindrical surface and a triaxial state of stress in the interior of the specimen. In order to compensate for this state of stress the true fracture strength was calculated using the Bridgman correction factor which is given by the following equation:

$$\sigma_f = \frac{P_f \big/ A_f}{\left(1 + 4R \big/ D_{\min}\right) \ln\left(1 + D_{\min} \big/ 4R\right)} \tag{2.6}$$

where R is the neck radius and D_{min} is the minimum diameter of the fracture location. This was only used for forged steel since the cast iron specimen did not show signs of necking. For cast iron the true fracture strength (σ_f) was calculated using the equation:

$$\sigma_f = \frac{P_f}{A_f} \tag{2.7}$$

where the area at fracture is calculated using the diameter of the specimen after fracture as measured with an optical comparator.

True fracture ductility (ε_f) was calculated using the equation:

$$\varepsilon_f = \ln\left(\frac{A_0}{A_f}\right) \tag{2.8}$$

where A_0 is the initial cross-sectional area.

The monotonic tensile test results for the two materials are summarized in Table 2.3. The monotonic properties for the two materials are shown in Table 2.4. The monotonic engineering stress-strain curves for the two materials are shown in Figure 2.7. These stress-strain curves for both materials are shown superimposed on the same plot in Figure 2.8.

2.1.3.2 Cyclic deformation properties and behavior

The resistance to deformation of a material can change when a cyclic load is applied rather than a monotonic load. The application of inelastic strain can change the properties of the material. As a cyclic load is applied, the material may cyclic soften or cyclic harden. These two terms refer to the decrease and increased resistance to deformation, respectively. This "cyclic transient behavior" can be observed by plotting stress amplitude versus the number of cycles. An increase in stress amplitude with applied strain cycles represents cyclic hardening behavior, while a decrease of stress

amplitude represents cyclic softening behavior. The transient response of the ductile cast iron and the forged steel are shown in semi-log format in Figure 2.9. The response is also shown normalized in Figure 2.10. One specimen from each strain amplitude is shown in the plots.

Although this "cyclic transient behavior" does exist, the material stabilizes with applied cyclic loading. This stabilization is important to the representation of cyclic material properties. If the material continues to change, material properties would be dependant on the cycles applied. The midlife of the test was taken as the stabilized state of the material, except where the test was switched from strain control to load control (for this case the hysteresis loop at the time of the switch was used). Therefore, the steady state hysteresis loops from the constant amplitude strain-controlled fatigue tests were used to determine the following cyclic properties: fatigue strength coefficient (σ_f'), fatigue strength exponent (b), fatigue ductility coefficient (ε_f'), fatigue ductility exponent (c), cyclic yield strength (YS'), cyclic strength coefficient (K'), and the cyclic strain hardening exponent (n'). The cyclic properties of ductile cast iron and forged steel are summarized in Table 2.4.

The steady-state hysteresis loops for the forged steel material and the cast iron material are shown in Figure 2.11. A summary of the constant amplitude completely reversed fatigue test data for the forged steel is shown in Table 2.5 and for the cast iron in Table 2.6.

In order to find the cyclic strength coefficient (K') and the cyclic strain hardening exponent (n'), the true plastic strain amplitude ($\Delta\varepsilon_p/2$) was calculated using the equation:

$$\frac{\Delta\varepsilon_p}{2} = \frac{\Delta\varepsilon}{2} - \frac{\Delta\sigma}{2E} \tag{2.9}$$

The cyclic strength coefficient (K') and the cyclic strain hardening exponent (n') were obtained by plotting the true stress amplitude ($\Delta\sigma/2$) versus true plastic strain amplitude ($\Delta\varepsilon_p/2$) in log-log scale. The cyclic strength coefficient (K') is the intercept of stress amplitude at a plastic strain amplitude of 1, and the cyclic strain hardening exponent (n') is the slope of the best fit line. To satisfy the ASTM Standard E739 [2004], the true plastic strain amplitude ($\Delta\varepsilon_p/2$) was the independent variable when performing the least squares fit of the data. The range of data used to obtain the K' and n' values were 0.25% $< \varepsilon_a <$ 2% for cast iron and 0.2% $< \varepsilon a <$ 2% for forged steel. This range represents the range in which significant plastic deformation occurred. The best fit line of the data is represented by the equation:

$$\frac{\Delta\sigma}{2} = K'\left(\frac{\Delta\varepsilon_p}{2}\right)^{n'} \tag{2.10}$$

The K' and n' values are used in the Ramberg-Osgood equation that characterizes the cyclic true stress-strain behavior of the material. The Ramberg-Osgood equation for cyclic behavior is given by:

$$\frac{\Delta\varepsilon}{2} = \frac{\Delta\varepsilon_e}{2} + \frac{\Delta\varepsilon_p}{2} = \frac{\Delta\sigma}{2E} + \left(\frac{\Delta\sigma}{2K'}\right)^{1/n'} \tag{2.11}$$

The plots of true stress amplitude ($\Delta\sigma/2$) versus true plastic strain amplitude ($\Delta\varepsilon_p/2$) in log-log scale for the two materials along with the best fit lines are shown in Figure 2.12.

Due to the "cyclic transient behavior" the cyclic stress-strain curve is different than the monotonic curve. The cyclic stress-strain curve was obtained using the applied strain amplitudes and the stress amplitudes from the stable hysteresis loops. The cyclic stress-strain curves for the two materials are shown in Figure 2.13. The cyclic stress-strain curve from both materials are shown superimposed on the same plot in Figure 2.14.

The cyclic stress-strain curves are shown superimposed with their respective monotonic stress-strain curve in Figure 2.15. The cyclic and monotonic stress-strain curves for the two materials are shown superimposed on the same plot in Figure 2.16. From Figure 2.15(a) it can be seen that the forged steel cyclic softens for the range of available cyclic stress-strain data. From Figure 2.15(b) it can be seen that the cast iron cyclic hardens.

2.1.3.3 Fatigue behavior and comparisons

When determining strain-life fatigue properties, such as σ_f', b, ε_f', and c, the stress amplitude ($\Delta\sigma/2$) and the plastic strain amplitude ($\Delta\varepsilon_p/2$) were considered the independent variables and the fatigue life ($2N_f$) was considered the dependent variable in the least squares fit. This is done in accordance with ASTM Standard E739 [2004].

The elastic fatigue behavior of the material can be described by Basquin's equation as:

$$\frac{\Delta\sigma}{2} = \sigma_f'\left(2N_f\right)^b \tag{2.12}$$

The fatigue strength coefficient (σ_f') and the fatigue strength exponent (b) were found by fitting a line to the true stress amplitude ($\Delta\sigma/2$) versus number of reversals to failure ($2N_f$) data in log-log scale. σ_f' is intercept at one reversal, $2N_f = 1$, and b is the slope of the best fit line. The range of data used to determine σ_f' and b were $0.2\% \leq \varepsilon_a \leq 2\%$ for forged steel and $0.16\% \leq \varepsilon_a \leq 2\%$ for cast iron. The plots of true stress amplitude ($\Delta\sigma/2$) versus reversals to failure ($2N_f$) along with the best fit lines for the two materials are shown in Figure 2.17. Superimposed plots of the two materials are shown in Figure 2.18. This figure shows that forged steel has a higher fatigue strength than ductile cast iron at any given life. For a given stress amplitude, the forged steel life is larger by at least an

order of magnitude than cast iron at shorter lives, and approximately 50 times larger at long lives. Since the component is a rotating component in an engine, it is subjected to a large number of cycles in service. Therefore, the fatigue performance at long life is the main area of interest. The fatigue limit, considered to be at 10^6 cycles for both materials, was 358.9 MPa for forged steel and 262.8 MPa for cast iron. The fatigue strength at 10^6 cycles for the forged steel material was 36% higher than the fatigue strength of the ductile cast iron material at the same life.

The relationship between the true plastic strain amplitude and the number of reversals to failure is given by the Manson-Coffin relationship:

$$\frac{\Delta\varepsilon_p}{2} = \varepsilon_f'(2N_f)^c \tag{2.13}$$

The fatigue ductility coefficient (ε_f') and the fatigue ductility exponent (c) were determined by fitting a line to the true plastic strain amplitude ($\Delta\varepsilon_p/2$) versus reversals to failure ($2N_f$) data in log-log scale. ε_f' is the intercept at one reversal, $2N_f = 1$, and c is the slope of the best fit line. The range of data used to determine ε_f' and c were $0.2\% \leq \varepsilon_a \leq 2\%$ for forged steel and $0.25\% \leq \varepsilon_a \leq 2\%$ for cast iron. This range was selected as the range where significant plastic deformation occurred. The plots of true plastic strain amplitude ($\Delta\varepsilon_p/2$) versus reversals to failure ($2N_f$) along with the best fit lines for the two materials are shown in Figure 2.19. Superimposed plots of the two materials are shown in Figure 2.20. Figure 2.20 shows that the forged steel material has a factor of 40 longer life than the ductile cast iron material for a given plastic strain amplitude in the long life region.

The total strain is related to the fatigue life by adding the elastic and plastic portions of the curve. The strain-life equation is given by:

$$\frac{\Delta\varepsilon}{2} = \varepsilon_a = \frac{\Delta\varepsilon_e}{2} + \frac{\Delta\varepsilon_p}{2} = \frac{\sigma_f'}{E}\left(2N_f\right)^b + \varepsilon_f'\left(2N_f\right)^c \tag{2.14}$$

The strain-life curves along with the elastic strain portion, plastic strain portion, and fatigue data for both materials are shown in Figure 2.21. The strain life curve for the two materials are shown superimposed on the same plot in Figure 2.22. From the figure it can be seen that the forged steel curve is above the cast iron curve at all lives. In the long life region, which is the region of importance of this study, there is a factor of approximately 10 between the life of the cast iron and forged steel.

A variation on the strain life curve is the Neuber's plot. Neuber's stress range is calculated by:

$$\sqrt{(\Delta\sigma)(\Delta\varepsilon)E} = 2\sqrt{\left(\sigma_f'\right)^2\left(2N_f\right)^{2b} + \sigma_f'\varepsilon_f'E\left(2N_f\right)^{b+c}} \tag{2.15}$$

In Equation 2.15 the term on the left is referred to as Neuber's parameter. The fatigue behavior at a notch is often controlled by the stress range and the strain range at the root of the notch. Neuber's parameter is significant when comparing the fatigue performance of crankshaft materials due to the presence of notches, or fillets, in the crankshaft since this parameter combines the stress range, strain range, and modulus of elasticity. The Neuber plots for forged steel and cast iron are shown in Figure 2.23. Superimposed Neuber plots for the two materials are shown in Figure 2.24. From the figure in can be seen that the forged steel material has superior fatigue performance to the ductile cast iron material when Neuber's parameter is used. In the long life region this amounts to a factor of 50 longer life for the forged steel than the ductile cast iron material for a given Neuber stress range.

2.2 Charpy V-Notch Tests

2.2.1 Specimen and test equipment

The specimen geometry was taken from the ASTM Standard E23 [2004]. The standard specifies several different geometries which may be used. Of the several options available, the most commonly used specimen geometry was chosen as the geometry used for this study. This is the 10mm X 10mm X 55mm specimen geometry with a v shaped notch which E23 labels as Charpy Impact Test Specimen Type A. The geometry of the specimens created is shown in Figure 2.25 along with the specified tolerances.

The specimens used for obtaining impact toughness data by means of the Charpy impact test were obtained from crankshafts identical to those used to obtain monotonic and fatigue specimens. The process of forging causes the inclusions to become elongated in the longitudinal (maximum grain flow) direction of the sample. This elongation of the inclusions results in lower impact toughness when the notch is oriented in the longitudinal direction. Therefore, two different specimen orientations were used for the forged steel specimens. The locations from which the specimens were removed from the crankshaft are shown in Figure 2.26. Two letter designations are used when referring to the specimen orientation. The letter "L" represents the longitudinal direction and the letter "T" represents the transverse direction as indicated in Figure 2.26. One set of specimens are in the L-T orientation and the other set in the T-L orientation. In this code, the first letter represents the direction which is normal to the crack plane, and the second letter designates the direction in which the notch is machined (and the direction of crack growth). The casting process results in inclusions or porosity which are randomly

distributed in the sample and not expected to be elongated in any particular direction. Therefore, only one set of cast iron specimens were manufactured.

The specimens were machined in The University of Toledo Mechanical, Industrial, and Manufacturing Engineering Machine Shop. First the rough shape was cut from the sections shown in Figure 2.26 as discussed previously. Four specimens were obtained from Section A (as indicated in the figure) of both cast iron and forged steel crankshafts (L-T). Four specimens were also obtained from each counterbalance section of the forged steel crankshaft labeled Section B. There are two counterbalance sections of the crankshaft; therefore 8 specimens in the T-L orientation were obtained from each crankshaft. The specimens were then machined on a milling machine to an oversized geometry from that required. The remaining material was removed using a grinding machine until the specimens were the proper dimensions. The notch was cut using a horizontal milling machine and a 45 degree double angle milling cutter which had a 0.25 mm radius. All specimen dimensions, including the notch depth and angle were measured using a 10X magnification optical comparator.

The Charpy impact tests were conducted using a Tinius Olsen pendulum type impact testing machine. The machine used in the testing is shown in Figure 2.27. The machine is fitted with a dial indicator that reads directly in energy (kg-m). The machine was verified prior to being used. A zero verification test was done to ensure that no uncompensated windage or frictional losses were present in the machine. The test was conducted with no specimen present, and it was verified that the reading was zero. A percentage friction and windage loss test was also done as outlined by ASTM Standard E23 [2004], to verify that the friction and windage loss did not exceed 0.4% of the

maximum scale value. The amount of friction and windage loss present in the machine was within the acceptable range. The pendulum is raised to its initial height and then released by a lever. The pendulum swings as it impacts the face opposite the notch and then reaches its final height. The difference between the initial and final heights of the pendulum results in a reading of absorbed energy on the dial gauge.

2.2.2 Test procedure

Since the impact toughness of a material changes with temperature, an absorbed energy versus temperature plot is usually constructed. The typical plot has a lower shelf region and an upper shelf region with a curve connecting the two. Due to the application of the crankshafts used in this study, less emphasis was put on obtaining the precise upper and lower shelf regions than conducting the test over a range of temperatures which would include the operating range of the crankshafts. Six temperature levels were used for the tests. The temperature levels for all three specimen types (Forged steel L-T, T-L, and ductile cast iron) ranged between -77°C and 200°C. Two specimens were tested for each orientation/material at each temperature. Room temperature specimens were tested first where the room temperature was 26.3°C as measured by a thermometer. For the 0°C tests, an ice bath was maintained at 0°C. For the tests at -40°C and -77.1°C, a temperature conditioning bath of dry ice and lab grade isopropanol alcohol was used. For the tests using a liquid medium the temperature was constantly monitored using a liquid thermocouple probe and a digital readout. The specimens were immersed in the temperature conditioning bath for at least 5 minutes prior to testing. The tongs used to hold the specimen were also immersed in the bath prior to the first test and in between

subsequent tests. To ensure even temperature distribution, the conditioning bath was manually stirred. For the tests conducted at 100°C and 200°C, a Fisher Scientific Isotemp Oven Model 851F with a digital controller was used. The specimens were placed in the preheated oven at the specified temperature for at least 1 hour prior to testing. The tongs were placed in the oven prior to the first test and in between each subsequent test. For all tests conducted at temperatures other than ambient, the test was conducted within five seconds of removing the specimen from its temperature conditioning environment.

2.2.3 Test results and comparisons

The results of the Charpy Impact tests are shown in Table 2.7. The average absorbed energy values obtained from duplicate Charpy V-notch impact tests at each temperature are shown as a bar chart in Figure 2.28. From this figure it can be seen that the forged steel in the L-T direction had a higher absorbed energy value over the entire range of temperatures. The figure also shows that the ductile cast iron values were the lowest of the three sets of values over the entire range of temperatures, as expected. Figure 2.29 shows the absorbed energy versus temperature curve for all three specimen types. The upper shelf region is shown for the three materials, however with the lowest temperature at -77°C, the lower shelf region is not clearly shown. The middle transition curve was obtained by fitting an n^{th} order polynomial to the data. This curve also indicates that forged steel in the L-T orientation has the highest impact toughness of the three material/orientations tested regardless of temperature.

The fracture surfaces of all specimens tested are shown in Figure 2.30. The percentage shear fracture (ductile fracture) was also observed for each specimen. The ASTM Standard E23 Annex 6 [2004] specifies four procedures for determining the percentage of ductile fracture. The second option, comparing the surface with the supplied fracture appearance chart, was chosen. The percentage shear, along with the energy data for each test is given in Table 2.7. The forged steel in both directions exhibited 100% ductile fracture at 100°C and 200°C. The forged steel specimens also showed little to no ductile fracture at the sub zero temperatures. The cast iron specimens exhibited brittle fracture over the entire temperature range tested.

Table 2.1: Chemical analysis of the forged steel and ductile cast iron as a percent weight, remaining Fe [Heitmann, 2006].

Element	Forged Steel	Ductile Cast Iron
C	0.45	3.44
Mn	0.81	0.48
P	0.016	0.019
S	0.024	0.004
Si	0.27	2.38
Al	0.033	0.01
Cr	0.1	0.09
Ni	0.05	0.06
Cu	0.13	0.31
N	0.008	--
O	13 ppm	--

Table 2.2: Hardness values for (a) forged steel and (b) ductile cast iron monotonic and fatigue specimens.

Specimen	FS-2*	FS-3	FS-4	FS-6	FS-8	FS-9	FS-10	FS-11*	FS-12	FS-13	FS-14	FS-15
Measured HRC	18	25	24	27	18	24	23.5	17.5	26	25	20.5	25.5
	18	25	24	27	18.5	25	24	18	27	26	22.5	26.5
	20	25.5	26.5	27.5	18.5	25.5	24.5	19	27.5	27.5	23	27.5
Measured HRB	97.5	101.5	100.5	102.5	98	102	101	97	102	103.5	102	102.5
	97.5	102	102	102.5	98.5	102	101	97.5	102.5	103.5	102	102.5
	98.5	103	103	103	99.5	102.5	101	98	103	103.5	102.5	102.5
Average HRC	18.7	25.2	24.8	27.2	18.3	24.8	24.0	18.2	26.8	26.2	22.0	26.5
Average HRB	97.8	102.2	101.8	102.7	98.7	102.2	101.0	97.5	102.5	103.5	102.2	102.5

(a)

Specimen	CI-1	CI-2	CI-4	CI-5	CI-6	CI-8	CI-9	CI-10	CI-11	CI-12*	CI-13	CI-14	CI-15	CI-16
Measured HRC	17	18	16.5	20.5	19.5	19	19	17	19	16	21	18.5	19.5	20
	18.5	18	15	19	19	19.5	19.5	18	21	15	19	17	18	18
	19	18	17	20	21	20	19	18.5	18.5	13.5	20	17	20	20
Measured HRB	99	97	94.5	97.5	98	97	98.5	98.5	98.5	94	97.5	98	97	97.5
	100	97.5	94.5	97.5	97	96.5	97.5	97	99	94.5	99	97	96.5	98
	100	98	94.5	97	98	97.5	98	96.5	97	93.5	98	97	97	97
Average HRC	18.2	18.0	16.2	19.8	19.8	19.5	19.2	17.8	19.5	14.8	20.0	17.5	19.2	19.3
Average HRB	99.7	97.5	94.5	97.3	97.7	97.0	98.0	97.3	98.2	94.0	98.2	97.3	96.8	97.5

* Test data were not considered due to low hardness levels

(b)

Table 2.3: Result summary of monotonic tensile tests.

Specimen ID	D_o, mm (in.)	D_f, mm (in.)	L_o, mm (in.)	L_f, mm (in.)	E, GPa (ksi)	YS 0.2% offset, MPa (ksi)	UYS, MPa (ksi)	LYS, MPa (ksi)	YPE, %	S_u, MPa (ksi)	K, MPa (ksi)	n	%EL	%RA	R, mm (in.)	σ_f^*, MPa (ksi)	ε_f
FS-12	5.13	3.33	5.99	9.22	221.3	625.0	681.9	623.8	0.44%	826.6	1,315.6	0.152	54%	58%	1.46	979.5	87%
CI-4	5.16	5.00	5.99	6.60	178.2	412.2	--	--	--	657.6	1,199.0	0.183	10%	6%	--	657.6	6%

* On the forged steel the value of true fracture strength is corrected for necking according to the Bridgman correction factor.

Table 2.4: Summary of monotonic and cyclic properties for the two materials.

Monotonic Properties	Forged Steel		Cast Iron		Ratio
Average Hardness, HRC	23		18		0.8
Average Hardness, HRB	101		97		0.96
Modulus of elasticity, E, Gpa (ksi)	221	(32,088)	178	(25,838)	0.81
Yield Strength (0.2%offset), YS, MPa (ksi)	625	(91)	412	(60)	0.66
Ultimate strength, S_u, MPa (ksi)	827	(120)	658	(95)	0.80
Percent elongation, %EL	54%		10%		0.19
Percent reduction in area, %RA	58%		6%		0.10
Strength coefficient, K, MPa (ksi)	1316	(191)	1199	(174)	0.91
Strain hardening exponent, n	0.152		0.183		1.20
True fracture strength, σ_f, MPa (ksi)	980	(142)	658	(95)	0.67
True fracture ductility, ε_f	87%		6%		0.07

Cyclic Properties	Forged Steel		Cast Iron		Ratio
Fatigue strength coefficient, σ_f', MPa (ksi)	1124	163	927	(134)	0.82
Fatigue strength exponent, b	-0.079		-0.087		1.10
Fatigue ductility coefficient, ε_f'	0.671		0.202		0.30
Fatigue ductility exponent, c	-0.597		-0.696		1.17
Cyclic yield strength, YS', MPa (ksi)	505	73	519	(75)	1.03
Cyclic strength coefficient, K', MPa (ksi)	1159	168	1061	(154)	0.91
Cyclic strain hardening exponent, n'	0.128		0.114		0.89
$S_f = \sigma_f'(2N_f)^b$ at $N_f = 10^6$, MPa (ksi)	359	(52)	263	(38)	0.73
Average E' Gpa (ksi)	204	(31,437)	174	(25,229)	0.85

Note: Forged steel taken as the base for all ratio calculations

Table 2.5: Summary of constant amplitude completely reversed fatigue test results for forged steel.

Spec. ID *	D_o, mm (in.)	E',Gpa (ksi)	Testing control mode	Test freq. Hz	$\Delta\varepsilon/2$, %	$\Delta\varepsilon_p/2$ (calc.)%	$\Delta\varepsilon_p/2$ (meas.) %	$\Delta\sigma/2$, MPa (ksi)	σ_m, MPa (ksi)	$N_{50\%}$, [a] cycles	$(N_f)_{10\%}$ [b] , cycles	$(N_f)_{20\%}$, [c] cycles	$(N_f)_{50\%}$, [d] cycles	Failure location [e]	Hardness (HRC)
FS-8	5.18 (0.204)	203.0 (29,448)	strain	0.10	1.981%	1.674%	1.637%	679.7 (98.6)	-3.6 -(0.5)	147	263	266	276	IGL	18.3
FS-14	5.21 (0.205)	191.1 (27,709)	strain	0.50	0.995%	0.711%	0.674%	629.0 (91.2)	-3.7 -(0.5)	574	1,001	1,035	1,132	IGL	22
FS-3	5.18 (0.204)	192.7 (27,947)	strain	0.50	0.999%	0.715%	0.677%	629.3 (91.3)	-2.7 -(0.4)	600	1,125	1,142	1,188	IGL	25.2
FS-9	5.18 (0.204)	207.6 (30,115)	strain	0.83	0.499%	0.253%	0.224%	543.1 (78.8)	14.5 (2.1)	2,450	4,827	4,847	4,894	IGL	24.8
FS-15	5.21 (0.205)	199.1 (28,881)	strain	0.83	0.501%	0.259%	0.232%	534.8 (77.6)	9.3 (1.3)	2,671	4,901	5,056	5,304	IGL	26.5
FS-10	5.13 (0.202)	194.0 (28,131)	strain	0.50	0.349%	0.135%	0.105%	472.7 (68.6)	27.5 (4.0)	8,105	13,515	13,567	13,635	IGL	24
FS-6	5.18 (0.204)	199.7 (28,957)	strain	0.50	0.348%	0.129%	0.124%	485.3 (70.4)	32.1 (4.7)	4,509	8,798	9,127	10,384	IGL	27.2
FS-11*	5.16 (0.203)	207.7 (30,128)	strain load	0.83	0.249%	0.080%	0.060%	374.3 (54.3)	37.4 (5.4)	37,345	--	--	74,691	IGL	18.2
FS-4	5.21 (0.205)	205.1 (29,739)	strain load	0.83	0.251%	0.051%	0.037%	442.7 (64.2)	45.1 (6.5)	55,742	--	--	111,484	IGL	24.8
FS-13	5.21 (0.205)	208.5 (30,243)	strain load	0.83	0.199%	0.020%	0.008%	396.9 (57.6)	43.0 (6.2)	9,352	--	--	509,935	IGL	26.2
FS-2*	5.13 (0.202)	210.5 (30,535)	strain load	1.00	0.200%	0.043%	0.035%	346.2 (50.2)	15.8 (2.3)	8,999	--	--	540,950	IGL	18.7
FS-16	5.16 (0.203)	NA NA	load	25.00	0.160%	0.000%	0.000%	342.0 (49.6)	0.0 (0.0)	--	--	--	5,000,000	NA	--
FS-7	5.13 (0.202)	228.1 (33,078)	strain load	25.00	0.160%	0.000%	0.000%	354.0 (51.3)	1.7 (0.3)	--	--	--	5,000,000	NA	--

[a] $N_{50\%}$ is defined as the midlife cycle. [b] $(N_f)_{10\%}$ is defined as 10% load drop. [c] $(N_f)_{20\%}$ is defined as 20% load drop. [d] $(N_f)_{50\%}$ is defined as 50% load drop.

[e] IGL = inside gage length; OGIT = outside gage length but inside test section. * Specimens were not included in fits due to low hardness values

Table 2.6: Summary of constant amplitude completely reversed fatigue test results for ductile cast iron.

Speci. ID	D_o, mm (in.)	E',Gpa (ksi)	Testing control mode	Test freq., Hz	$\Delta\varepsilon/2$, %	$\Delta\varepsilon_p/2$ (calc.) %	$\Delta\varepsilon_p/2$ (meas.) %	$\Delta\sigma/2$, MPa (ksi)	σ_m, MPa (ksi)	$N_{50\%}$, [a] cycles	$(N_f)_{10\%}$, [b] cycles	$(N_f)_{20\%}$, [c] cycles	$(N_f)_{50\%}$, [d] cycles	Failure location [e]	Hardness, HRC
CI-14	5.21 (0.205)	150.3 (21,794)	strain	0.10	1.994%	1.612%	1.549%	680.1 (98.6)	-25.9 -(3.8)	7	NA	NA	14	IGL	17.5
CI-9	5.16 (0.203)	161.8 (23,459)	strain	0.50	1.000%	0.665%	0.634%	595.2 (86.3)	-16.3 -(2.4)	35	75	76	76	IGL	19.2
CI-13	5.18 (0.204)	161.8 (23,459)	strain	0.50	0.995%	0.659%	0.630%	597.9 (86.7)	-20.5 -(3.0)	32	89	90	91	IGL	20.0
CI-15	5.16 (0.203)	177.9 (25,808)	strain	0.50	0.499%	0.212%	0.202%	510.0 (74.0)	-8.2 -(1.2)	200	291	313	371	IGL	19.2
CI-12	5.16 (0.203)	163.7 (23,735)	strain	0.50	0.498%	0.221%	0.201%	492.8 (71.5)	-5.6 -(0.8)	450	757	771	789	OGIT	14.8
CI-8	5.21 (0.205)	179.5 (26,031)	strain	0.50	0.349%	0.083%	0.076%	474.3 (68.8)	10.3 (1.5)	512	975	1,015	1,164	IGL	19.5
CI-11	5.16 (0.203)	174.9 (25,368)	strain	0.83	0.250%	0.021%	0.016%	407.8 (59.1)	12.5 (1.8)	2,916	5,646	5,703	5,770	IGL	19.5
CI-5	5.16 (0.203)	173.9 (25,218)	strain load	0.83	0.250%	0.021%	0.022%	407.8 (59.1)	41.3 (6.0)	8,291	--	--	16,581	IGL	19.8
CI-10	5.16 (0.203)	176.3 (25,575)	strain load	1.00	0.200%	0.008%	0.005%	341.2 (49.5)	30.0 (4.3)	8,184	--	--	45,105	IGL	17.8
CI-16	5.21 (0.205)	172.8 (25,065)	strain load	1.00	0.199%	0.008%	0.005%	333.5 (48.4)	30.5 (4.4)	7,613	--	--	57,445	OGIT	19.3
CI-1	5.21 (0.205)	-- --	strain load	10.00	0.160%	0.000%	0.000%	285.0 (41.3)	0.0 (0.0)	--	--	--	317,014	IGL	18.2
CI-6	5.16 (0.203)	-- --	load	10.00	0.160%	0.000%	0.000%	286.8 (41.6)	0.0 (0.0)	--	--	--	144,928	IGL	19.8
CI-2	5.18 (0.204)	183.4 (26,598)	strain load	0.75 20.00	0.160%	-0.001%	0.002%	286.2 (41.5)	20.0 (2.9)	9,377	--	--	880,814	IGL	18.0
CI-7	5.13 (0.202)	-- --	load	20.00	0.135%	0.000%	0.000%	240.5 (34.9)	0.0 (0.0)	--	--	--	5,000,000	NA	--
CI-3	5.16 (0.203)	-- --	load	20.00	0.135%	0.000%	0.000%	240.5 (34.9)	0.0 (0.0)	--	--	--	5,000,000	NA	--

[a] $N_{50\%}$ is defined as the midlife cycle.
[b] $(N_f)_{10\%}$ is defined as 10% load drop.
[c] $(N_f)_{20\%}$ is defined as 20% load drop.
[d] $(N_f)_{50\%}$ is defined as 50% load drop.
[e] IGL = inside gage length; AKP = at knife point; OGIT = outside gage length but inside test section.
* Specimens were not included in fits due to low hardness values

Table 2.7: Summary of results from Charpy impact tests for (a) forged steel L-T, (b) forged steel T-L, and (c) cast iron.

(a)

Temperature (˚C)	Absorbed Energy (kg-m)	Joules	Percent Shear
-77	1.4	13.7	0%
-77	1.3	12.7	0%
-45	2.5	24.5	10%
-45	3.4	33.3	10%
0	4.3	42.2	30%
0	3.8	37.3	40%
26	6.4	62.7	60%
26	5.5	53.9	50%
100	9.5	93.1	100%
100	8	78.4	100%
200	8.8	86.3	100%
200	7.5	73.5	100%

(b)

Temperature (˚C)	Absorbed Energy (kg-m)	Joules	Percent Shear
-77	1.0	9.8	0%
-77	1.2	11.8	0%
-44	1.3	12.3	0%
-44	1.6	15.7	0%
0	2.1	20.6	20%
0	2.4	23.5	10%
26	3.5	34.3	60%
26	4.3	42.2	50%
100	3.2	31.4	100%
100	5.3	52.0	100%
200	5.1	50.0	100%
200	6.6	64.7	100%

(c)

Temperature (˚C)	Absorbed Energy (kg-m)	Joules	Percent Shear
-77	0.3	2.9	0%
-77	0.2	2.0	0%
-41	0.5	4.9	0%
-41	0.3	2.9	0%
0	0.3	2.9	0%
0	0.4	3.9	0%
26	0.5	4.9	0%
26	0.5	4.9	0%
100	0.8	7.8	0%
100	0.9	8.8	0%
200	1.4	13.7	0%
200	1	9.8	0%

(a)

(b)

Figure 2.1: Forged steel (a) and ductile cast iron (b) crankshafts used to obtain test specimens.

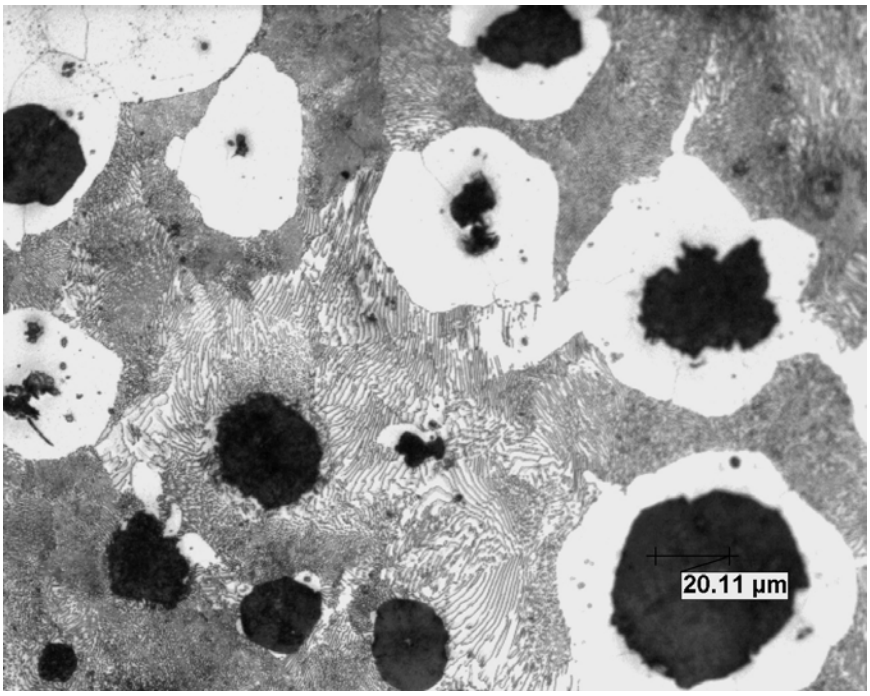

(a)

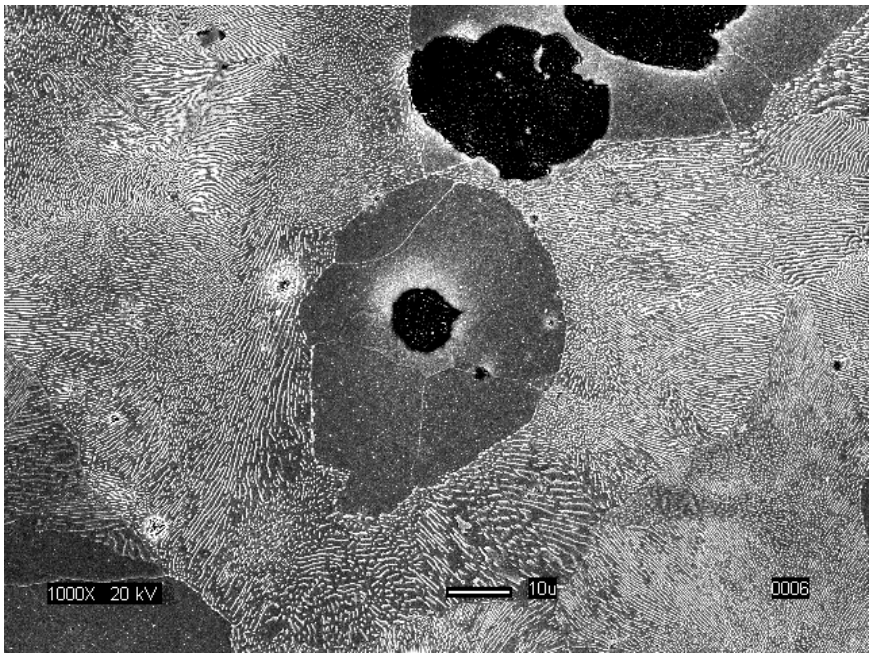

(b)

Figure 2.2: Photomicrographs of the ductile cast iron material at (a) 500X and (b) 1000X [Laus and Heitmann, 2007].

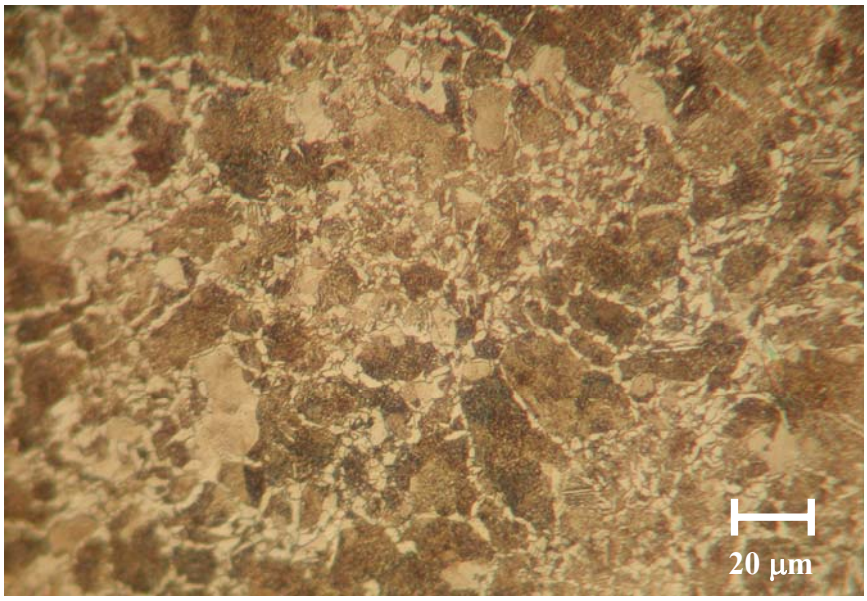

Figure 2.3: Photomicrograph of the forged steel material at 500X.

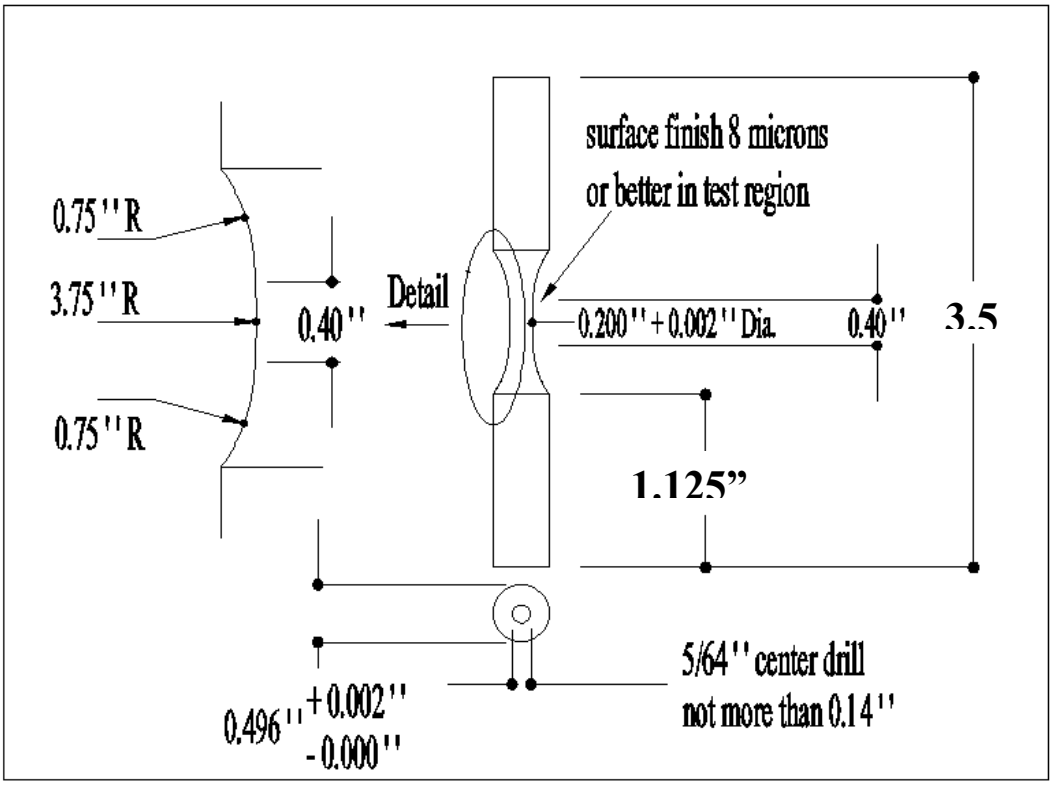

Figure 2.4: Specimen geometry for monotonic tensile tests and constant amplitude fatigue tests.

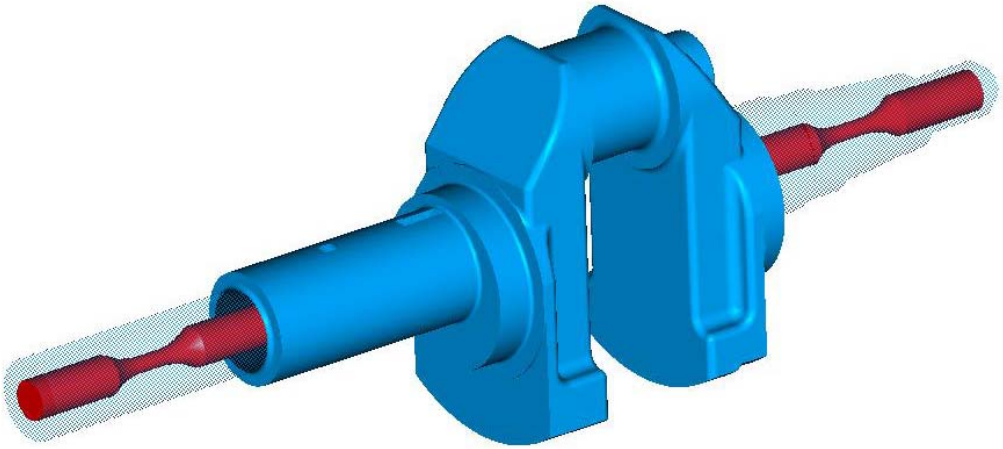

(a)

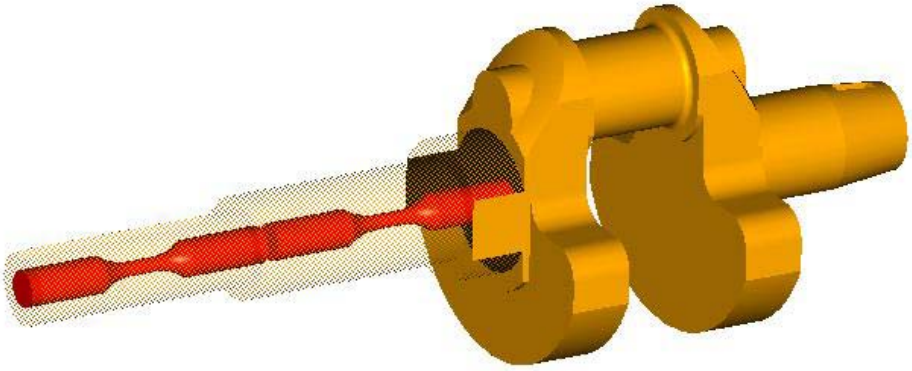

(b)

Figure 2.5: Locations where the monotonic and fatigue specimens were removed from for forged steel (a) and cast iron (b).

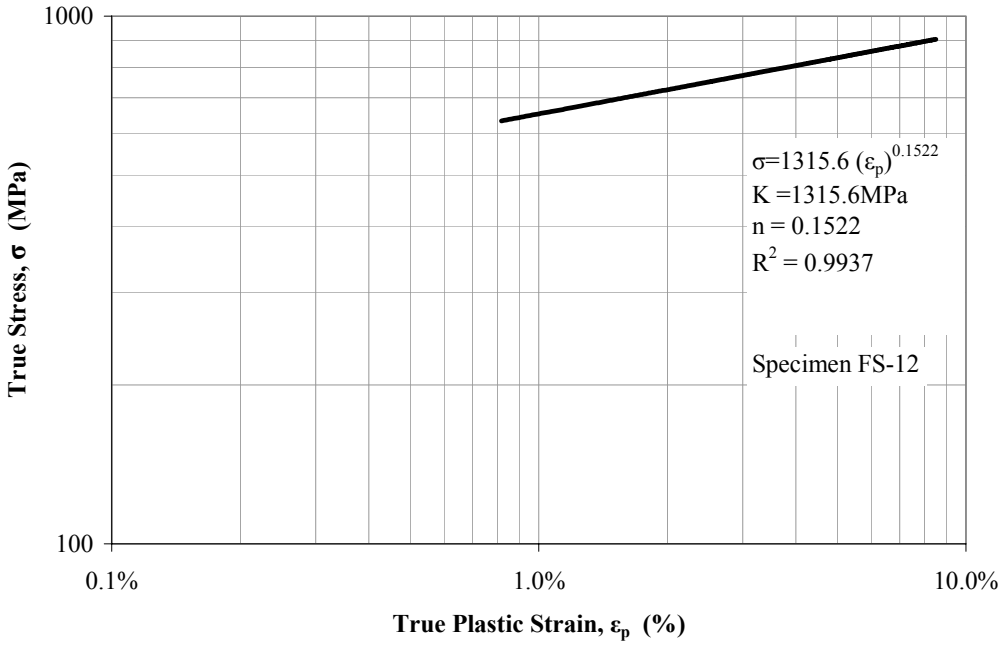

(a)

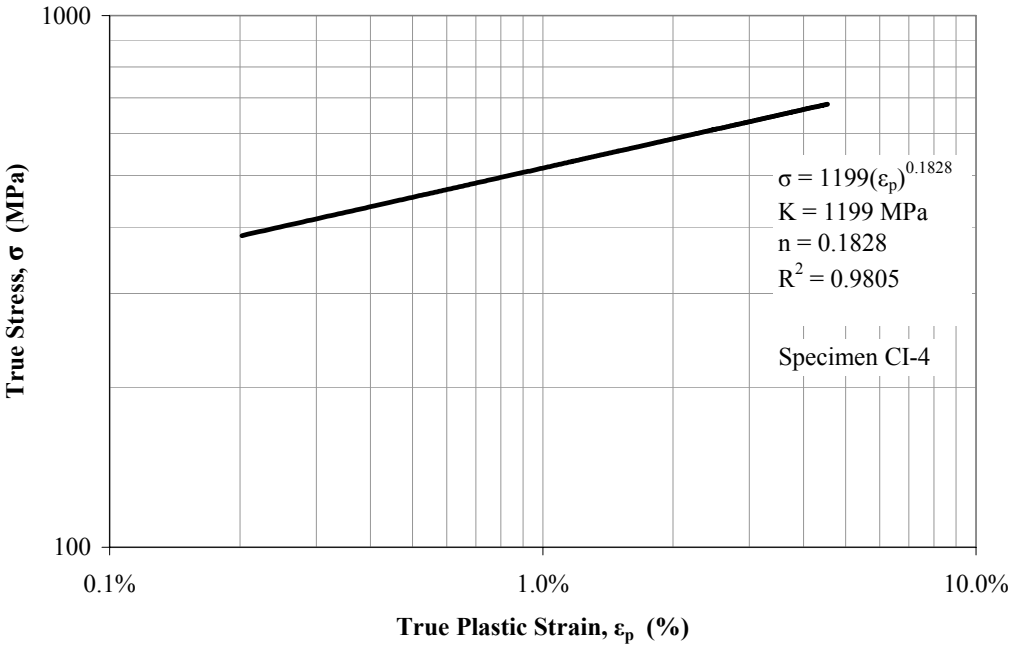

(b)

Figure 2.6: True stress versus true plastic strain for (a) forged steel and (b) ductile cast iron.

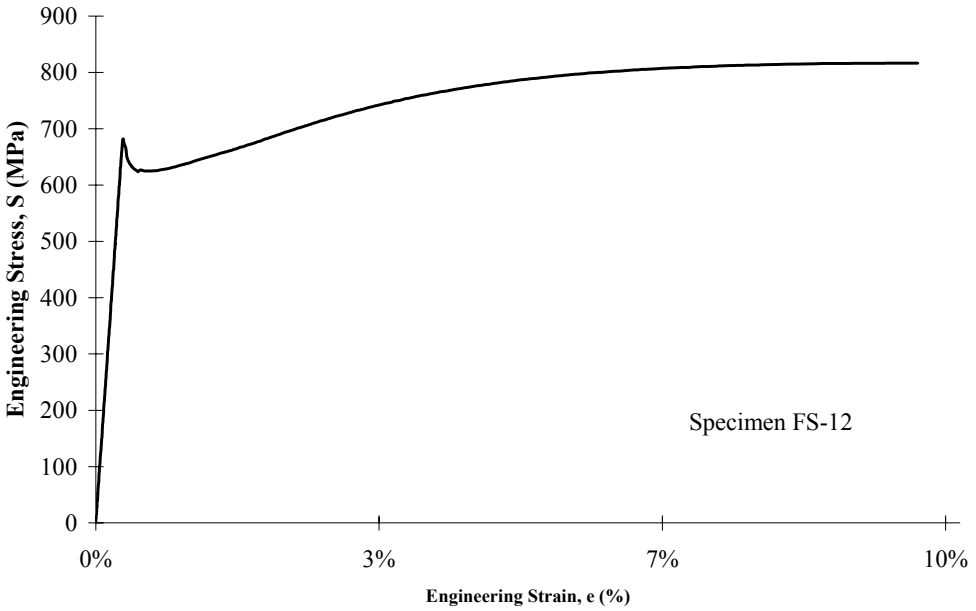

(a)

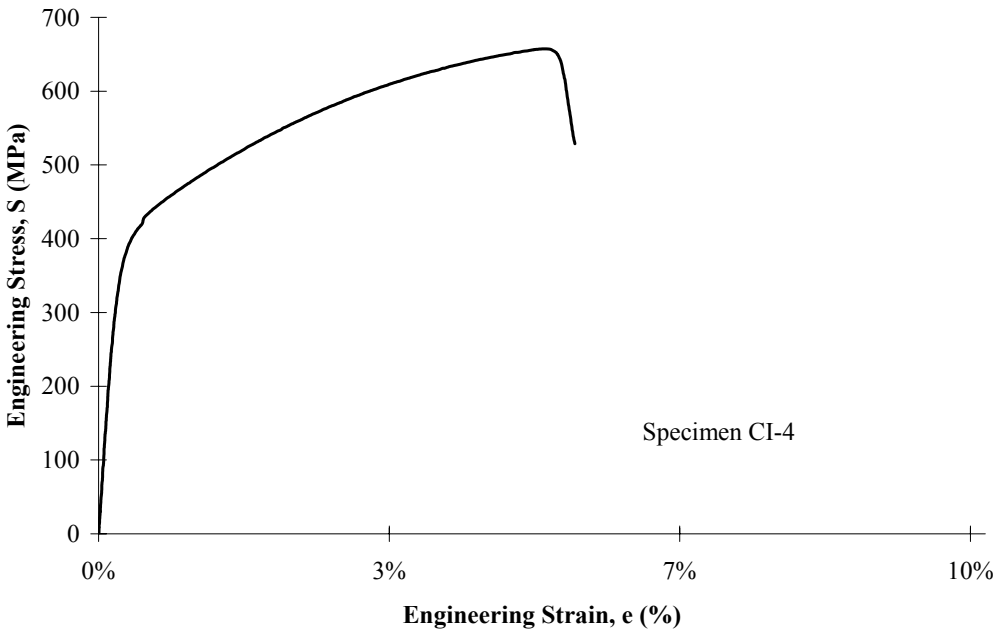

(b)

Figure 2.7: Monotonic engineering stress versus strain curves for (a) forged steel and (b) ductile cast iron.

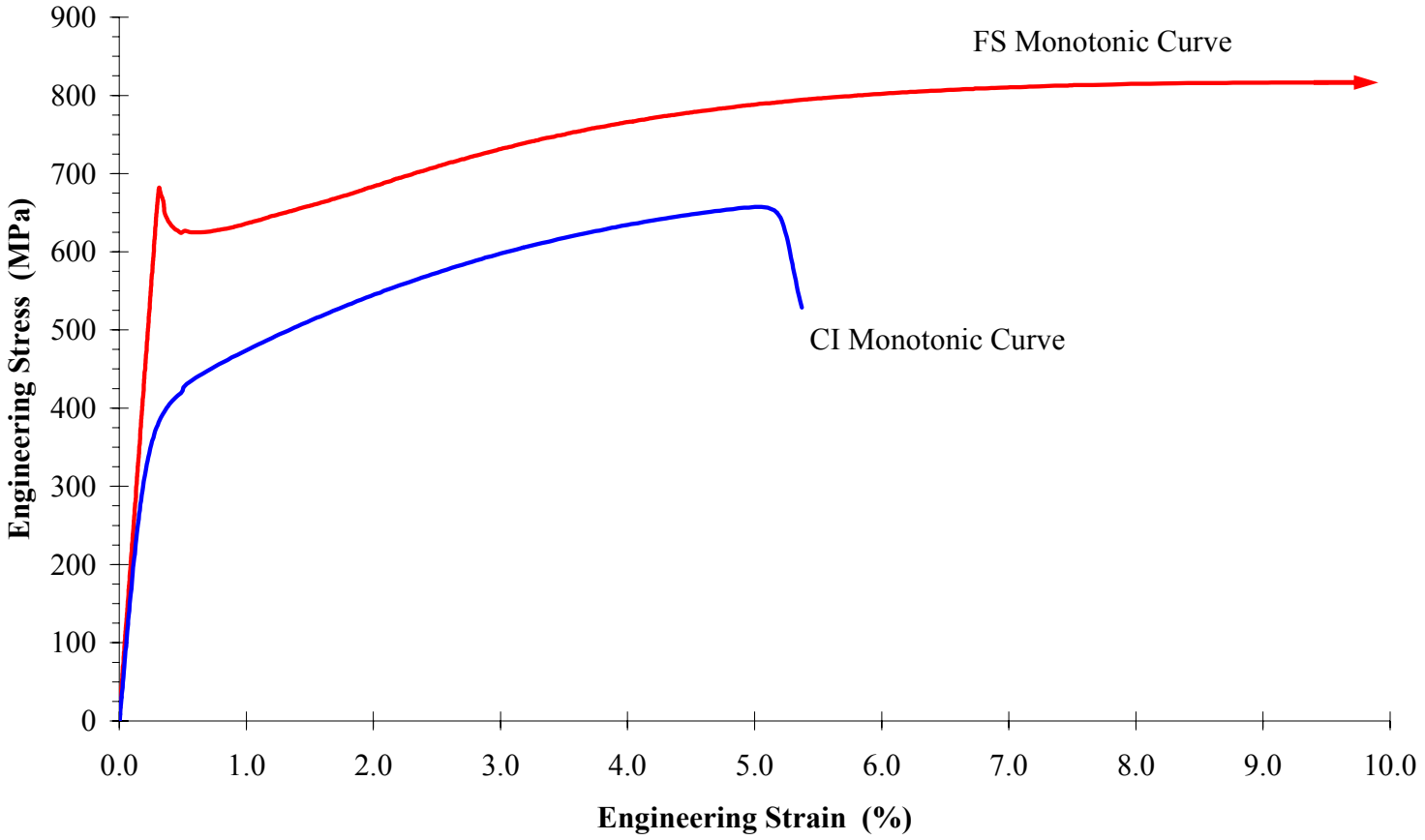

Figure 2.8: Superimposed monotonic engineering stress versus strain curves for forged steel and ductile cast iron.

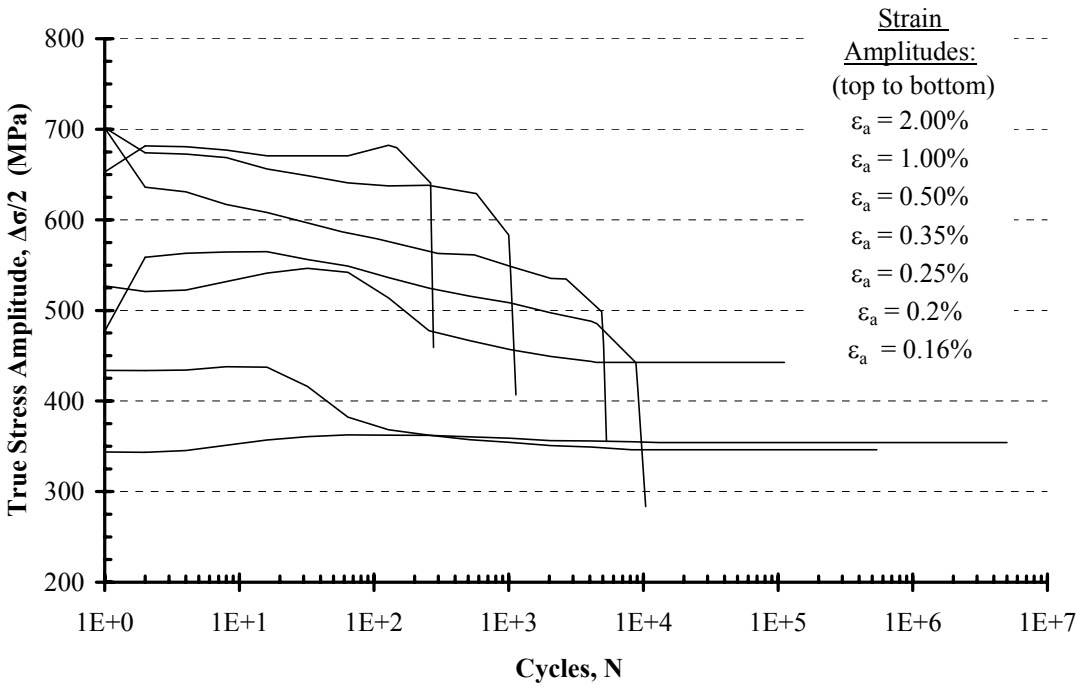

(a)

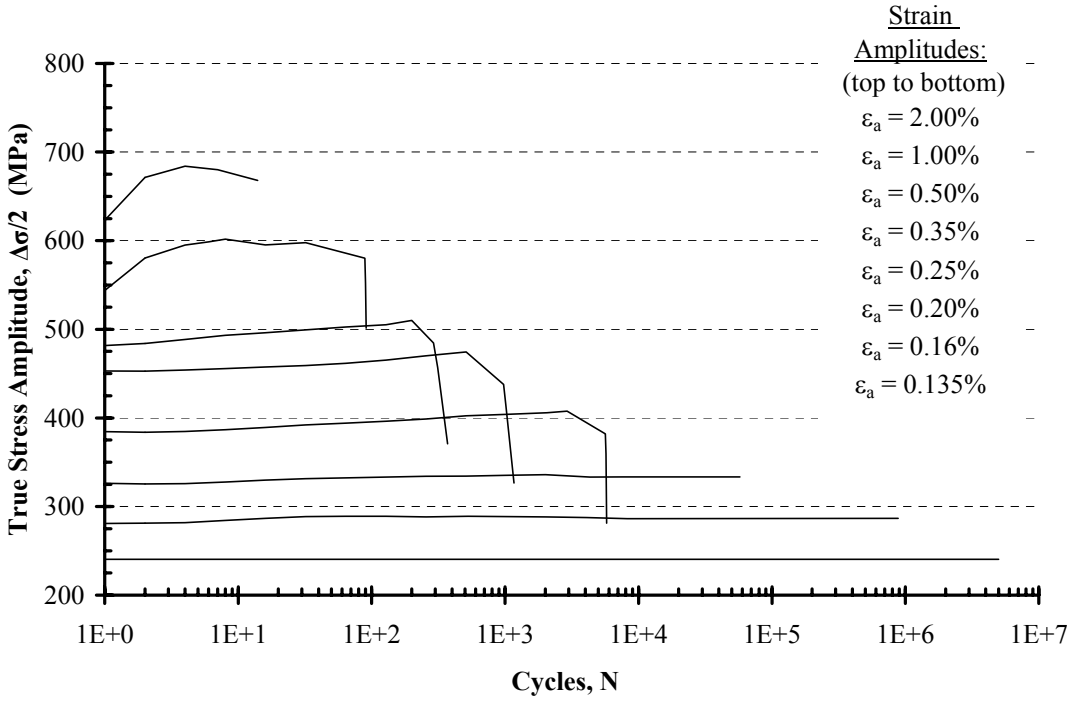

(b)

Figure 2.9: True stress amplitude versus number of cycles for (a) forged steel and (b) ductile cast iron.

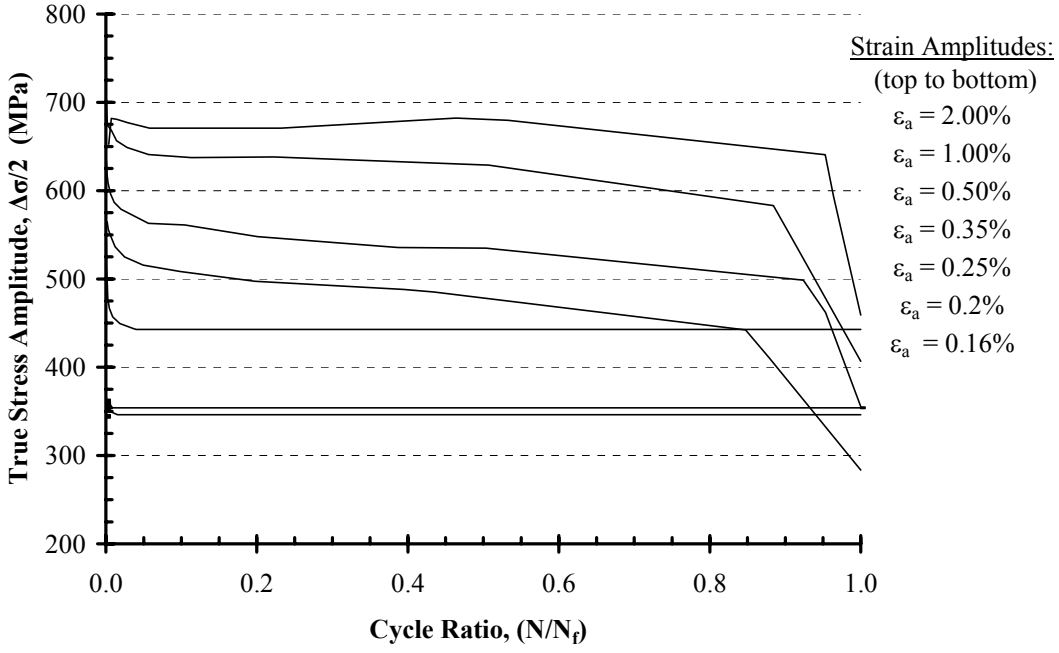

(a)

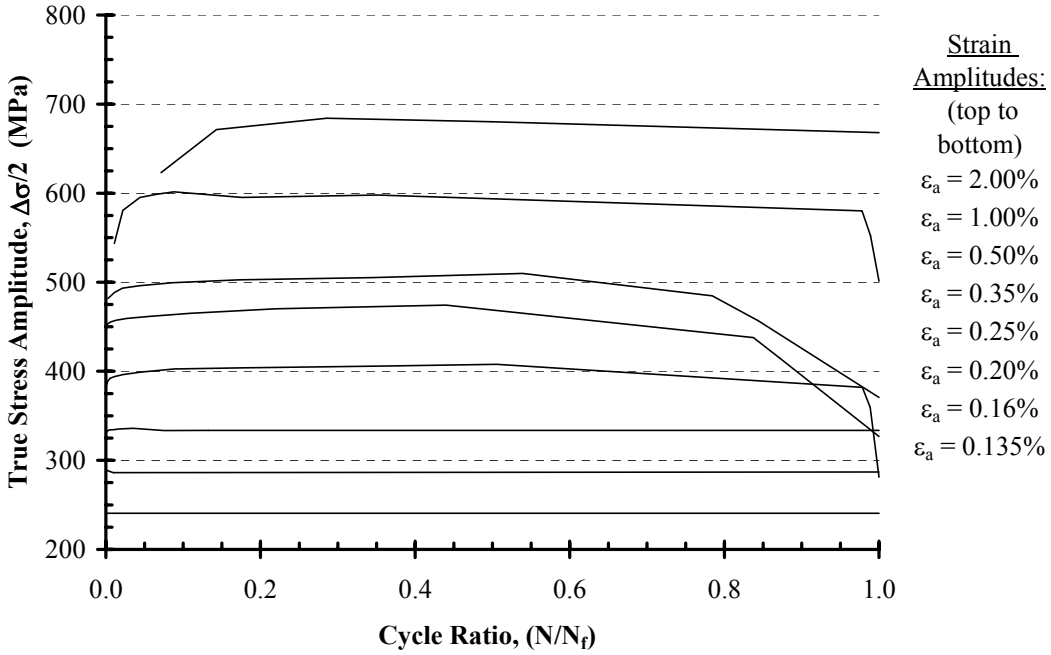

(b)

Figure 2.10: True stress amplitude versus normalized number of cycles for (a) forged steel and (b) ductile cast iron.

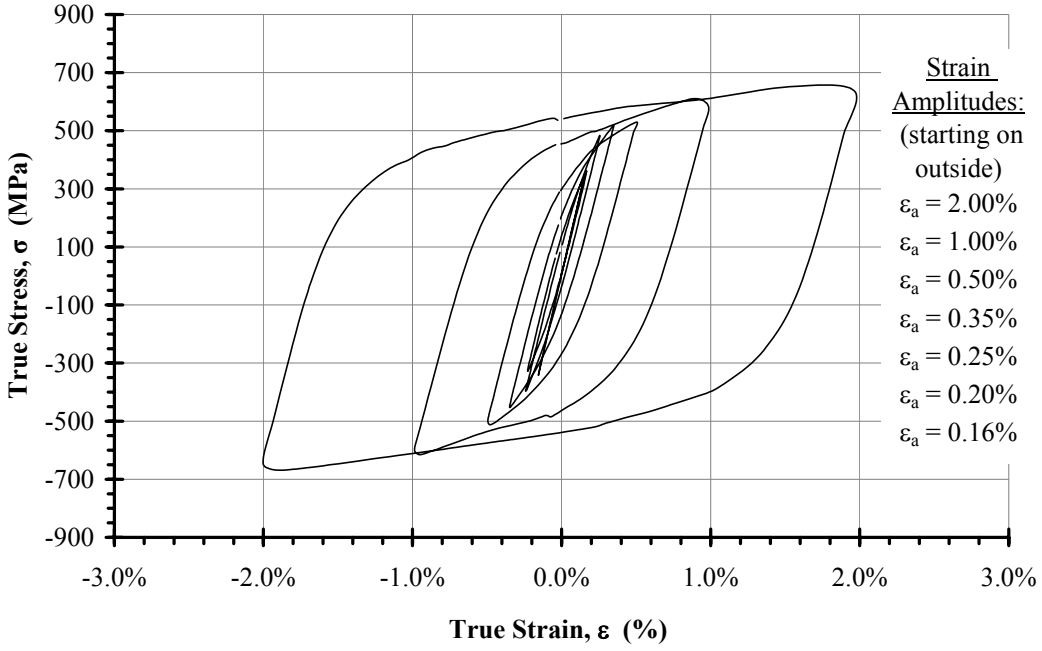

(a)

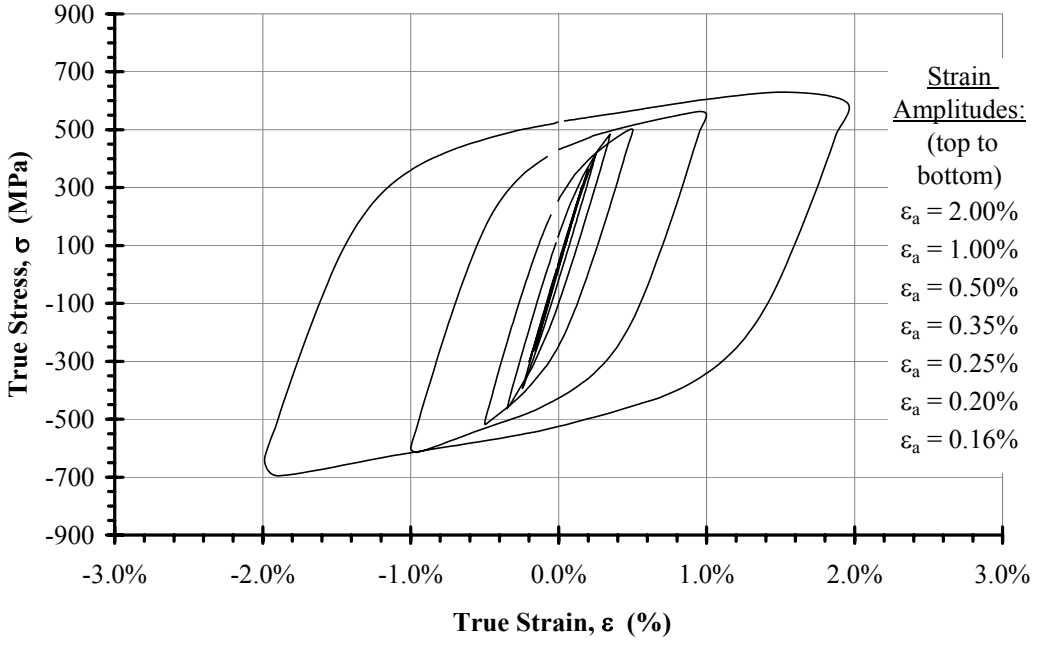

(b)

Figure 2.11: Plots of midlife hysteresis loops for (a) forged steel and (b) cast iron.

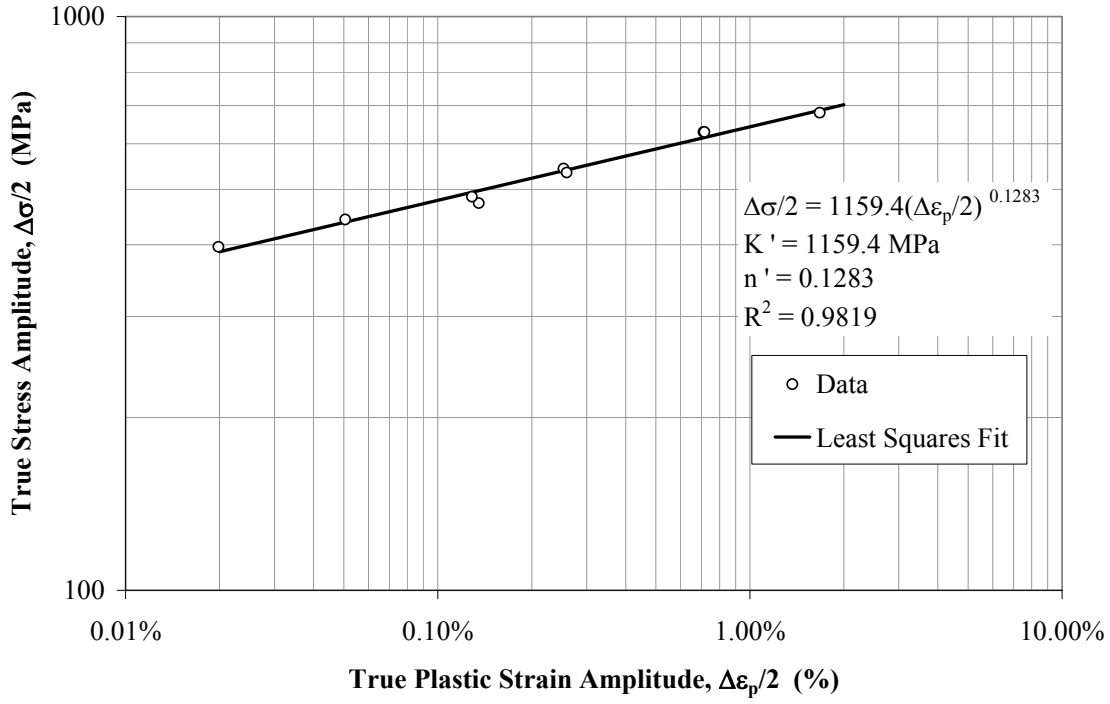

(a)

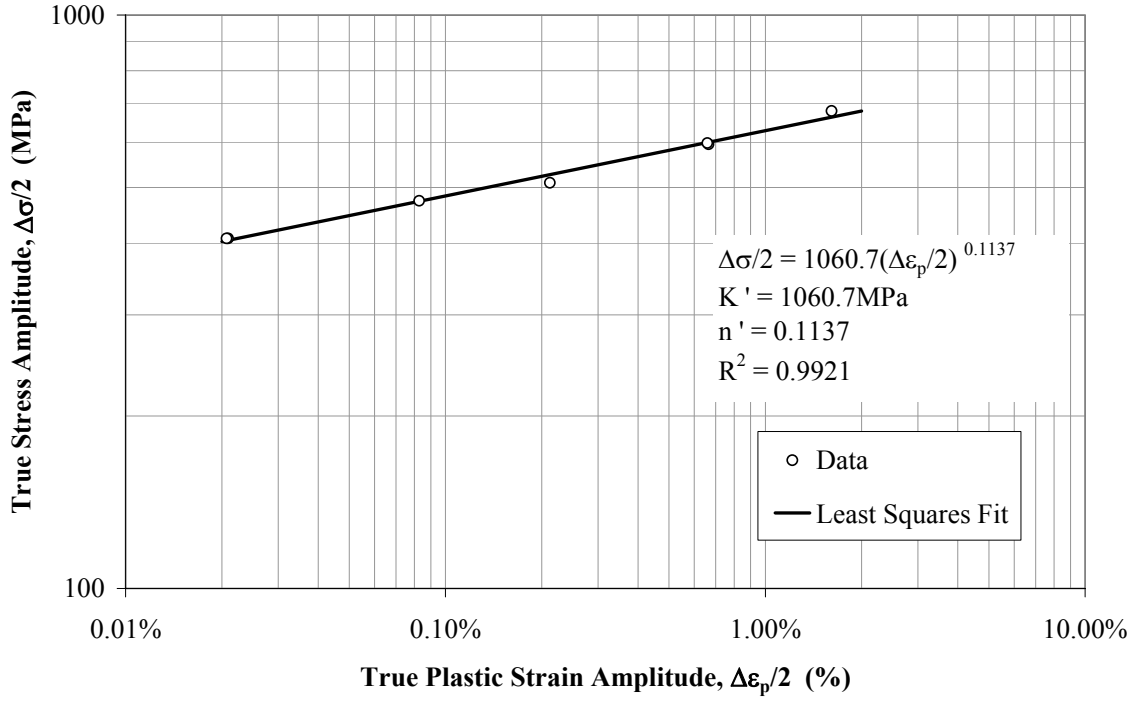

(b)

Figure 2.12: True stress amplitude versus true plastic strain amplitude for (a) forged steel and (b) ductile cast iron.

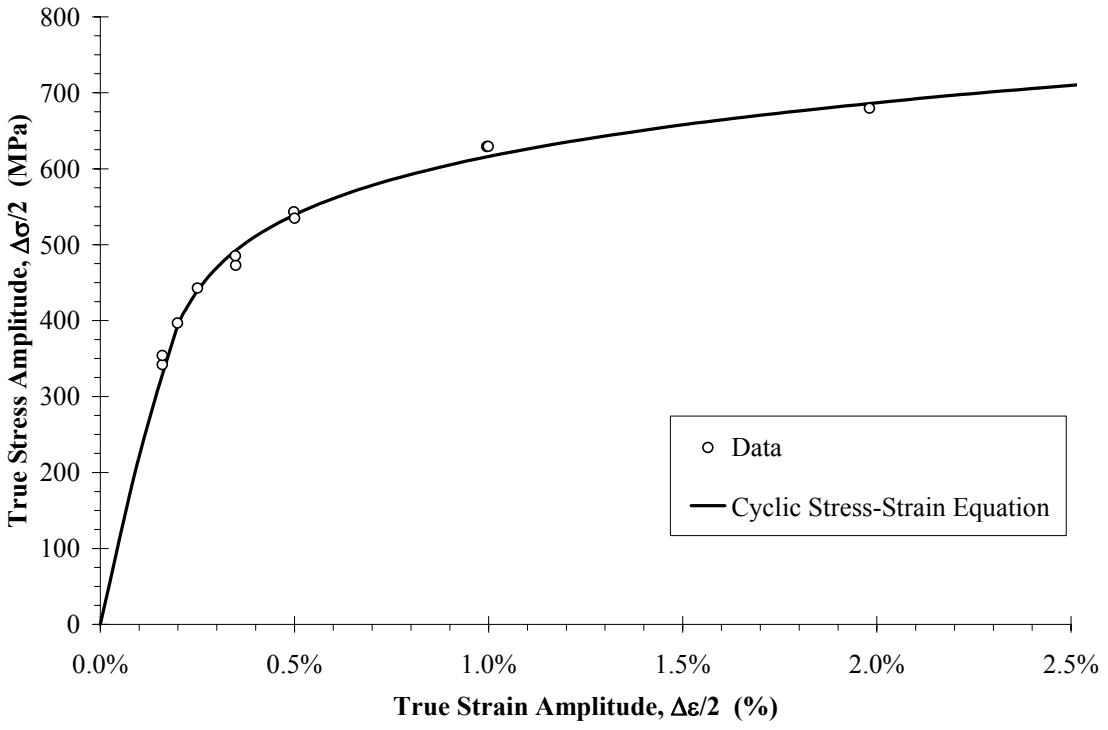

(a)

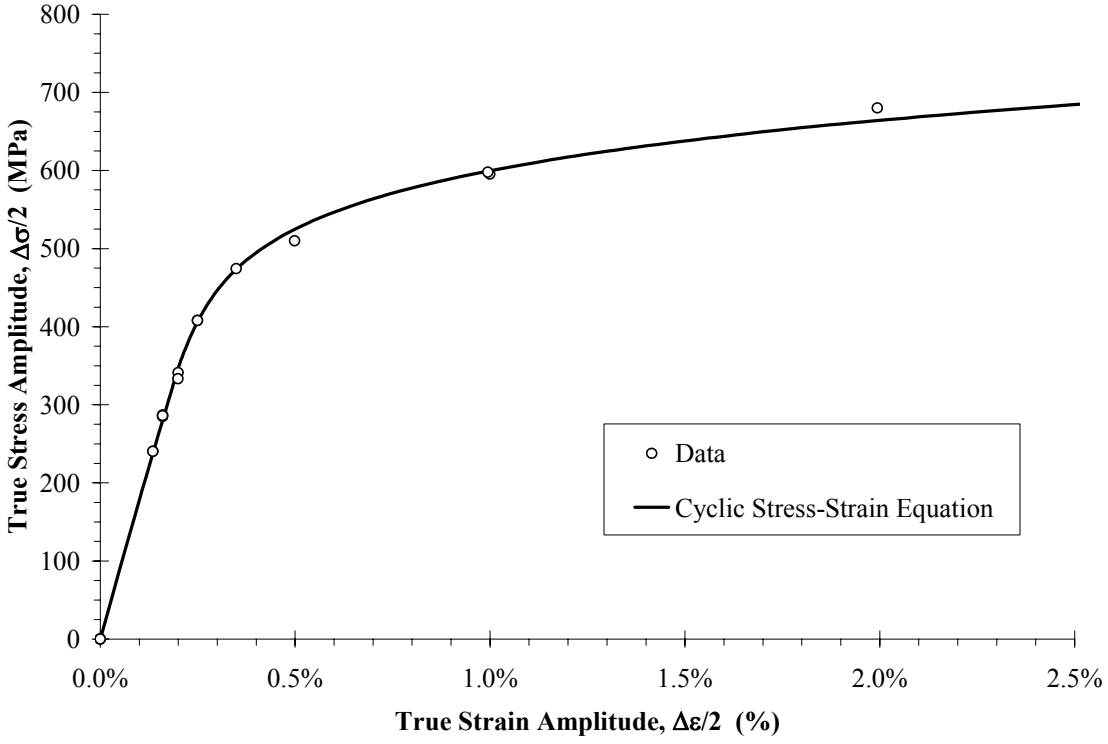

(b)

Figure 2.13: True stress amplitude versus true strain amplitude for (a) forged steel and (b) ductile cast iron.

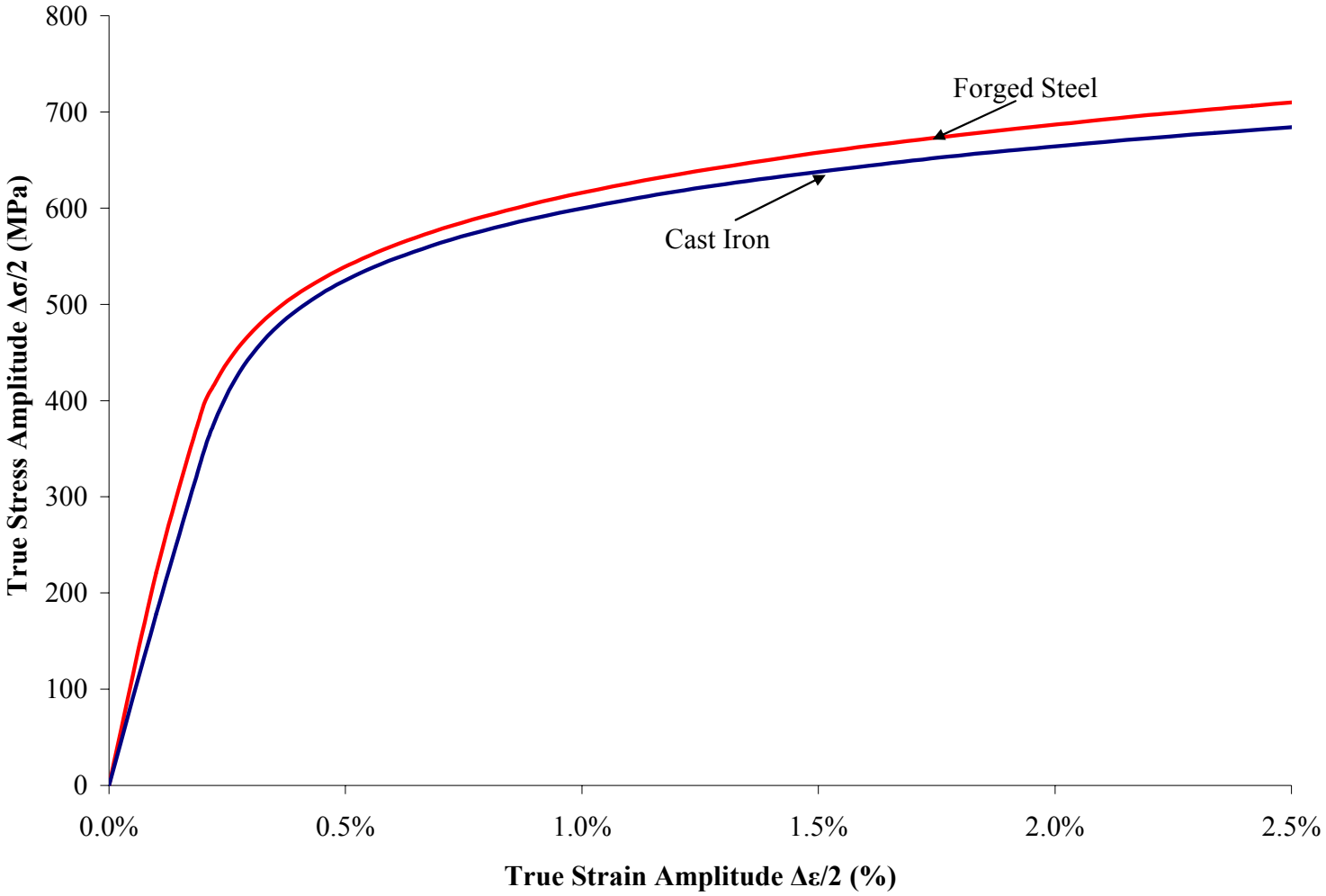

Figure 2.14: Superimposed cyclic stress-strain curves for forged steel and ductile cast iron.

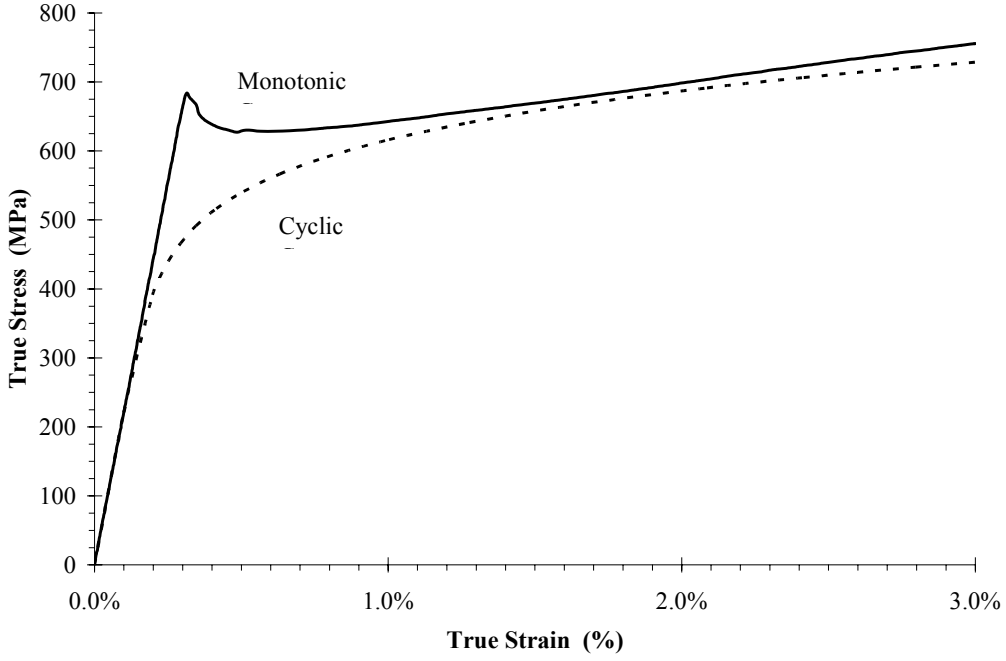

(a)

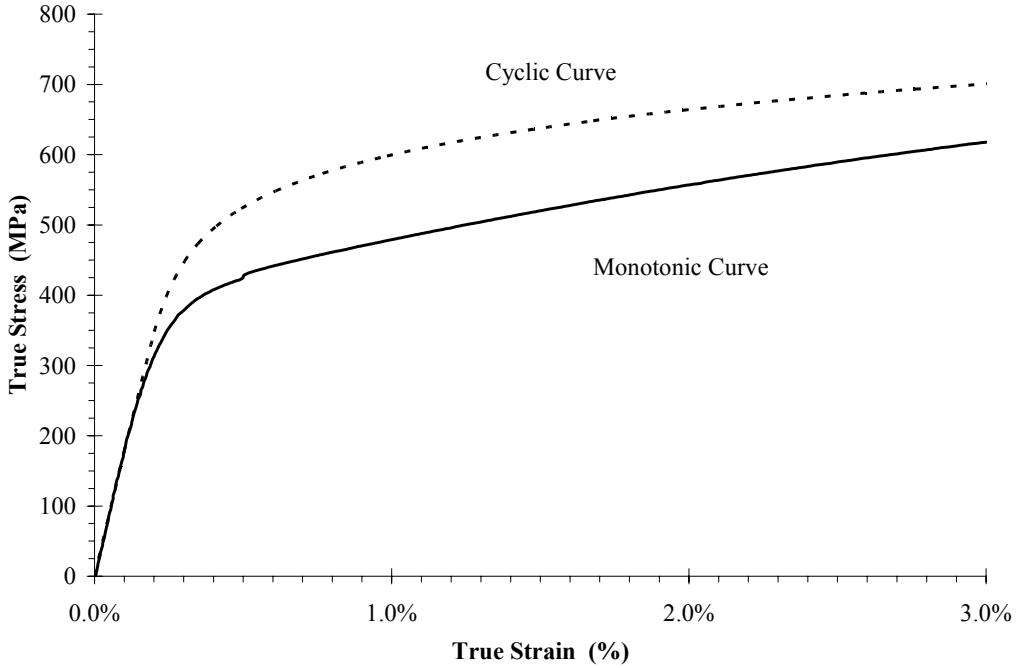

(b)

Figure 2.15: Superimposed plots of monotonic and cyclic true stress versus true strain curves for (a) forged steel and (b) ductile cast iron.

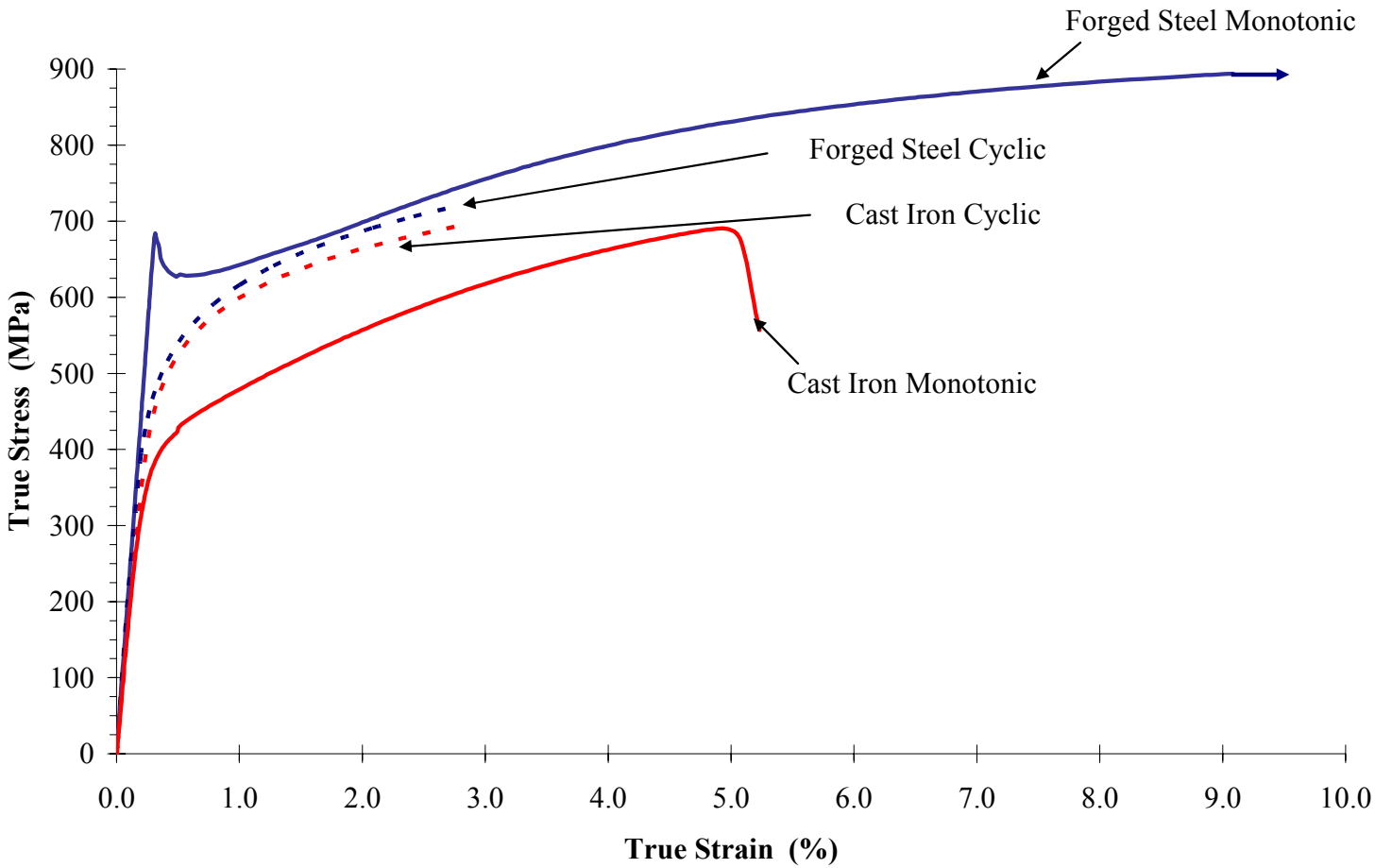

Figure 2.16: Superimposed plots of monotonic and cyclic true stress versus true strain curves for forged steel and ductile cast iron.

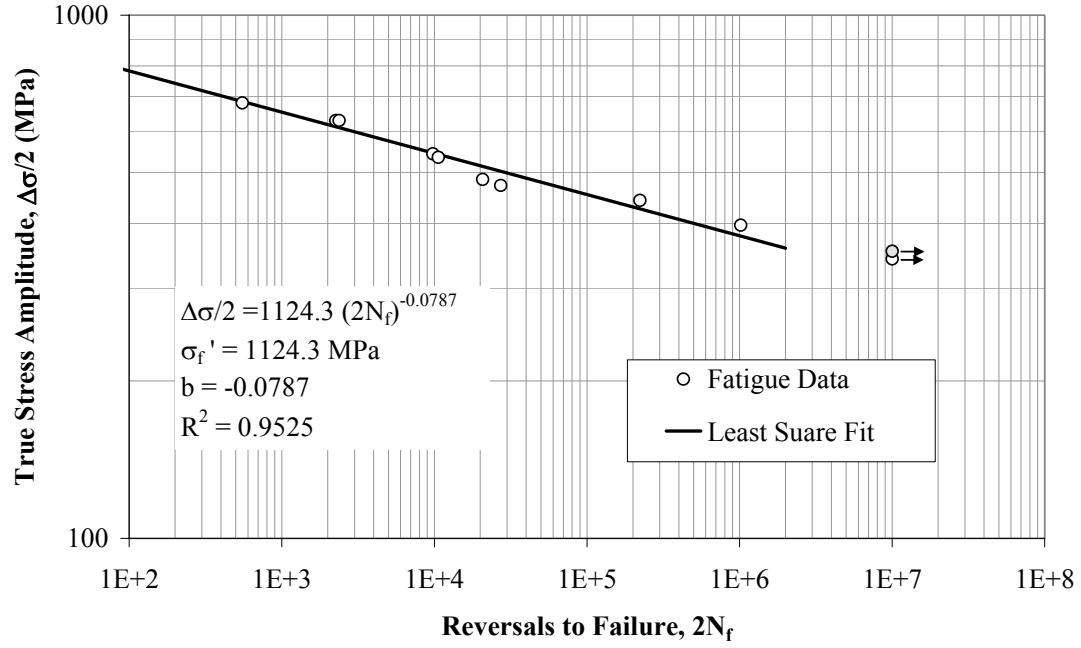

(a)

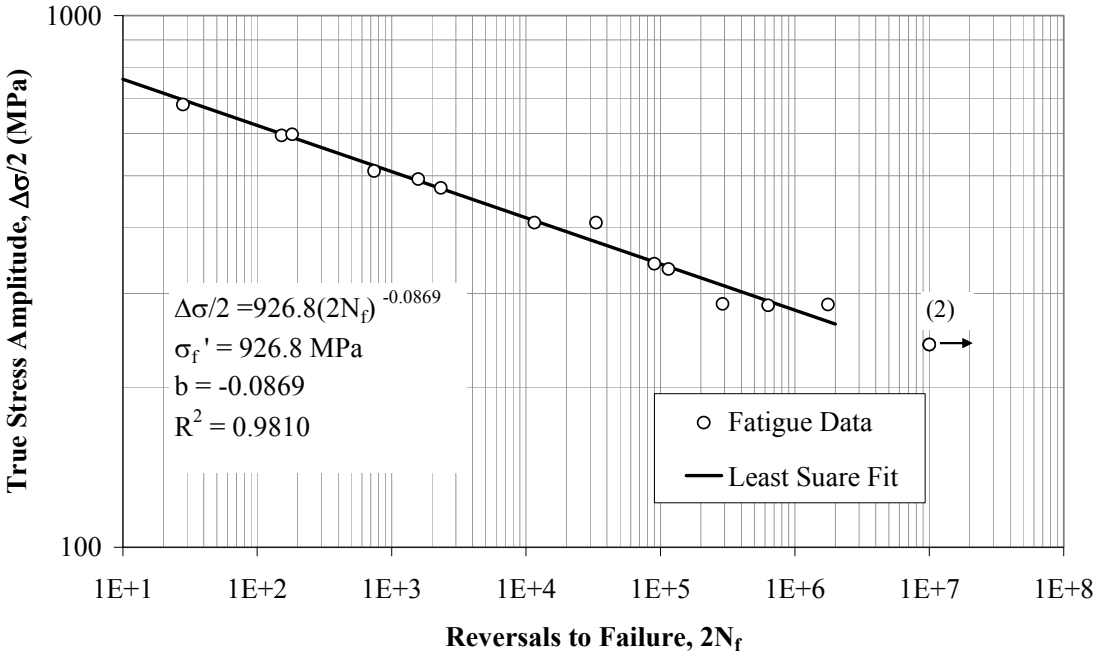

(b)

Figure 2.17: True stress amplitude versus reversals to failure for (a) forged steel and (b) ductile cast iron.

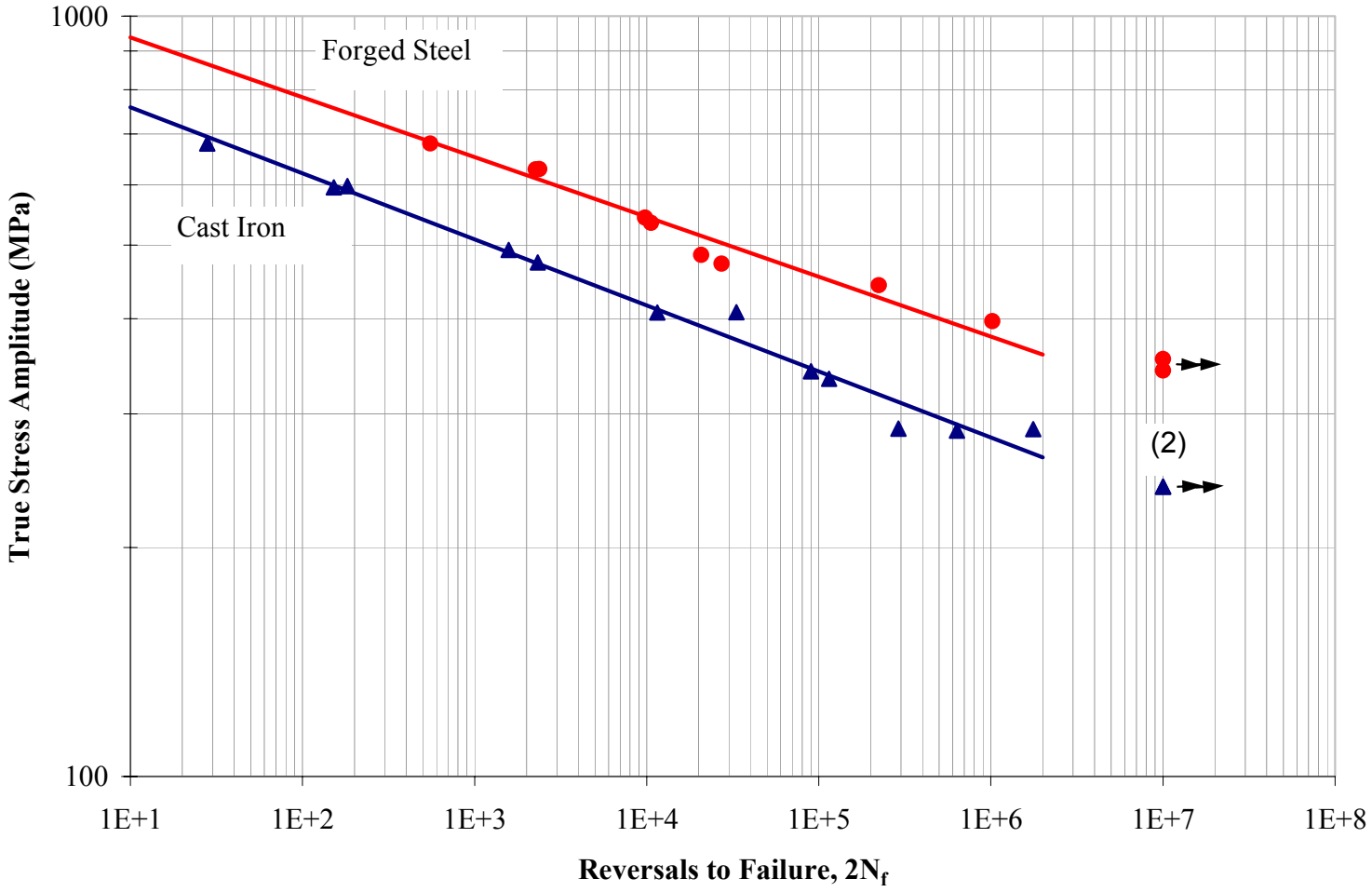

Figure 2.18: Superimposed plots of true stress amplitude versus reversals to failure for forged steel and ductile cast iron.

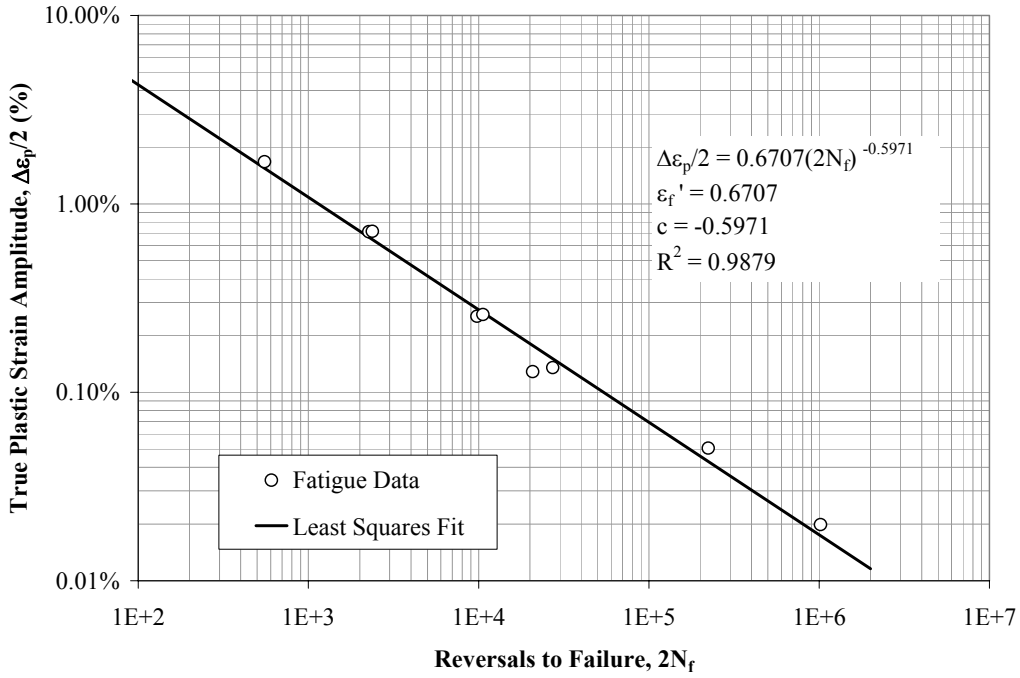

(a)

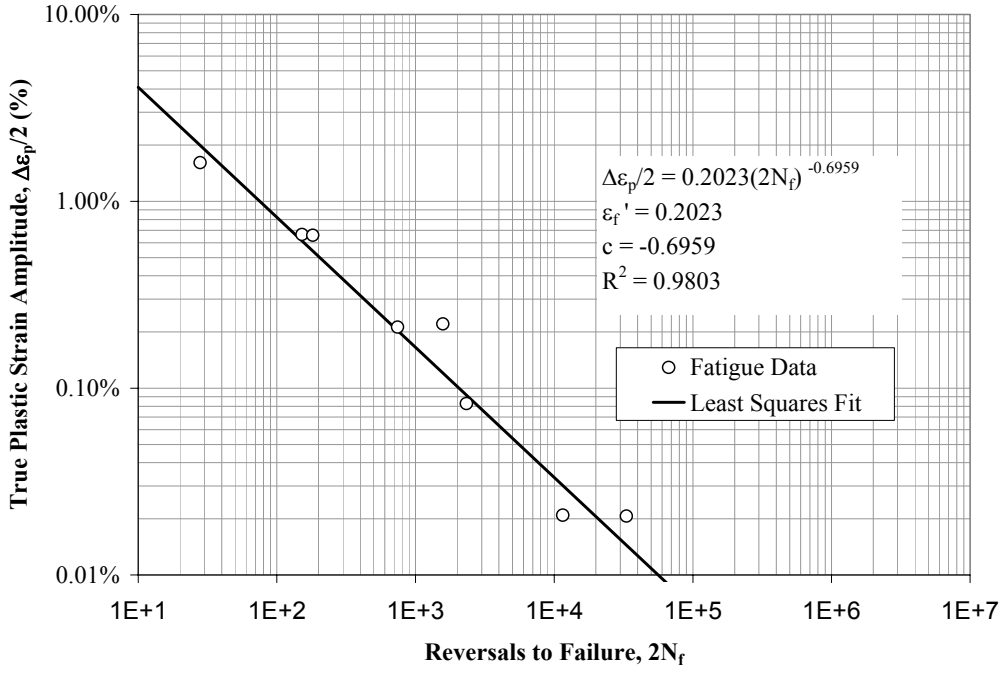

(b)

Figure 2.19: True plastic strain amplitude versus reversals to failure for (a) forged steel and (b) ductile cast iron.

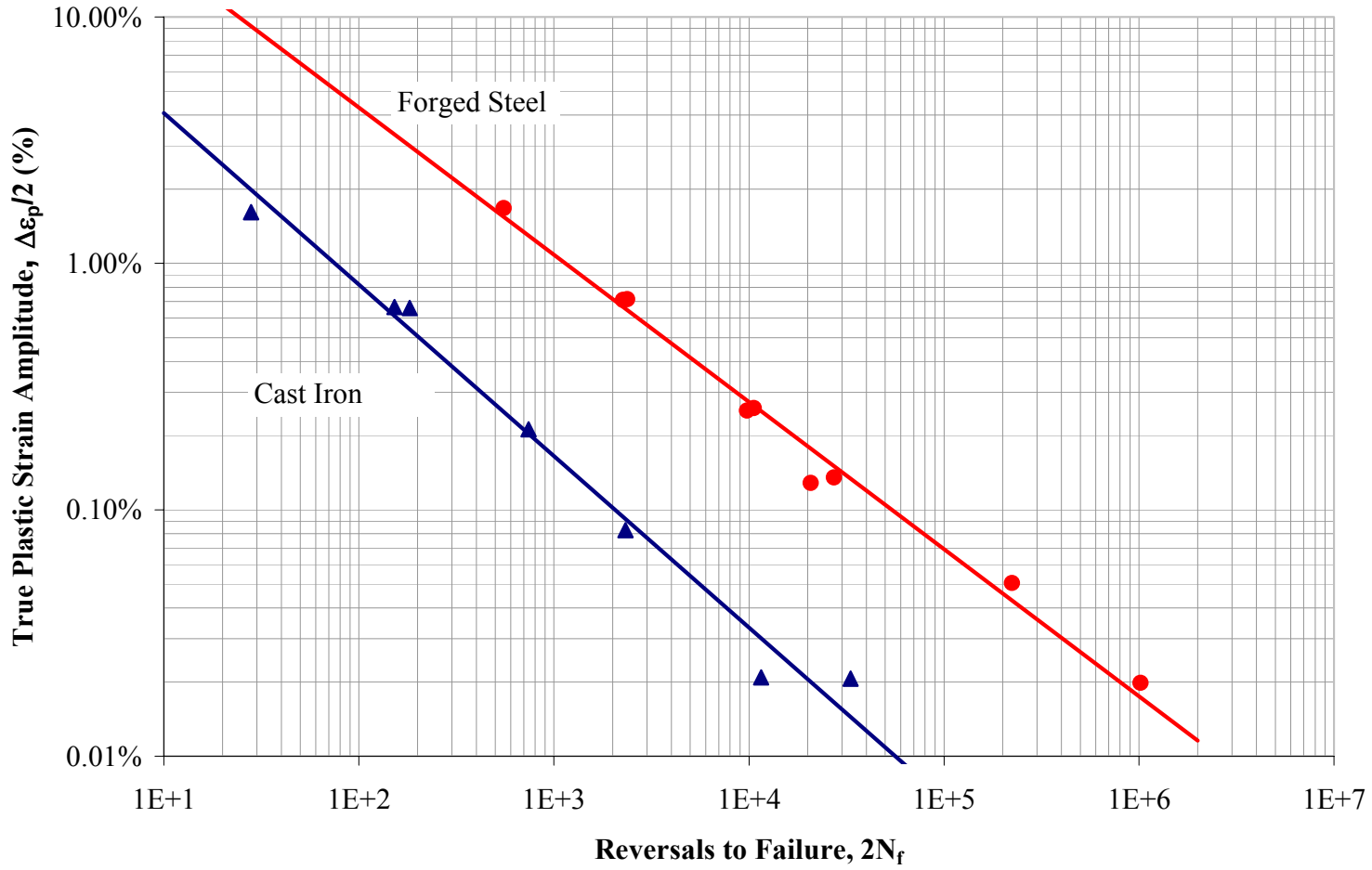

Figure 2.20: Superimposed plots of true plastic strain versus reversals to failure for forged steel and ductile cast iron.

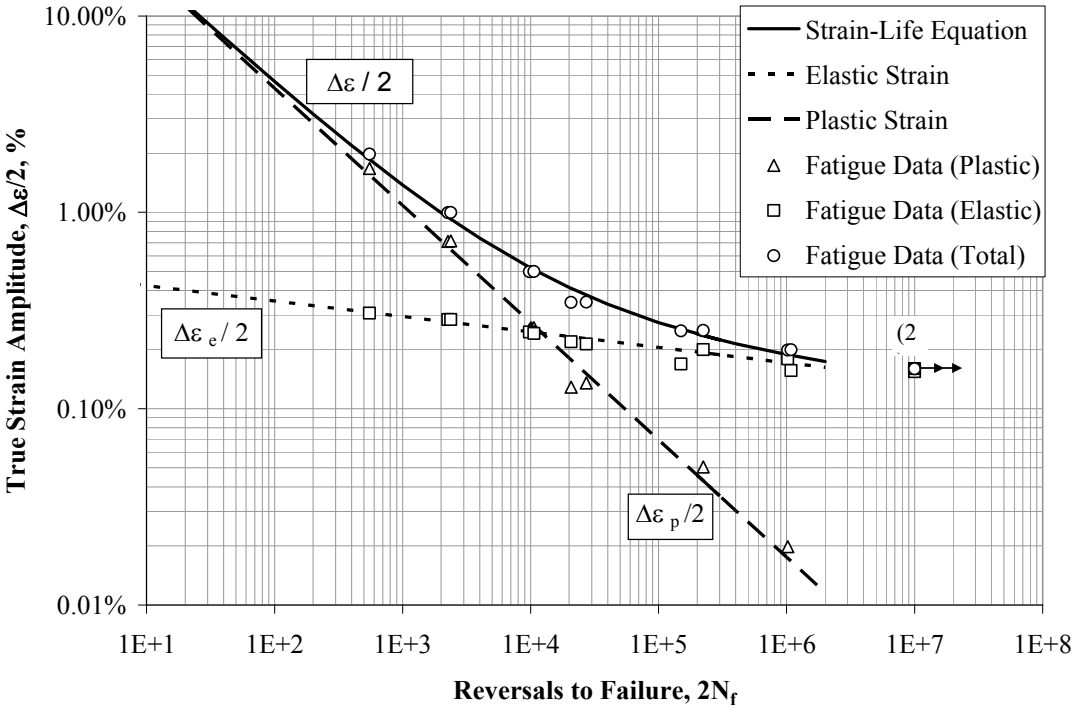

(a)

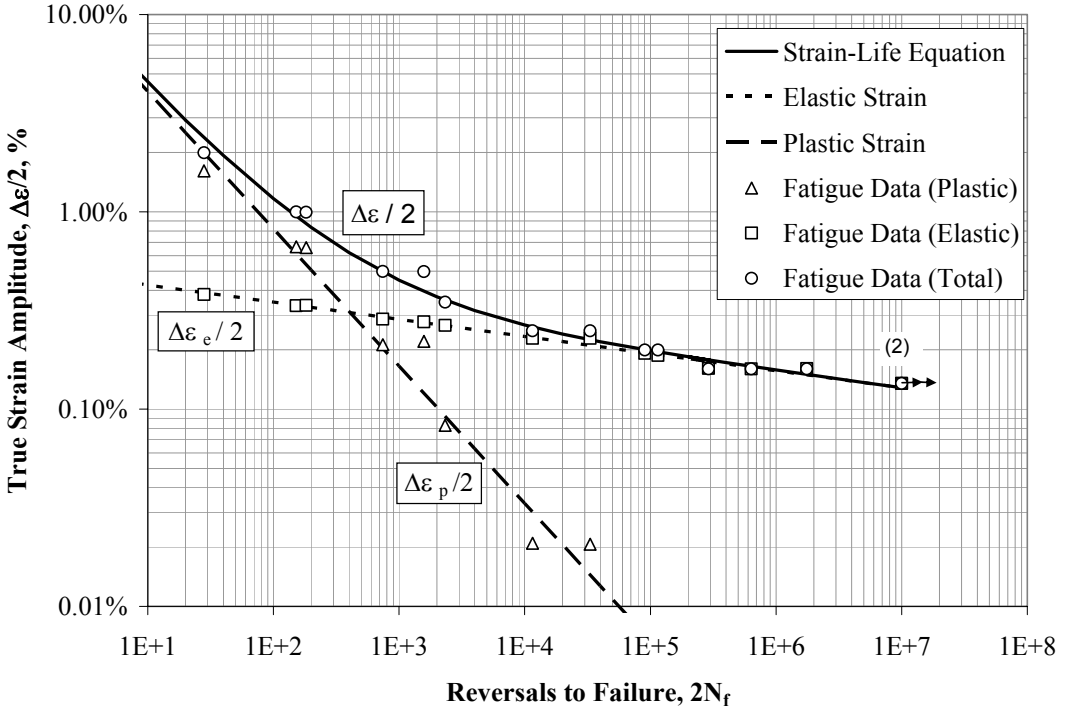

(b)

Figure 2.21: True strain amplitude versus reversals to failure for (a) forged steel and (b) ductile cast

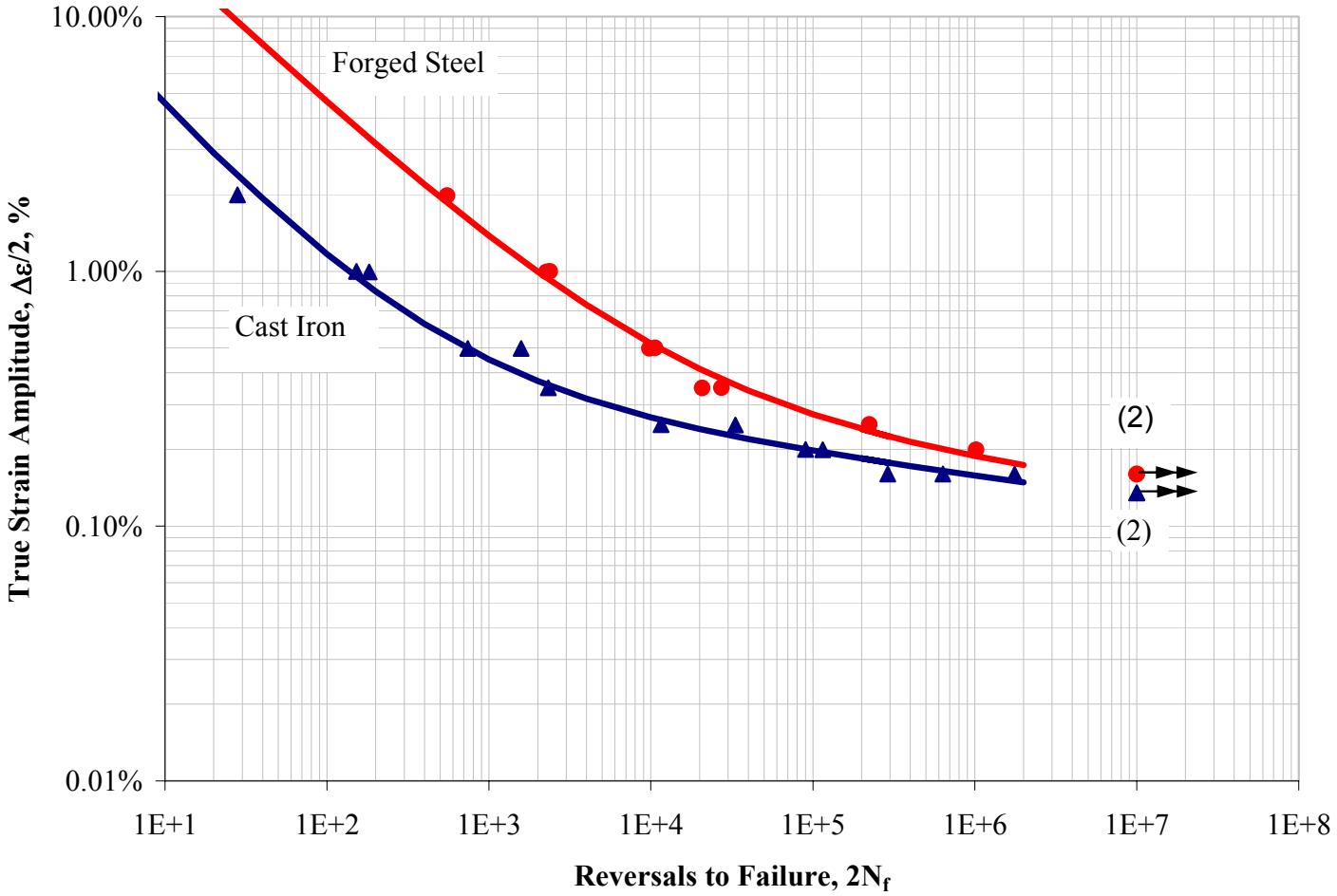

Figure 2.22: True strain amplitude versus reversals to failure for forged steel and ductile cast iron.

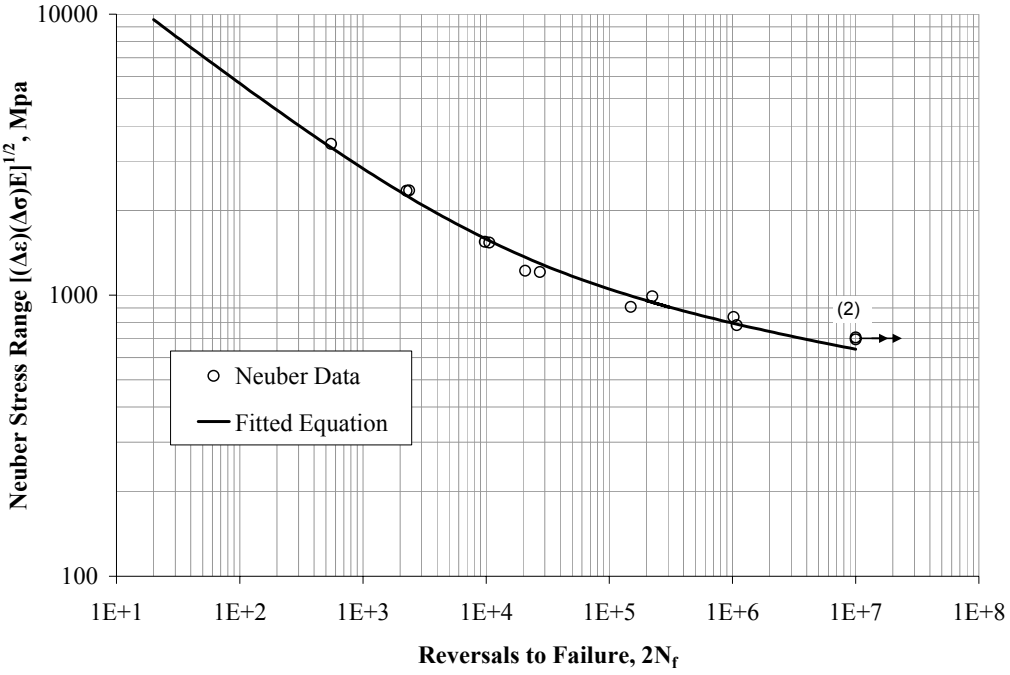

(a)

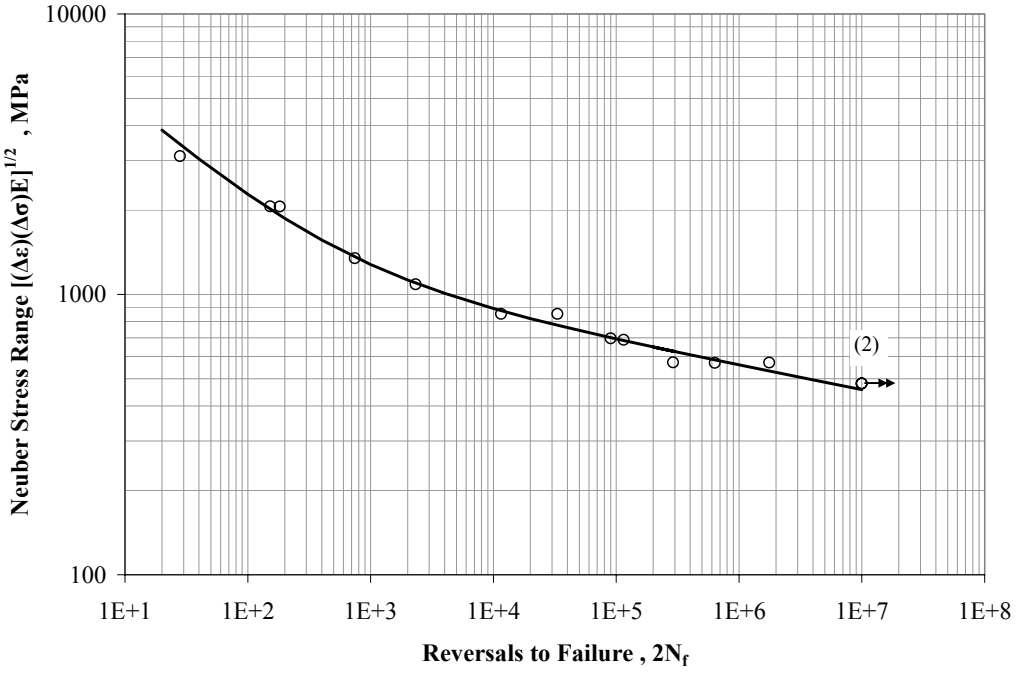

(b)

Figure 2.23: Neuber stress range versus reversals to failure for (a) forged steel and (b) ductile cast iron.

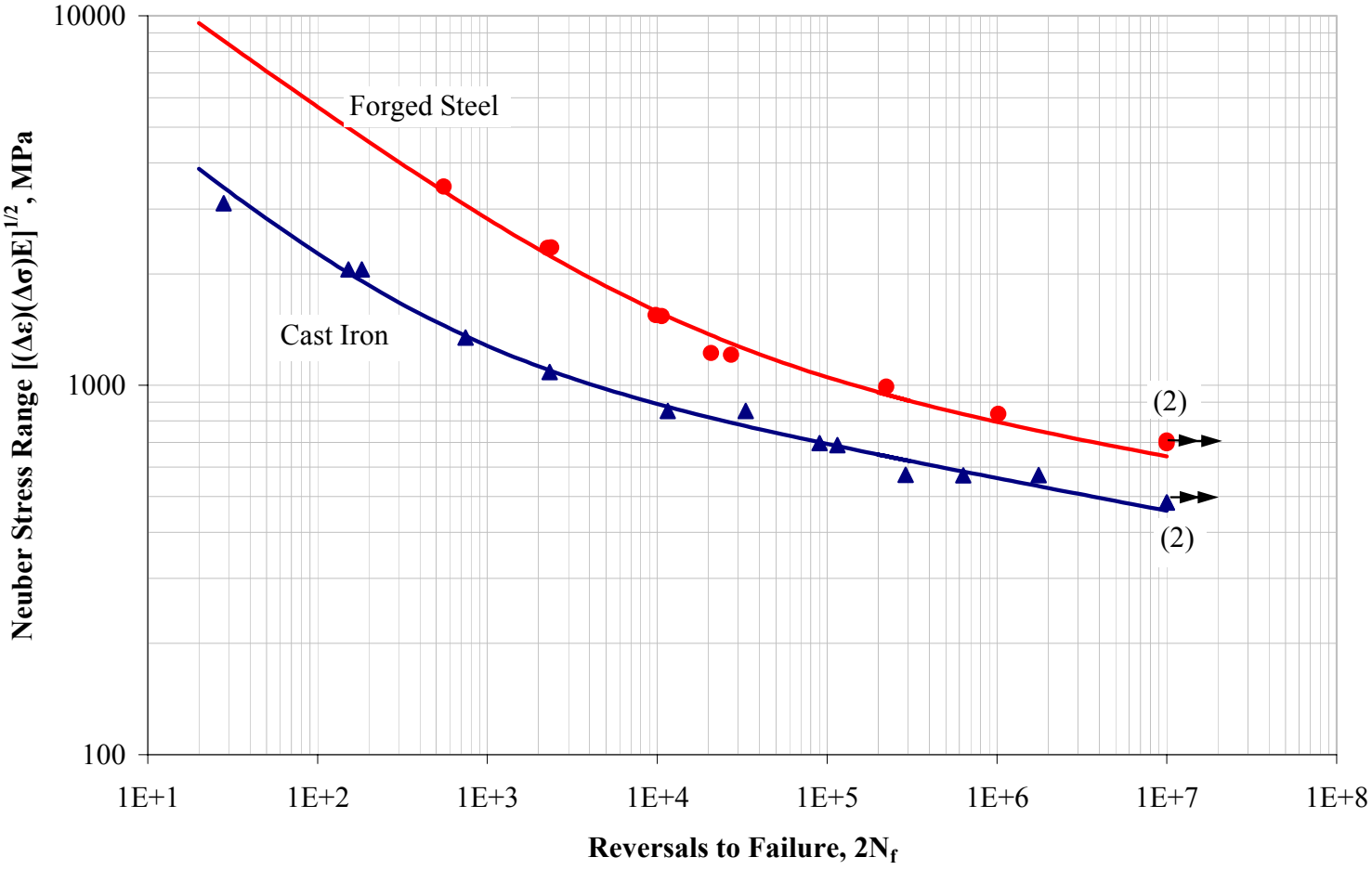

Figure 2.24: Superimposed Neuber stress range versus reversals to failure for forged steel and ductile cast iron.

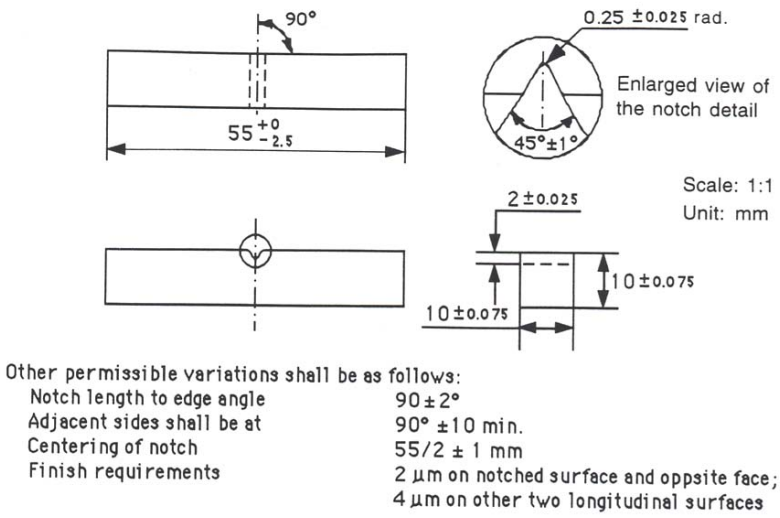

Figure 2.25: Charpy impact specimen geometry.

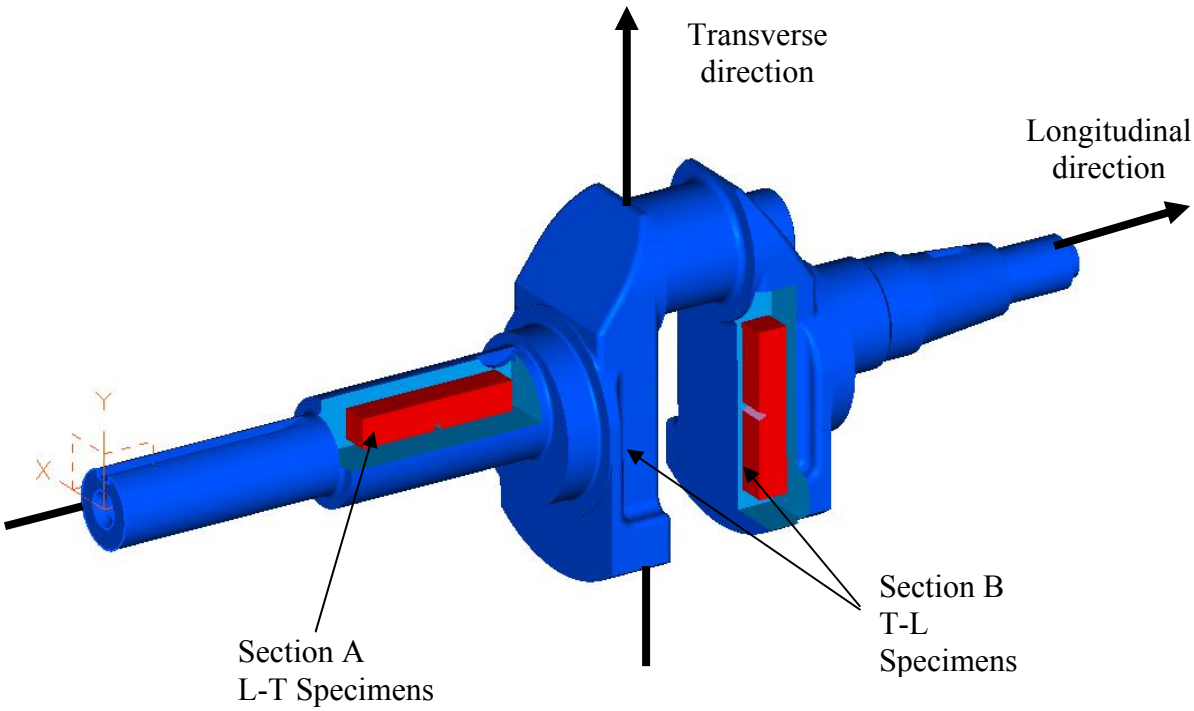

Figure 2.26: Locations on the crankshaft where Charpy v-notch specimens were machined from.

Figure 2.27: Tinius Olsen impact test machine.

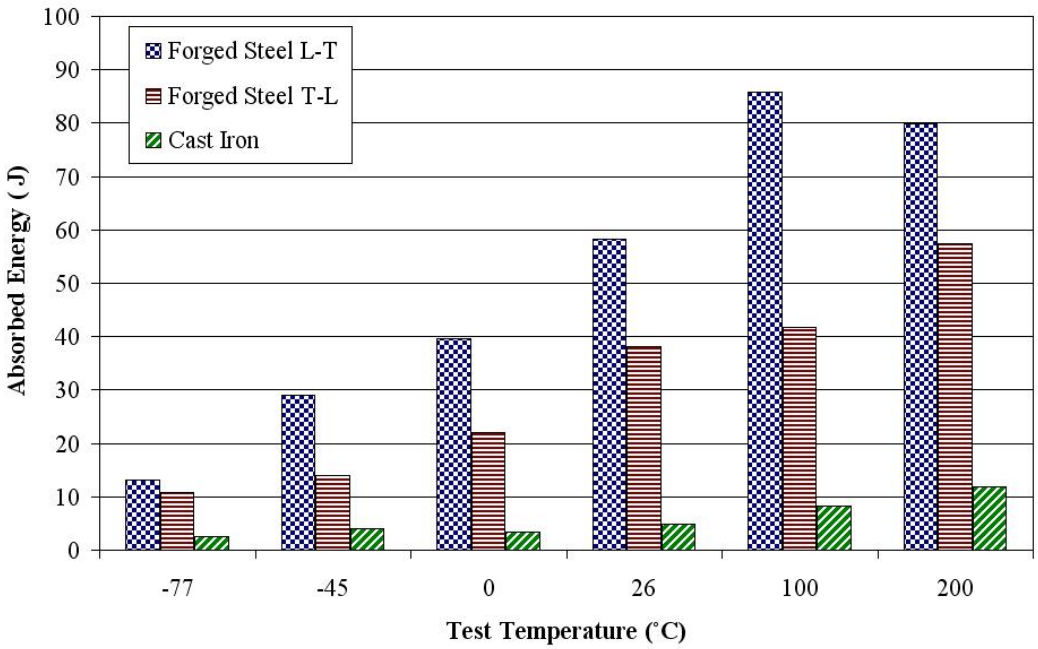

Figure 2.28: Average absorbed energy values at the different test temperatures for forged steel (L-T, T-L) and ductile cast iron.

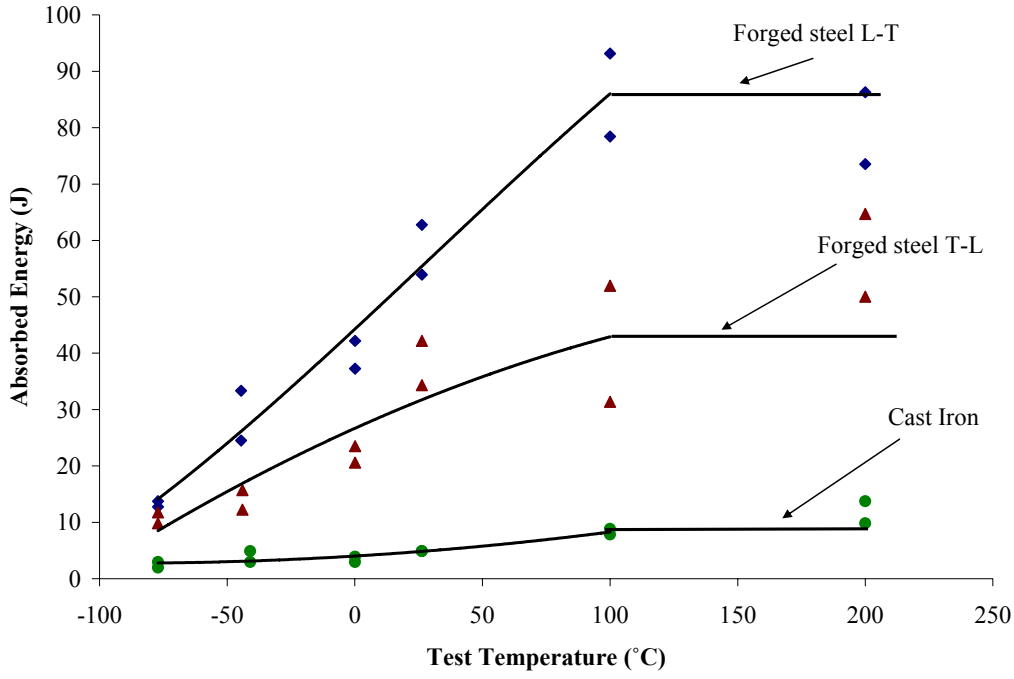

Figure 2.29: Absorbed energy versus test temperature for forged steel (L-T, T-L) and cast iron specimens.

(a)

(b)

(c)

Figure 2.30: Fracture surfaces of (a) forged steel L-T, (b) forged steel T-L, and (c) ductile cast iron specimens in order of increasing temperature from left to right.

CHAPTER 3

COMPONENT TESTING PROCEDURES AND RESULTS

3.1 Test Apparatus and Procedures

3.1.1 Loading conditions and test fixture

In order to compare the fatigue lives of the forged steel and ductile cast iron crankshafts, constant amplitude, load-controlled fatigue tests were performed on the two crankshafts. A crankshaft experiences two types of in service loading, bending and torsion. Previous studies and the dynamic load analysis of the engine showed that the effect of torsion was negligible compared to bending. Since bending was the primary in service loading mechanism, it was used as the loading mechanism for the component fatigue tests. In order to minimize the magnitude of the applied loads necessary to achieve the desired stress levels, cantilever bending was used, rather than three-point bending. While the cantilever bending fixture did minimize the loads required, it did decrease the rigidity of the test fixture. This increased deflection was the limiting factor in the test frequency.

Finite element analysis in conjunction with the dynamic loading analysis of the engine identified the critical location, or highest stresses location, of the crankshafts. For details on identification of the critical location refer to Chapter 4. In order to isolate the critical location in the crankshafts, the crankshaft was tested such that the critical

crankpin fillet had a higher bending moment than the non-critical crankpin fillet. This was accomplished by orienting the crankshaft such that the critical crankpin fillet had a longer moment arm. Figure 3.1 shows the production, as tested forged steel crankshaft with the critical location identified. Figure 3.2 shows the same for the ductile cast iron crankshaft.

The test fixture was designed so there was a vertical support that clamped onto the main bearing section of the crankshaft and the load was applied through a moment arm attached to the nose of the crankshaft. The test fixture was machined from a solid bar of 4" by 3" steel. The vertical support of the test fixture was welded to a ¾" thick plate of steel so that the fixture could be bolted to the machine test bed. A hole was bored into the vertical support that had the same diameter as the main bearing sections of both crankshafts. Identical diameters allowed the test fixture to be used for both crankshafts. The moment arm was machined from the same 4" by 3" bar steel. A hole the precise size of the nose section of the crankshafts was bored into the end of the moment arm for attachment to the crankshaft. Clamping the crankshaft was accomplished with four ½" diameter bolts on both the vertical support and the moment arm. All bolts were tightened with a dial gage torque wrench to the same torque prior to testing to ensure an evenly distributed clamping force. A schematic of the test fixture and set-up is shown in Figure 3.3, where the forged steel crankshaft is shown only as an example. The test set-up for the forged steel crankshaft is shown in Figure 3.4 and for the cast iron crankshaft in Figure 3.5.

A rod end bearing was used to apply the load to minimize any misalignment in the test set-up. As mentioned previously, bending was the only loading desired for the

test. However, often times in applying a bending load, an axial force is also present. In order to minimize this unwanted axial force, the motion between the moment arm and the loading applicator was not constrained horizontally. Slots were machined into the loading end of the moment arm. A rod fitted with needle roller bearings was attached to the rod end bearing. The roller bearings were necessary to minimize the frictional force that would be present if the rod was allowed to slide in the moment arm slots, rather than roll. Figure 3.6 shows the rod end bearing and slotted end of the moment arm with the roller bearings. To verify that there was no significant axial force present, a crankshaft was fitted with strain gages and loads were applied. The results were compared to those obtained from FEA and analytical (i.e. Mc/I) calculations. The results showed that there was no axial force present. The verification of the test fixture is presented in Chapter 4 as part of the stress analysis.

3.1.2 Test procedures

The bending fatigue tests were performed at room temperature, which was monitored with a digital thermometer and recorded for each test along with the humidity which was measured using a precision hydrometer. Tests were conducted using a sinusoidal waveform and constant amplitude load control. Test frequencies between 1.4 and 3 Hz were used for all tests, with the lower frequency used for the higher load levels and the higher frequency used for lower load levels. The stress ratio, or R-ratio, is the ratio of maximum stress to minimum stress. The dynamic load analysis that was performed resulted in load versus crank angle data for both crankshafts as shown by Montazersadgh and Fatemi [2007]. As the crankshaft rotates through the engine cycles,

the loading, which is primarily bending, changes. The loads are also dependent on the rpm of the engine. The dynamic analysis showed that the average ratio of minimum load to maximum load was approximately equal to -0.2 for both crankshafts [Montazersadgh, 2007]. Therefore, an applied R ratio of -0.2 was used for all tests.

Four load levels were used for both crankshafts, with three tests at each load level to assess variability and scatter. The load levels resulted in lives between 10^3 and 4 x 10^6 cycles. The parameters for each test, along with the results are summarized in Table 3.1. In the table, a positive load value is applied upwards, causing compressive stress on the top of the crankshaft and tensile stress at the bottom where the critical section was located.

The forged steel and ductile iron crankshafts were designed to operate in very similar engines. The crankshafts were of similar size and similar mass, 3.9 kg for the forged steel and 3.7 kg for the cast iron crankshaft. Due to their similar size and application, both crankshafts would experience similar in service loading. Therefore, both crankshafts were tested at the same bending moment levels.

3.2 Failure Criterion

Initially the crankshafts were tested until the point which they could no longer maintain the applied cyclic load. At this point the displacement versus cycles curve reached an asymptotic value and the crankshaft was considered to be fractured. After several tests were completed, it was found that the crack growth life of the component was one-half to two-thirds the life of the component. Failure of the crankshaft could, therefore, not be the point when the crankshaft fractured. The crankshaft, being a

rotating engine component, could not function in a state of increased deflection. Crack initiation was used as a failure criterion for the crankshafts. In order to use crack initiation as a failure criterion, however, the point at which the crack initiated must be clearly identifiable. Each test was stopped at intervals corresponding to ten to twenty percent of the expected life of the component, at which point the crankshaft was inspected for the presence of a crack. If no crack was present the test was continued. If a crack was present, the crack was measured and recorded. A light white coating of paint was applied to the critical fillet area in order to help detect a crack, as shown in Figure 3.7. The physical crack length was monitored using putty that was molded to the cracked area and then removed leaving a raised imprint of the crack, as shown in Figure 3.8. The crack length was then measured from the putty using a digital caliper. As the crack grew, the test was stopped at intervals corresponding to ten to twenty percent of the expected life and the crack length was measured and recorded. It was found that by the time the crack was detected it was on the order of 6 mm or longer. Crack initiation, for life prediction purposes, is usually defined as a crack on the order of 1 mm or 2 mm. Therefore, the point at which a crack was visually detected was not a desired definition of initiation point, since the crack was already long at this point.

When a crack was present and as it grew, there was, as expected, a decrease in stiffness, or in other words an increase in deflection. Using the measured crack length data, along with the recorded displacement amplitude data for each test, a correlation between the change in displacement amplitude and the crack length was developed for both forged steel and ductile cast iron crankshafts. For both materials, the change in displacement amplitude versus measured crack length was plotted. The base for

determining the change in displacement amplitude for each test was taken as the point where the displacement amplitude was stable, as indicated by a horizontal line in Figure 3.9.

The change in displacement amplitude versus measured crack length plot is shown in Figure 3.10 for the forged steel crankshaft and in Figure 3.11 for the cast iron crankshaft. In Figures 3.10 and 3.11 each test is shown in a different color. The data are shown superimposed in Figure 3.12.

Measured crack length versus cycle data for the forged steel crankshafts are shown in Figure 3.13 and for the cast iron crankshafts in Figure 3.14. For a given change in displacement amplitude the size of a crack can be determined from Figures 3.10 and 3.11. Then from Figures 3.13 and 3.14, knowing the size of the crack, the number of cycles can be determined. This method allows for the change in displacement amplitude versus crack length data to be extrapolated to find the change in displacement amplitude corresponding to a given length. Then the cycles where the crack initiation (i.e. a crack on the order of 2 mm) occurred can be determined from the data.

Using the fitted equation for each crankshaft, the change in displacement amplitude was extrapolated for a crack length of 2 mm. From the relationship between the change in displacement amplitude and crack length, a crack length of 2 mm would result in a very small change in displacement amplitude. The change in displacement amplitude for a 2 mm crack was on the order of a micrometer, such that the position transducer of the test frame could not accurately detect this change. However, when there was any recorded increase in displacement amplitude the relationship suggests that there was a crack present. The data from each test was analyzed and the cycle at which

there was a measurable increase in displacement amplitude was determined to be the crack initiation point. An expanded scale plot of the displacement amplitude versus cycles plot for the forged steel crankshafts is shown in Figure 3.15 and in Figure 3.16 for the ductile cast iron crankshafts. These figures show that the displacement amplitude is relatively steady for a period in the test after the full load is applied and prior to the formation of a crack. At the point where a crack develops, an increase in the displacement amplitude is observed.

The predicted crack lengths obtained from the change in displacement amplitude versus crack length plots shown in Figures 3.10 and 3.11 were compared with the measured crack lengths. The predicted crack length versus measured crack length is shown in Figure 3.17 for the forged steel crankshafts and in Figure 3.18 for the ductile cast iron crankshafts. Scatter bands at factors of plus and minus two are also plotted. The figures show that the predicted crack lengths are within a factor of two of the measured crack lengths for both the forged steel and ductile cast iron crankshafts.

A change in displacement amplitude of 5% was also used as a failure criterion for comparison purposes. A 5% change was much more apparent than the small change in displacement amplitude that was used for determining crack initiation. From the displacement amplitude versus cycles plot shown in Figure 3.9, it can be seen that the displacement amplitude reached a constant value while no crack was present and then began to increase as the crack grew. The figures also show that for some of the short life tests the displacement amplitude curves reached an asymptotic value; this was determined to be the point of fracture. This fracture point was only reached for several tests due to the significant amount of time it took to grow the crack to that length.

3.3 Results and Comparisons

The moment amplitude versus cycles to failure for both forged steel and cast iron crankshafts using the crack initiation criterion is shown in Figure 3.19. The figure shows that for a given applied moment, the life of the forged steel crankshaft is approximately six times longer than the life of the ductile cast iron crankshaft. The moment amplitude versus cycles to failure for the forged steel and ductile cast iron crankshafts using the 5% change in displacement amplitude criterion is shown in Figure 3.20. Using the 5% change in displacement criterion, the difference in life is less at shorter lives when compared to the crack initiation criterion, but the difference is greater at long lives. At long life, there is approximately an order of magnitude difference between the life of the forged steel and cast iron crankshafts. The divergence of the curves at longer lives suggests that the forged steel crankshaft had a slower crack growth rate than the ductile cast iron crankshaft.

A fatigue limit is important for a long life component; if the loads or stresses are below the fatigue limit, failure will likely not occur. When tested at a moment amplitude of 431 N-m, the forged steel crankshaft had a life greater than 4×10^6 cycles and was considered a run-out. Two forged steel crankshafts were tested at this level with no failures. The cast iron crankshafts at this load level failed between 75,200 and 82,200 cycles. The issue of fatigue limit is important when comparing the fatigue lives for a long life component such as a crankshaft. The cast iron crankshaft has fatigue strength of 316 N-m at 10^6 cycles based on either the crack initiation or 5% increase in displacement amplitude criteria. This suggests a 36% higher fatigue strength for the forged steel

crankshaft as compared to the cast iron crankshaft. The fatigue strength at 10^6 cycles for the two materials obtained from specimen tests in Chapter 2 show the fatigue strength of the cast iron to be 263 MPa and for the forged steel to be 359 MPa. This also suggests a 36% higher fatigue strength for the forged steel as compared to the cast iron. Therefore, the differences in fatigue strengths of the cast iron and forged steel for the components and for the materials are the same. One contributing factor to the same ratio is that the geometries of the two crankshafts were very similar, therefore the primary difference in the two crankshafts for component testing purposes was the difference in material properties.

The literature suggests that fatigue behavior of cast iron is similar to steel and therefore cast iron should also have a fatigue limit at about 10^6 cycles [Juvinall and Marshek, 1991]. The existence of a fatigue limit for the cast iron crankshaft could not be verified with the limited number of components available for testing and the length of time required for high cycle testing.

As shown in Figures 3.19 and 3.20, the scatter in the component fatigue life test data is small for both the crack initiation and 5% change in displacement criteria (within a factor of about 2 for the forged steel crankshaft and a factor of about 3 for the cast iron crankshaft). The scatter was similar to what was seen in the specimen fatigue tests. For both the specimen tests and the component tests, the scatter for the cast iron was somewhat better than expected. Porosity that is typically present in castings can contribute to increased scatter due to its random distribution and size. Cracks can develop from the porosity and therefore their randomness in size and distribution can influence the fatigue life.

Based on the specimen tests conducted on the cast iron specimens, the cast iron exhibits a cyclically hardening behavior as shown in Chapter 2. The component tests on the cast iron crankshafts also showed a cyclically hardening behavior. The hardening behavior does not, however, directly correlate to the hardening behavior observed in the specimen tests. In the specimen tests the entire gage section experiences the cyclically hardening. In the component tests the stresses in the crankshaft are completely elastic with the exception of the fillets where there is plastic deformation. Therefore, the entire crankshaft is not cyclically hardening, but rather there is local hardening in the highly stressed fillet locations. Since this hardening is localized, the amount of hardening is not as large as would be seen in specimen testing. This hardening behavior is shown in Figures 3.21 and 3.22. The figure shows that the displacement amplitude for the cast iron crankshafts decreases at the beginning of the test before reaching a stable value. The forged steel crankshafts showed neither a cyclically hardening nor softening behavior, as expected from the specimen tests.

The ultimate cause of failure for each crankshaft was a crack that developed and grew in the critical location (crankpin fillet). Therefore all crankshafts that failed, had the same failure location. On one forged steel and several cast iron crankshafts a secondary crank grew in the crankpin fillet opposite to the critical crankpin fillet. These cracks developed after the cracks at the critical location and were not considered the cause of failure. The crankshafts where these secondary cracks developed are indicated in Table 3.1.

A typical fatigue fracture of the forged steel crankshaft is shown in Figures 3.23 and Figure 3.24. A typical fatigue fracture for the cast iron crankshaft is shown in

Figures 3.25 and 3.26. The figures show that the fracture surface is smoother for the forged steel when compared to the cast iron. The figures also show that the crack grew through the circular cross section for the cast iron crankshaft, but not for the forged steel crankshaft. The crack in the forged steel crankshaft grew approximately half way through the circular cross section and then veered off at approximately a 45 degree angle which is attributed to the geometry of the component. The component was no longer the weakest through the circular cross section once the crack grew long.

The cross section picture for the cast iron crankshaft shows the eccentricity of the center hole in the crankpin. This eccentricity increased the amount of material in the highest stressed location of section, at the bottom of Figure 3.25. The eccentricity of the oil bore was accounted for in the finite element model and also the analytical stress calculations presented in Chapter 4.

Table 3.1: Test parameters and results for the forged steel and ductile cast iron crankshaft fatigue tests.

Crank ID	Freq (Hz)	R-Ratio	M_a (N-m)	P_{max} (kN)	P_{min} (kN)	P_a (kN)	P_m (kN)	Observed Crack Length (mm)	N, Crack Observed	N_f, Crack Initiation from Disp. Data Extrapolation	N_f, 5% Change in Disp. Amp.	Failure Location
Forged Steel Crankshaft												
FS-2	1.4	-0.2	630	2.67	-0.53	1.60	-1.07	44.96	98,198	29,248	45,568	1
FS-3	1.4	-0.2	630	2.67	-0.53	1.60	-1.07	51.82	120,492	45,302	69,670	1
FS-4	1.4	-0.2	630	2.67	-0.53	1.60	-1.07	--	--	58,236	90,853	1
FS-5	2.5	-0.2	517	2.18	-0.44	1.31	-0.87	10.52	165,000	145,000	234,289	1
FS-6	2.5	-0.2	517	2.18	-0.44	1.31	-0.87	11.71	120,000	98,741	213,885	1
FS-7	2.5	-0.2	517	2.18	-0.44	1.31	-0.87	--	--	204,174	396,011	1 & 2
FS-9	3	-0.2	431	1.82	-0.36	1.09	-0.73	None	>2,090,000 Runout			No crack
FS-10	3	-0.2	431	1.82	-0.36	1.09	-0.73	None	>3,980,000 Runout			No crack
FS-8	3	-0.2	350	1.48	-0.30	0.89	-0.59	None	>3,240,000 Runout			No crack
Cast Iron Crankshaft												
CI-2	1.4	-0.2	630	2.67	-0.53	1.60	-1.07	11.43	11,504	7,132	17,353	1
CI-3	1.4	-0.2	630	2.67	-0.53	1.60	-1.07	5.08	11,692	9,256	17,380	1
CI-4	1.4	-0.2	630	2.67	-0.53	1.60	-1.07	3.175	8,021	8,021	20,957	1
CI-5	2	-0.2	517	2.18	-0.44	1.31	-0.87	8.51	31,464	25,512	47,513	1 & 2
CI-6	2	-0.2	517	2.18	-0.44	1.31	-0.87	8.81	34,898	24,096	52,790	1 & 2
CI-7	2	-0.2	517	2.18	-0.44	1.31	-0.87	12.55	42,750	37,380	54,966	1 & 2
CI-1	2.5	-0.2	431	1.82	-0.36	1.09	-0.73	7.62	113,043	75,200	132,877	1
CI-9	2.5	-0.2	431	1.82	-0.36	1.09	-0.73	13.60	90,175	78,367	121,866	1
CI-10	2.5	-0.2	431	1.82	-0.36	1.09	-0.73	37.06	--	82,200	143,259	1 & 2
CI-8	2.5	-0.2	350	1.48	-0.30	0.89	-0.59	19.79	985,496	920,783	1,005,665	1 & 2
CI-11	2.5	-0.2	350	1.48	-0.3	0.8896	-0.59	32.72	--	301,774	370,216	1 & 2

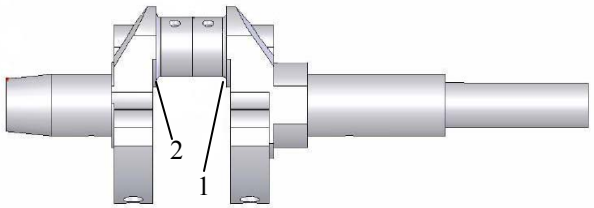

Figure 3.1: Forged steel crankshaft in its final machined condition.

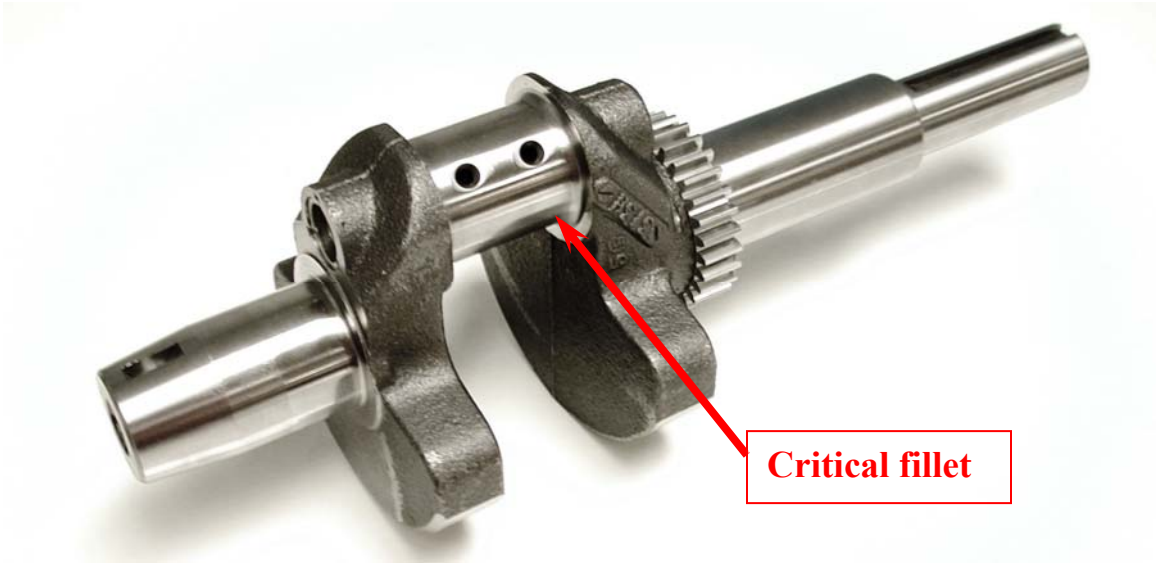

Figure 3.2: Ductile cast iron crankshaft in its final machined condition.

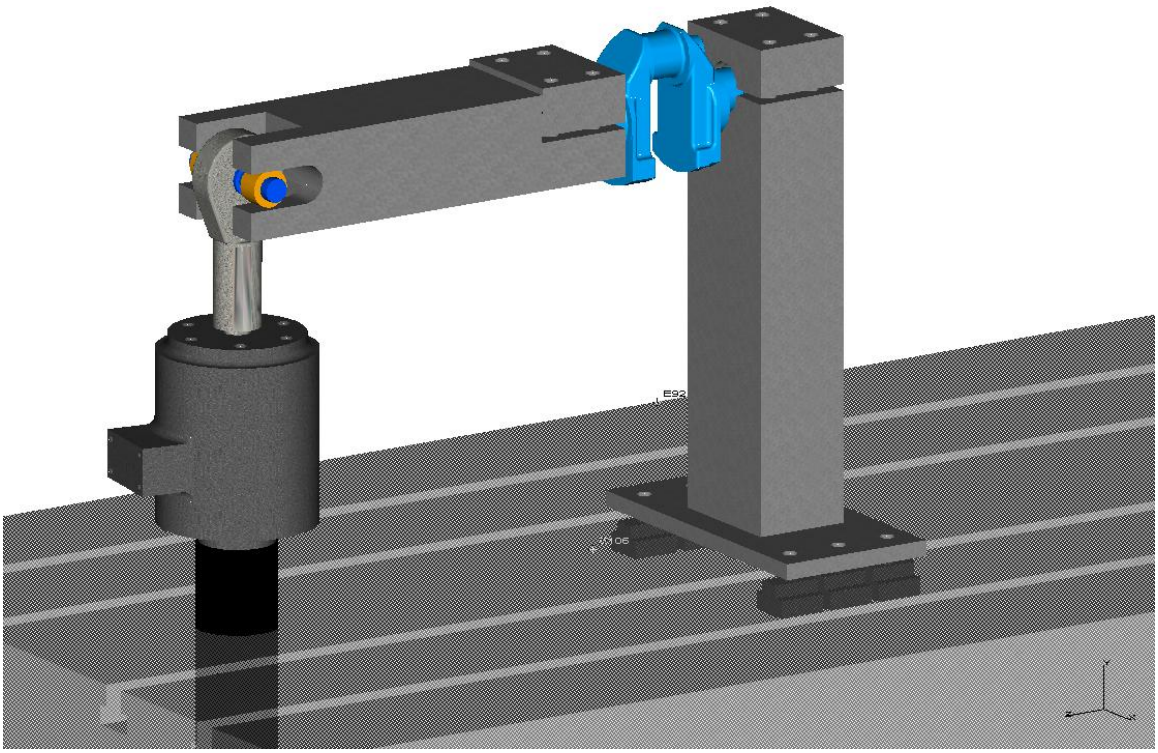

Figure 3.3: Schematic of test set-up.

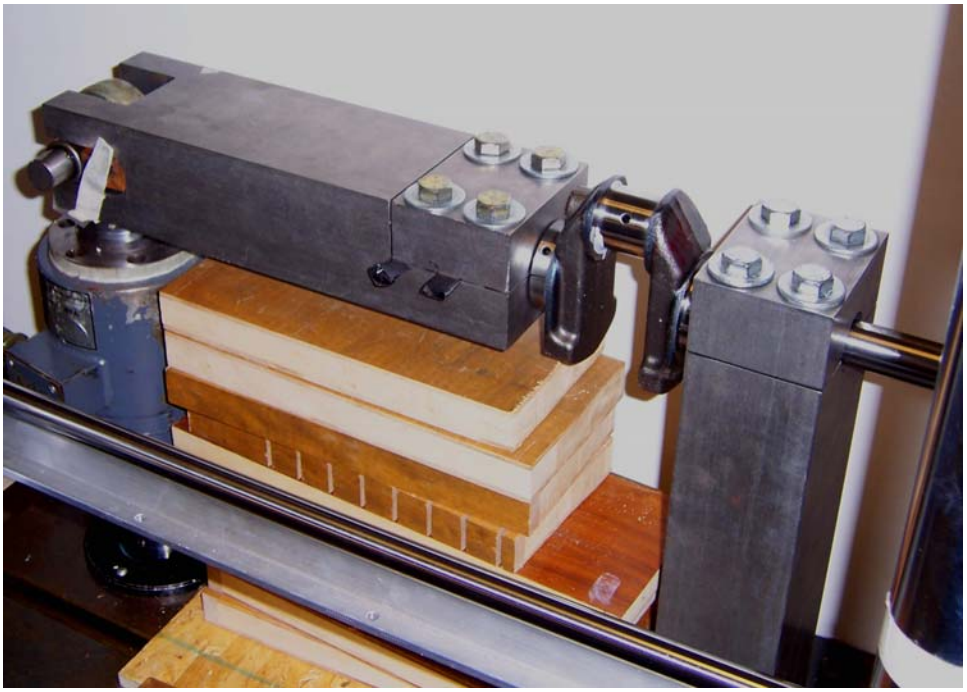

Figure 3.4: Test set-up for the forged steel crankshaft.

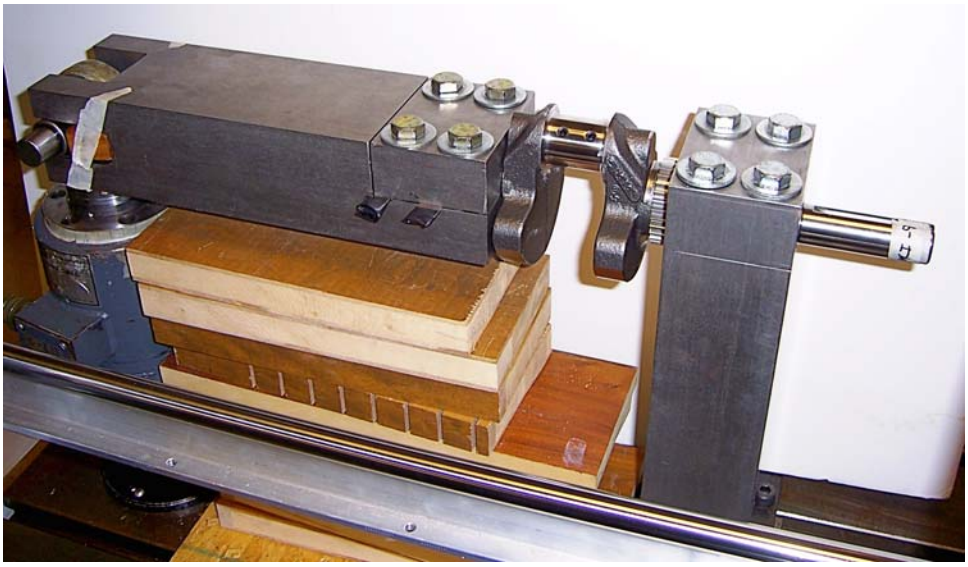

Figure 3.5: Test set-up for the ductile cast iron crankshaft.

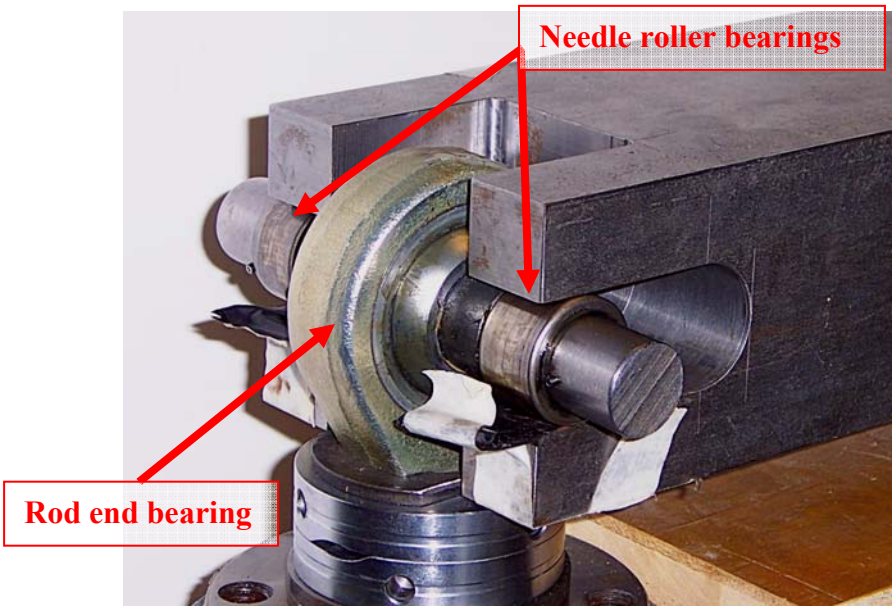

Figure 3.6: Close up of load application area of moment arm showing rod end bearing and roller bearings.

Figure 3.7: Critical fillet area of crankshaft painted to better observe crack.

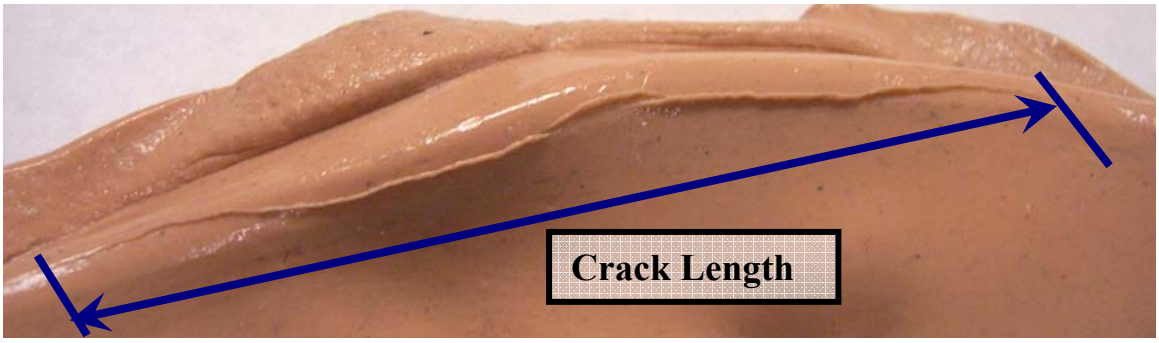

Figure 3.8: Imprint of crack with putty.

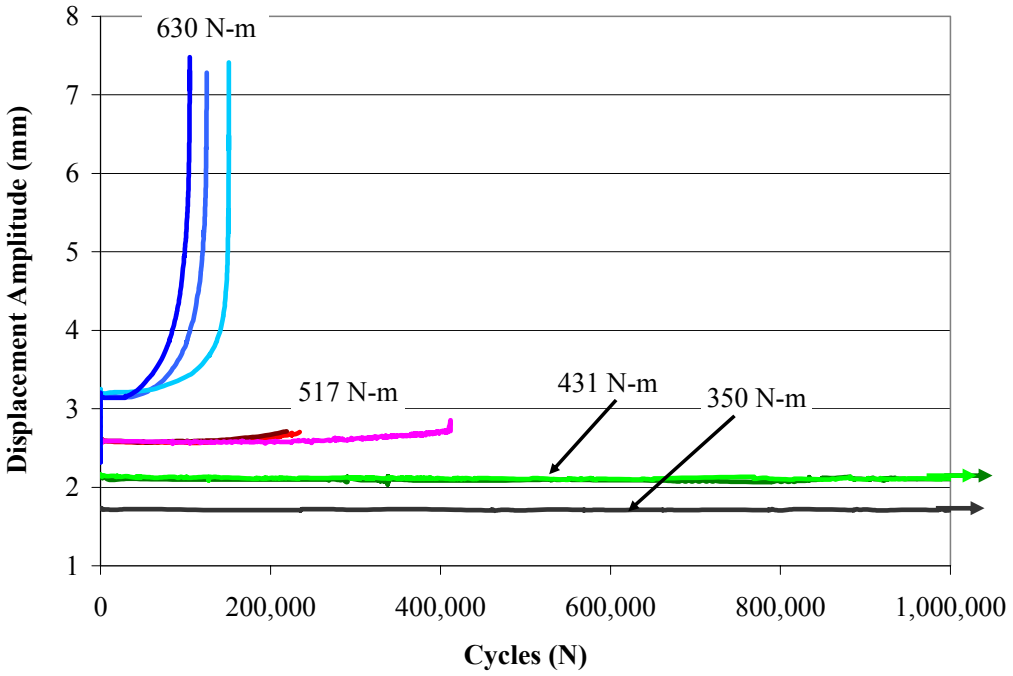

(a)

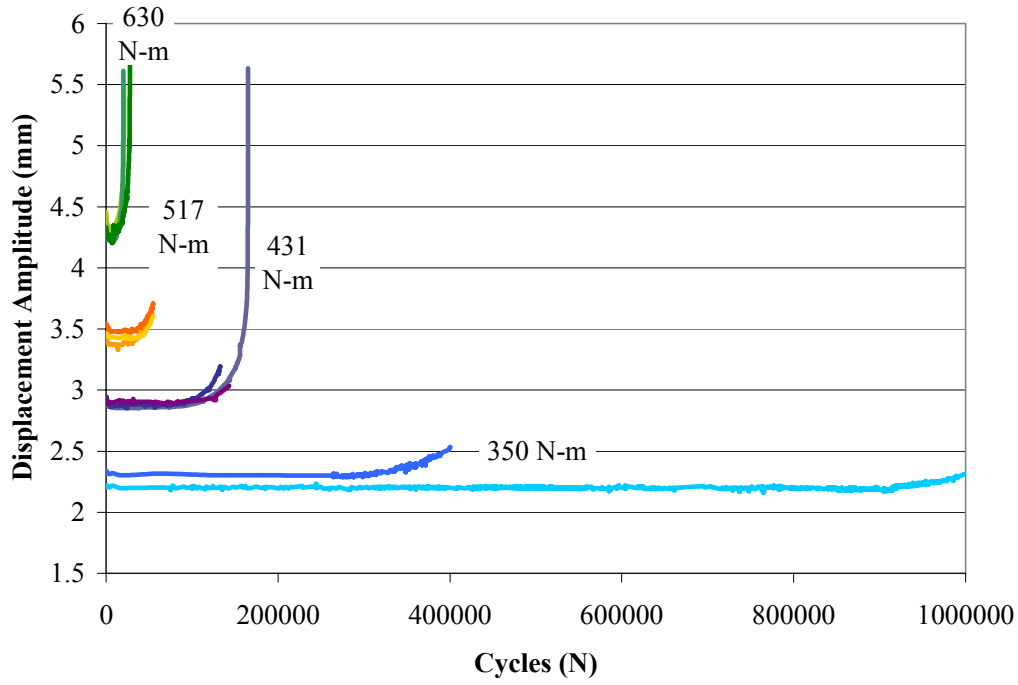

(b)

Figure 3.9: Displacement amplitude versus number of cycles for the (a) forged steel crankshafts and (b) ductile cast iron crankshafts.

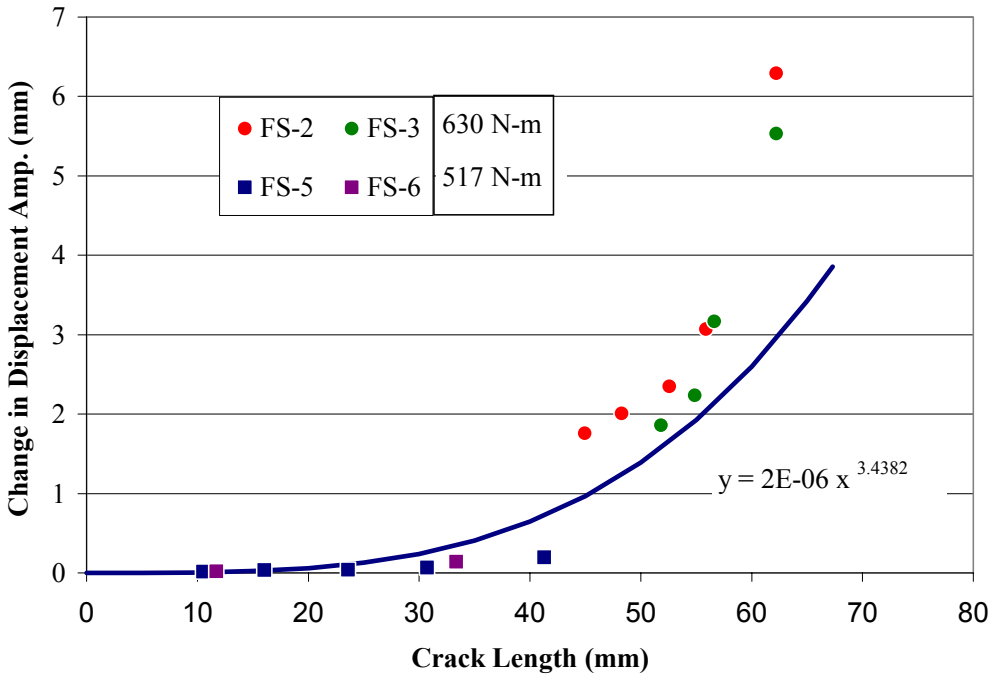

Figure 3.10: Change in displacement amplitude versus crack length for the forged steel crankshafts.

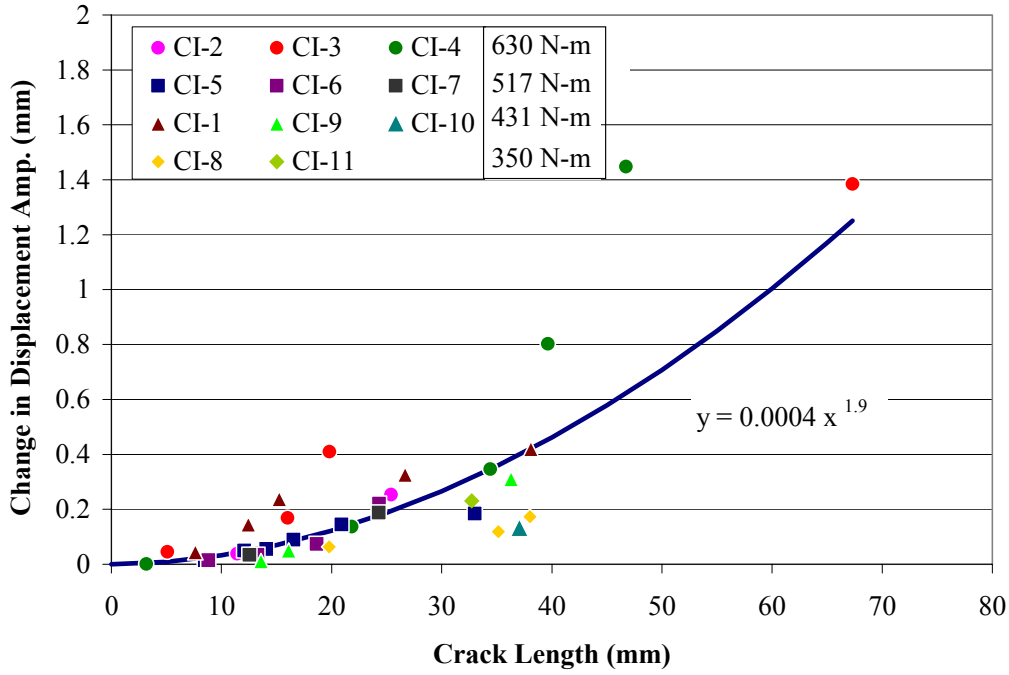

Figure 3.11: Change in displacement amplitude versus crack length for the cast iron crankshafts.

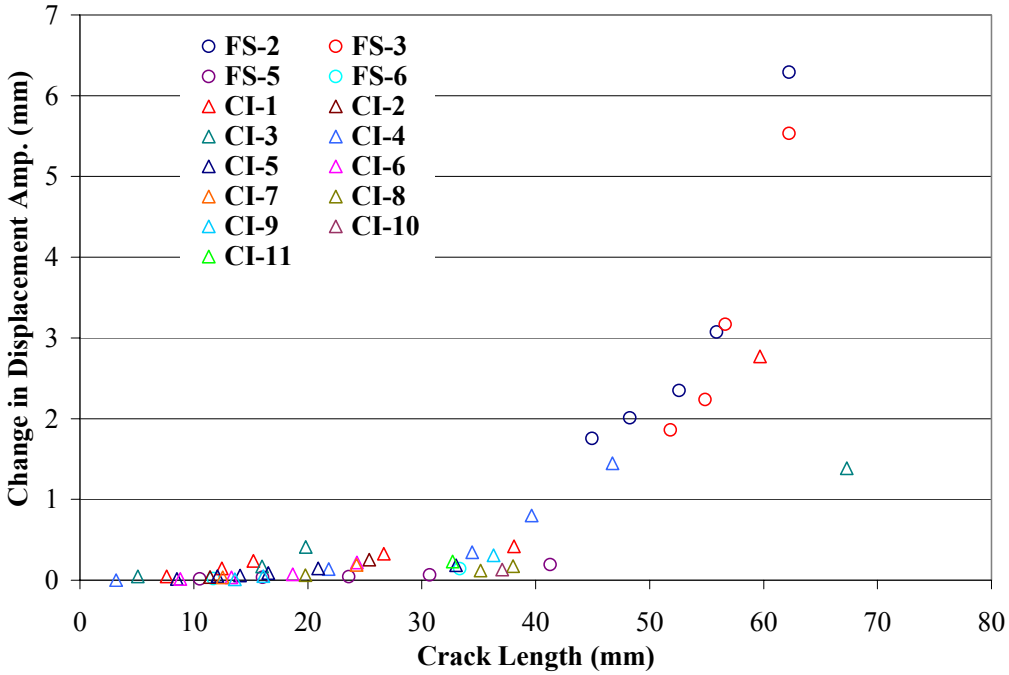

Figure 3.12: Superimposed plot of change in displacement amplitude versus crack length for the forged steel and cast iron crankshafts.

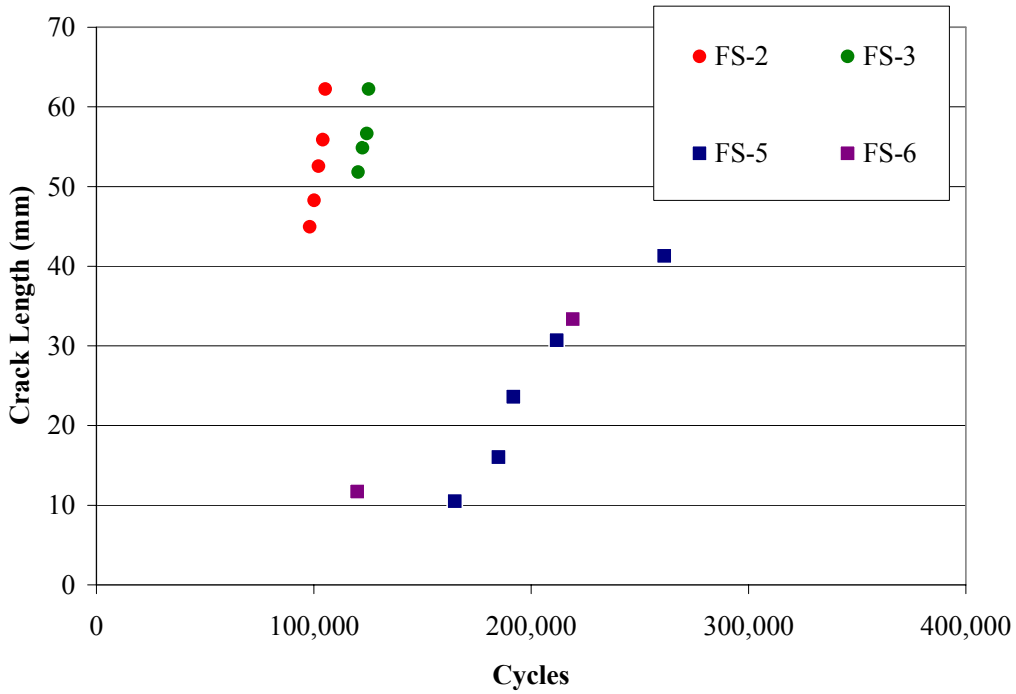

Figure 3.13: Measured crack length versus cycles for the forged steel crankshafts.

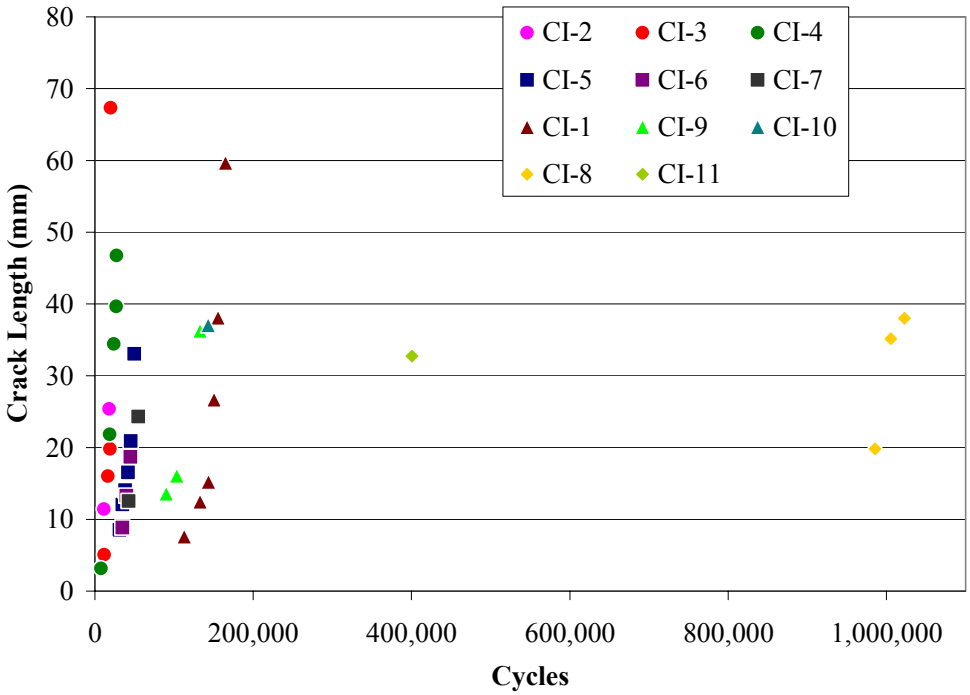

Figure 3.14: Measured crack length versus cycles for the ductile cast iron crankshafts.

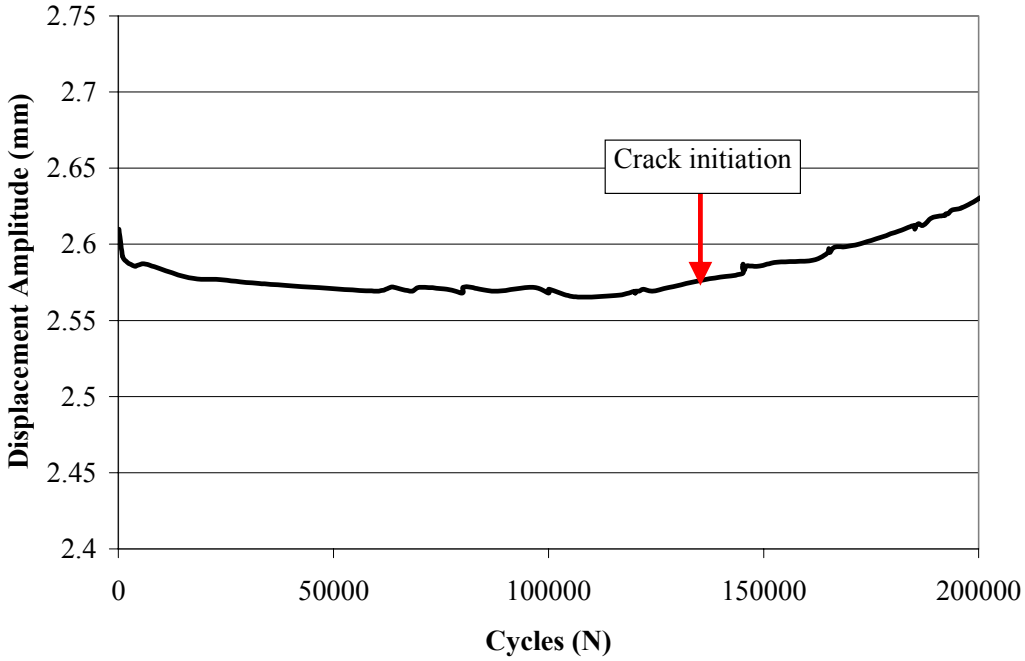

Figure 3.15: Displacement amplitude versus cycles for a forged steel crankshaft with the crack initiation point highlighted.

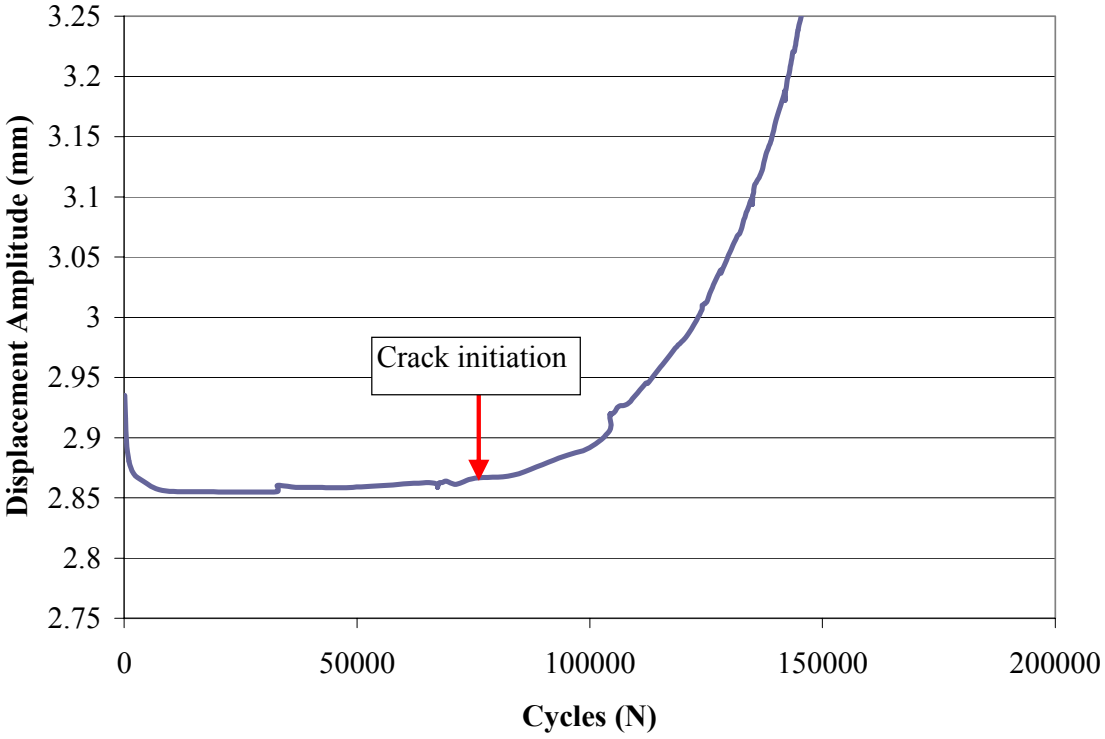

Figure 3.16: Displacement amplitude versus cycles for a ductile cast iron crankshaft with the crack initiation point highlighted.

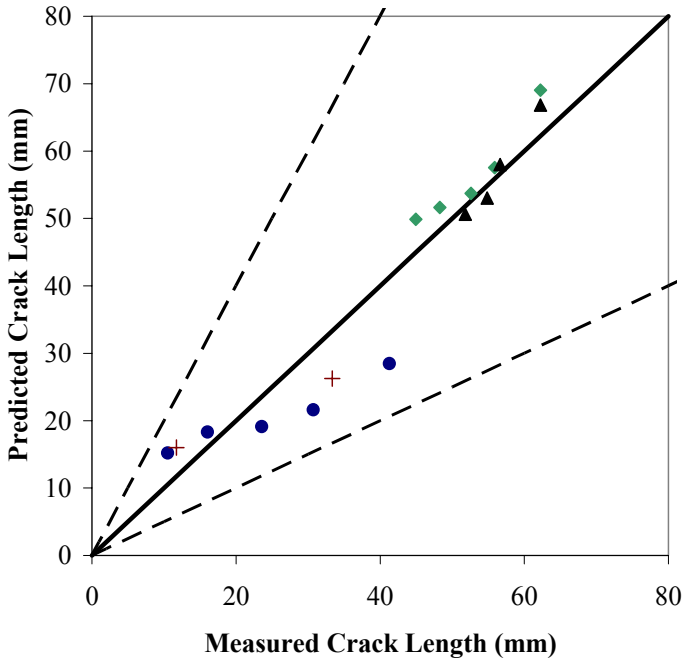

Figure 3.17: Predicted crack length versus measured crack length for the forged steel crankshafts. The same symbols correspond to crack lengths of the same crankshaft.

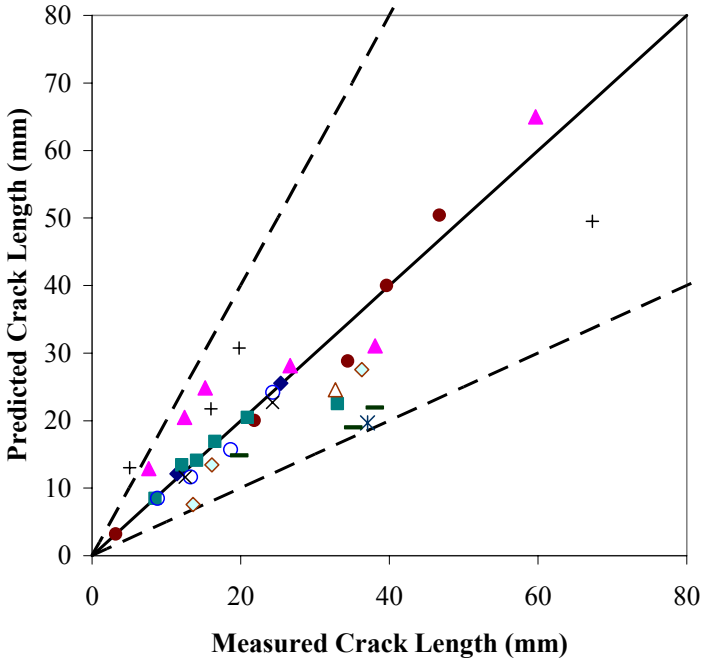

Figure 3.18: Predicted crack length versus measured crack length for the ductile cast iron crankshafts. The same symbols correspond to crack lengths of the same crankshaft.

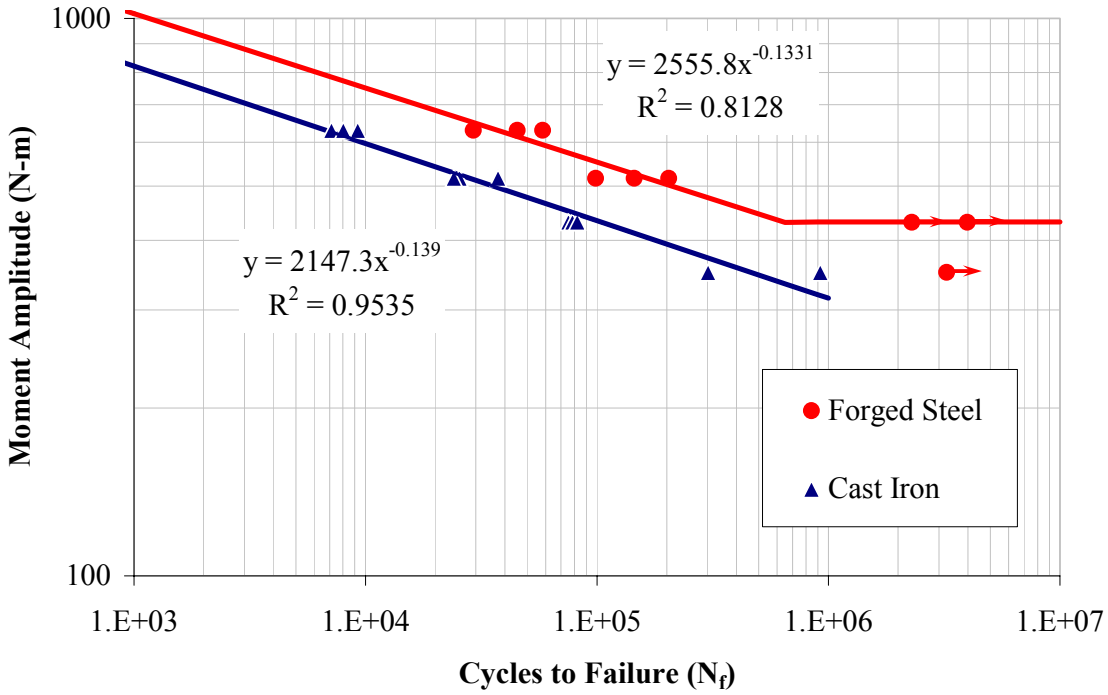

Figure 3.19: Moment amplitude versus cycles to failure using the crack initiation failure criterion.

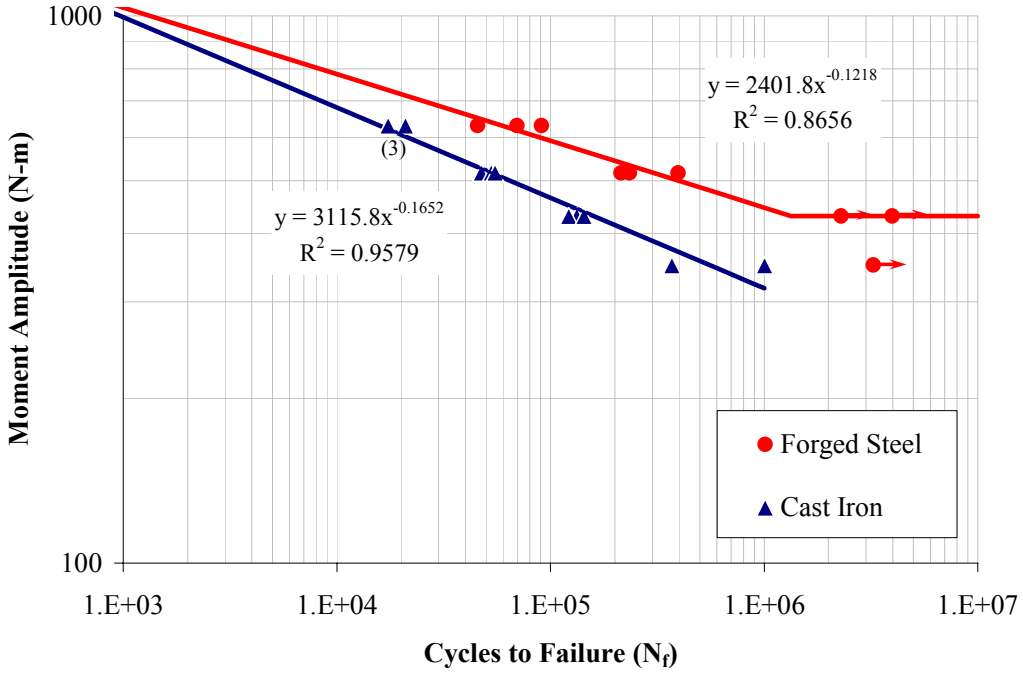

Figure 3.20: Moment amplitude versus cycles to failure using the 5% change in displacement amplitude failure criterion.

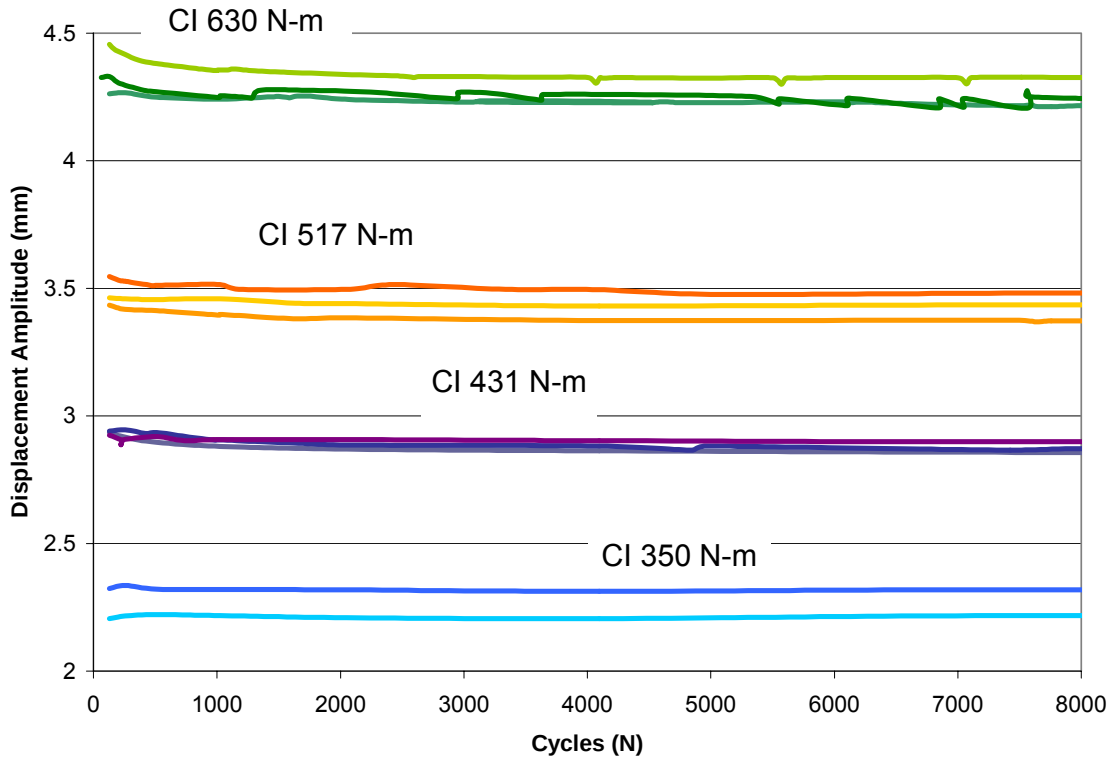

Figure 3.21: Cast Iron displacement amplitude versus cycles plot showing hardening behavior.

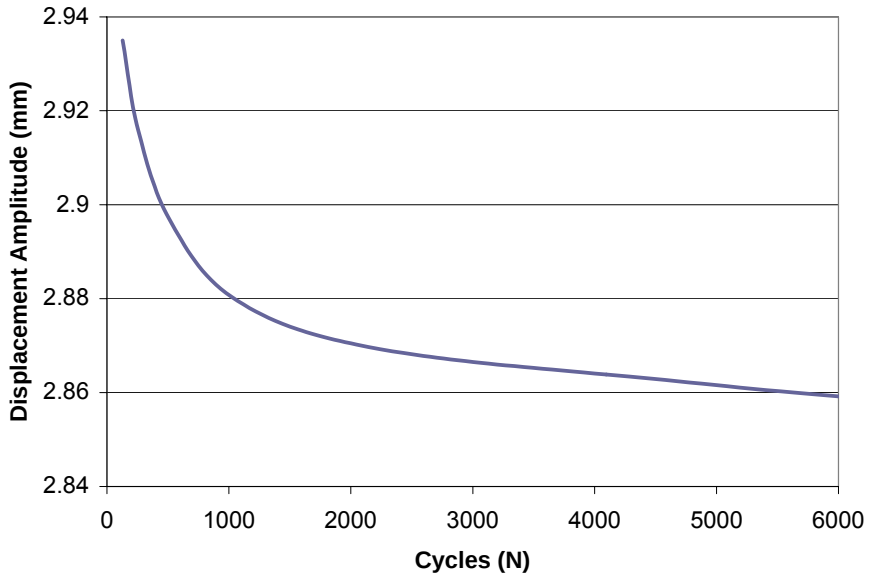

Figure 3.22: Expanded view of the displacement amplitude versus cycles plot for a cast iron crankshaft tested at 431 N-m.

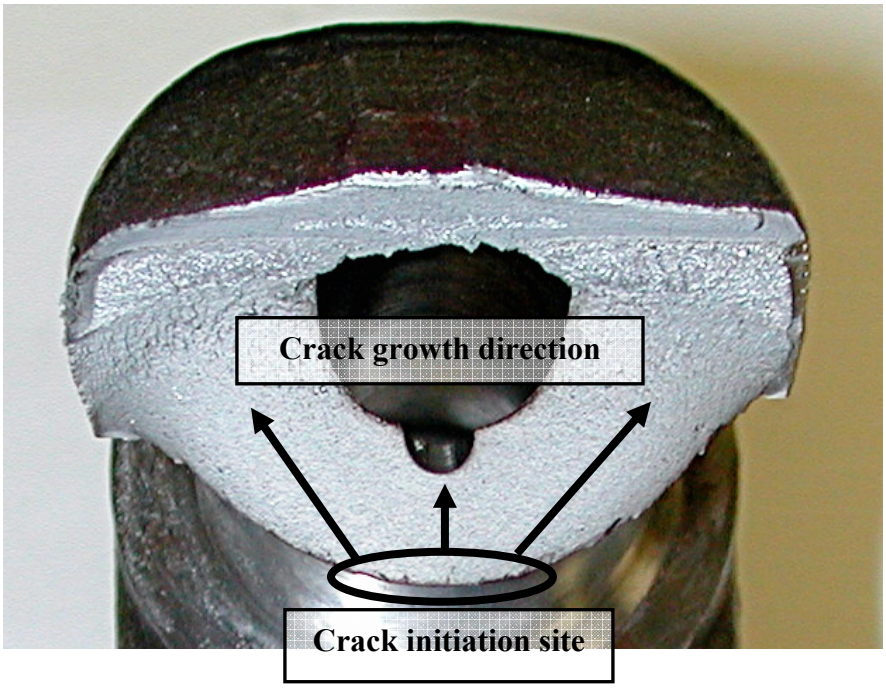

Figure 3.23: Example of a typical fatigue fracture surface for the forged steel crankshaft.

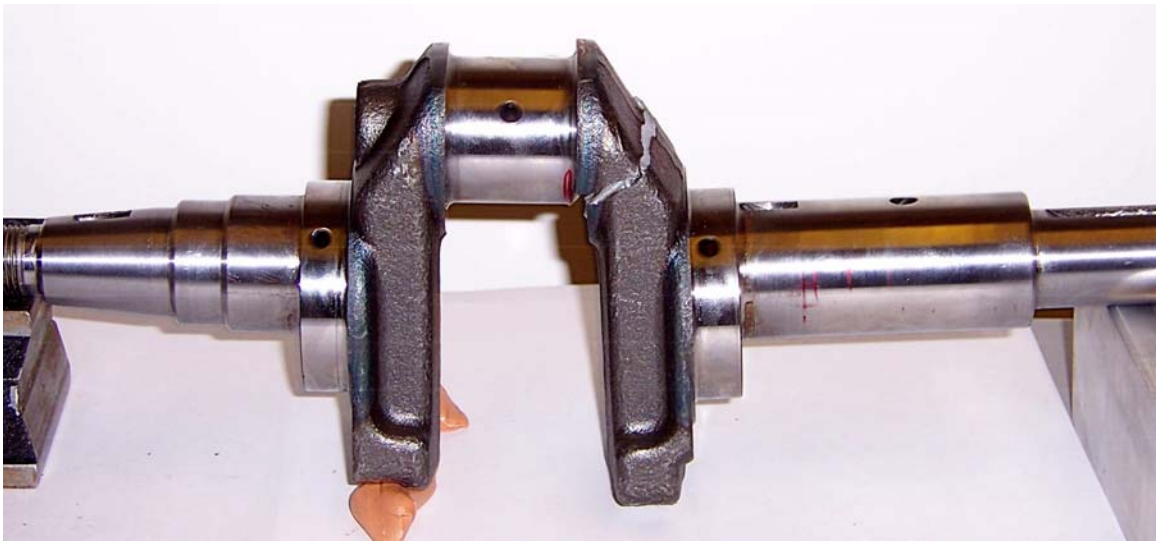

Figure 3.24: Side view of typical fatigue fractured forged steel crankshaft.

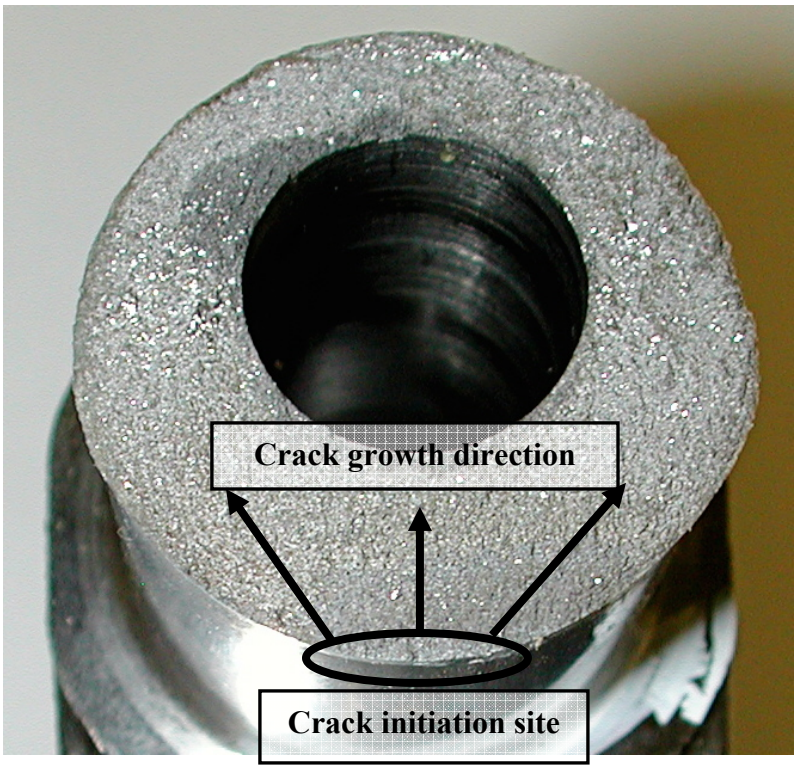

Figure 3.25: Example of a typical fatigue fracture surface for the cast iron crankshaft.

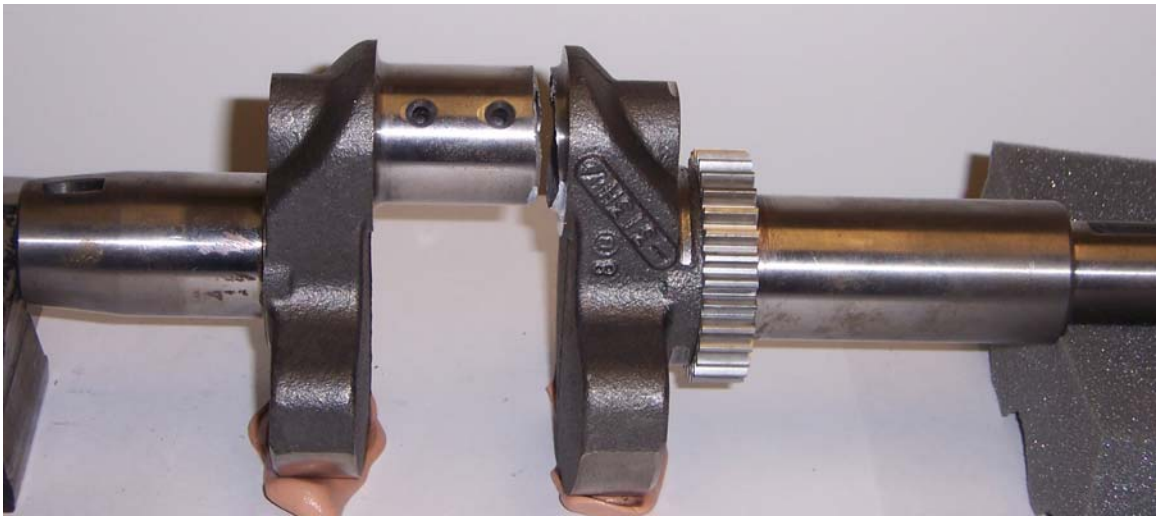

Figure 3.26: Side view of typical fatigue fractured cast iron crankshaft.

CHAPTER 4

STRESS ANALYSIS AND FATIGUE LIFE PREDICTIONS

4.1 Analytical Stress Calculations

To verify the nominal stress obtained from FEA which was used for the life predictions, analytical stress calculations were performed. Since the component was loading in bending only, the stress was calculated using the equation:

$$S_a = \frac{M_a c}{I} \tag{4.1}$$

where S_a is the stress amplitude, M_a is the moment amplitude, c is the distance from the centroid to the location where the stress is calculated and I is the area moment of inertia. The forged steel crankshaft had an outer crankpin diameter of 3.68 cm and an inner diameter of 1.70 cm, which were used to calculate the area moment of inertia, which is 8.59 cm^4.

For the cast iron crankshaft, the calculation was slightly more complex. The oil bore through the crank pin was not centered, creating a non standard cross section. The outer diameter of the crankpin of the ductile cast iron crankshaft was 3.30 cm and the inner diameter was 1.70 cm. In order to calculate the stress in the cast iron crank-pin, first the vertical distance to the centroid was found to be 1.57 cm from the bottom of the cross section shown in Figure 3.23. The area moment of inertia, *I*, for the cross section was then calculated using the parallel axis theorem to be 5.29 cm^4. The flexure formula,

given by Equation 4.1, could then be used to analytically determine the nominal stress at the critical location. Due to the non-standard cross-section the stress on the top of the crankpin differed from the stress on the underside of the crankpin. Since the critical section was determined to be on the underside of the crankpin, the distance from the centroid to the underside of the crankpin of the cast iron crankshaft, which was 1.57 cm, was used for *c*.

The analytical stress results for the forged steel and ductile cast iron crankshafts at the critical location, which was the crankpin fillet, and without consideration of stress concentration caused by the fillet, are shown in Table 4.1 (with the locations identified in Figure 4.2) along with the FEA results from Montazersadgh [2007].

4.2 Finite Element Modeling and Analysis

Finite element modeling was preformed on the forged steel and the ductile cast iron crankshafts. A linear elastic analysis was used due to the high cycle fatigue situation which requires nominally elastic loading. The finite element analysis (FEA) was used to determine the critical location of the crankshafts, determine the stress concentration factors for the critical fillet locations, and determine the nominal stress applied for the purpose of life prediction. Using the stress concentration factor approach rather than directly using the local stress and strain at the critical locations from FEA eliminates the need for a separate analysis for each load level.

The FEA analysis also validated what was revealed from the experimental stress results obtained from strain gages. Based on simple analytical calculations of bending stress (i.e. Mc/I), the stress in the forged steel crankshaft on the top and bottom of the crankpin should be equal in magnitude due to the symmetry of the crankpin cross-section.

The stress results obtained from strain gage readings, however, revealed that there was a larger stress at the bottom than at the top. This result was confirmed with FEA. The relatively complex geometry of the crankshaft results in stresses that are not easily calculated with simple analytical techniques. Finite element analysis was necessary in this instance in order to account for the complex geometry.

Two types of analyses were performed. First the crankshafts were modeled according to the dynamic load analysis to determine the critical location of each crankshaft under in service loading. Second, boundary conditions resembling those of the test fixture were used in order to determine the stresses for the purpose of life prediction and to compare with the experimental stress results from strain gages. Details of the finite element modeling including geometry generation, meshing, boundary conditions, and loading are presented in Montazersadgh and Fatemi [2007], and Montazersadgh [2007]. The results relevant to this study are presented in the subsequent sections.

4.2.1 Critical locations

The critical location is the location of the crankshaft subjected to the highest stress and therefore the location where fatigue cracks initiate and ultimately lead to failure. Identification of the critical location was necessary before the component fatigue testing described in Chapter 3 could be started since the design of the component fatigue test fixture was based on the location of the critical location. It was expected that the critical location would be in one of the fillets due to the high stress concentrations at these locations. The stress contour provided by the FEA based on the dynamic analysis is

shown in Figure 4.1. Based on the graphical representation of the stresses, several locations were selected as potential critical locations of the crankshaft, which are labeled as locations 1 through 6 in Figure 4.2. The analysis of the critical section is presented for the forged steel crankshaft, however similar results were obtained for the ductile cast iron crankshaft.

A plot of the von Mises stresses as a function of crank angle for the locations in Figure 4.2 are shown in Figure 4.3. The figure shows that a crank angle of 355 degrees represents the position where the highest stress levels occur. At the crank angle of 355 degrees it can be seen that location 2 identified in Figure 4.2 is the highest stressed location of the crankshaft. A plot of minimum and maximum stresses, stress range and mean stress for the critical locations is shown in Figure 4.4. The figure shows that location number 2, which was determined to have the highest von Mises stress, is also the location with the highest stress range and mean stress. In fatigue analysis the stress range and mean stress can be more important than the maximum stress.

Based on the plot of von Mises stress and the stress range and mean stress plot, location 2 was identified as the critical location of the crankshaft. This location was in agreement with the literature which has shown that the crankpin fillets are the highest stressed locations in a crankshaft [Jensen, 1970]. The critical location defined by the FEA analysis was verified during the component fatigue testing by the fact that all of the failed crankshafts developed cracks in this crankpin fillet location which then grew to a large crack which ultimately led to failure.

4.2.2 Comparison between FEA, analytical, and experimental results

The boundary conditions in the finite element model were changed from the dynamic loading condition to resemble the component test assembly. This was done to investigate the stresses in the component as a result of being loaded in the test apparatus. As mentioned previously, based on analytical bending stress calculations for the forged steel crankshaft, the stress at the top and bottom of the crankpin should be symmetric. However, both experimental and FEA results revealed that the stresses were not symmetric. The comparison between FEA and experimental values was also done to validate the finite element model. The experimental results were only obtained and compared to the FEA results for the forged steel crankshaft. It was not necessary to repeat the procedure for the cast iron crankshaft since it was modeled and tested the same way as the forged steel crankshaft. The details of the finite element analysis are given in Montazersadgh and Fatemi [2007].

Strain gages were mounted at the four locations labeled *a*, *b*, *c*, and *d* in Figure 4.2. The crankshaft was installed in the test fixture such that locations *a* and *b* were on the top and bottom respectively. The front main bearing was clamped in the support arm and the rear main bearing (the right side of Figure 4.2) was clamped in the moment arm. It should be noted that this was not the position the crankshafts were tested in as this comparison was done prior to properly identifying the critical fillet. In the tests, as described in Chapter 3, the crankshaft was switched such that the rear main bearing was in the support arm and moment arm was clamped to the front main bearing. Despite this change, the results were applicable since they were used for comparison purposes. The load was applied vertically through the moment arm attached to the right of Figure 4.2.

The crankshaft was also rotated 90 degrees so that locations *c* and *d* (Figure 4.2) were on the top and bottom, respectively. This was done to see the effects of the different offsets of the crank-pin.

The results from FEA, analytical calculations, and experimental results from strain gages are shown in Table 4.2. The table shows good agreement between the experimental results obtained from strain gages and the results from FEA. All of the differences between FEA and experimental results were 6.5% or less. The results from the analytical analysis are also close to the FEA and experimental results considering the complex geometry.

The analytical results, discussed in Section 4.2, suggest that the stress at location *a* and location *b* should be equal and opposite. FEA is necessary in order to obtain accurate stresses in the component which, in a case where the geometry is complex, could otherwise not be obtained. Both FEA and experimental results show that the magnitudes of the stresses at locations *a* and *b* (identified in Figure 4.2) are not equal due to the complexity of the geometry. However, when the crankshaft was rotated 90 degrees, the FEA results show that stresses at location *c* and location *d* are equal in magnitude, which is confirmed by the experimental results from the strain gages. Some difference is seen in the strain gage readings which can be attributed to errors in placing the gages.

4.2.3 FEA results used for life predictions

The finite element analysis with the boundary conditions resembling the component test fixture was used to determine the nominal stresses in the crankshafts. This nominal stress was used for life prediction purposes. For this analysis a point load

of 4.45kN was applied at B, as shown in Figure 4.2 for the forged steel crankshaft, which was the same for the cast iron crankshaft. The FEA results of the test condition are shown in Table 4.3 for forged steel and Table 4.4 for the cast iron crankshaft where the locations are identified in Figure 4.2. The finite element analysis based on the component test fixture showed that the highest stress was at the previously identified critical section, indicating that the test set-up would produce failures in the critical section. The stress at location *b* as shown in Figures 4.2 was extrapolated to determine the nominal stress at the critical location, point 2 in Figure 4.2. For the forged steel crankshaft the moment arm to location 4 was 12.6 cm resulting in a nominal stress of 121.6 MPa when 4.45 kN force was applied. To obtain the nominal stress at the critical location a ratio was used to accommodate a longer moment arm and different loads corresponding to the actual tests. The ratio related the stress from FEA, which was obtained from a given bending moment, to the stress resulting from a different bending moment. This was possible because of the uniform cross-section and the stress being linearly related to the bending moment. A similar procedure was used for the ductile cast iron crankshaft.

The nominal stress values at the critical fillet, location *b* in Figure 4.2, obtained from the FEA [Montazersadgh, 2007] for the forged steel and ductile cast iron crankshafts are shown in Table 4.1 for the different applied moments. The results were used in the life predictions discussed in Sections 4.3 and 4.4.

Determining the stress concentration factor (K_t) was also necessary for life predictions. The stress concentration factor allowed the stress at the fillets to be calculated knowing the nominal stress which was obtained from the linear elastic finite

element analysis. As shown in Table 4.3 for forged steel, the stress obtained from FEA with a 4.45 kN applied load was 121.6 MPa for location *b* and 539.7 MPa for location 2 (locations identified in Figure 4.2). Location *b* was considered to be far enough away from fillets such that it was not affected by stress concentrations. Therefore, as was done above, this stress was used to determine the nominal stress at location 2 by equating the ratio of the stresses to the ratio of the moment arms. The distance from the applied load to location *b* was 12.6 cm and to location 2 was 14.3 cm. The nominal stress at the critical location was determined to be 137.1 MPa. The stress concentration factor, K_t, was calculated by dividing the stress at the critical location from FEA by the nominal stress at the critical location:

$$K_t = \frac{S}{S_{nom}} \tag{4.2}$$

The stress concentration factor for forged steel was determined to be 3.94. A similar procedure was followed for the cast iron crankshaft where the nominal stress at the critical location was determined to be 160.7 MPa and the stress concentration factor, K_t, was 3.09.

4.3 Stress-Life Approach and Life Predictions

4.3.1 Procedures and predictions

In service the crankshaft is subjected to very high cycle fatigue, requiring the stresses to be elastic. In situations where stresses are predominately elastic and high cycle fatigue is present, the stress-life (S-N) approach is commonly used. The S-N approach uses the nominal stress rather than the localized stress at the root of the notch. To account for the

stress concentration at the notch, the fatigue limit is reduced by the fatigue notch factor. The effect of mean stress can be accounted for by an equation such as the modified Goodman equation. The S-N line can also be modified to account for other effects such as surface finish effect.

As a starting point, the stress-life curve for a smooth, unnotched member, subjected to completely reversed loading, was constructed from the fatigue strength coefficient, σ_f', and the fatigue strength exponent, b. Both σ_f' and b were obtained from the specimen tests as presented in Chapter 2 and the values for both materials are listed in Table 2.4. The S-N line for the smooth, unnotched member is represented by the equation:

$$S_f = \sigma_f' \left(2 \times 10^6\right)^b \tag{4.3}$$

The effect of the notch was taken into account by the fatigue notch factor, K_f. The fatigue notch factor depends on the geometry of the notch and also notch sensitivity of the material. The notch sensitivity of a material is defined by:

$$q = \frac{K_f - 1}{K_t - 1} \tag{4.4}$$

where K_f is the fatigue notch factor and K_t is the stress concentration factor. A value for $q = 0$ indicates no sensitivity to notches and $q = 1$ is defined as full notch sensitivity. When a material has large sensitivity to notches K_f is approximately equal to K_t. There are several equations for estimating the notch sensitivity of a material, including Peterson's equation given by [Stephens et al., 2000]:

$$q = \frac{1}{1 + a/r} \tag{4.5}$$

where q is the notch sensitivity, r is the radius of the notch and a is the material characteristic length. The following equation was used to calculate the material characteristic length, a (in millimeters) for the forged steel material [Stephens et al., 2000]:

$$a = 0.0254 \left(\frac{2070}{S_u}\right)^{1.8} \tag{4.6}$$

where S_u is the ultimate strength of the material in MPa. The notch sensitivity for the forged steel was calculated to be 0.95, indicating very high notch sensitivity. The fatigue notch factor for the forged steel crankshaft with a notch radius of r = 2.38 mm was then calculated to be 3.78.

For the ductile cast iron crankshafts, Peterson's equation (Equation 4.5) was also used along with the equation for characteristic length, a, intended for steels (Equation 4.6). Using this approach the notch sensitivity was calculated to be 0.92, which for the ductile cast iron crankshaft with a fillet radius of r = 2.45 mm resulted in K_f = 2.93. The life predictions using this approach were conservative. The difference in stress concentrations between the forged steel and ductile cast iron crankshafts can be attributed to the geometric differences in the two crankshafts. The ductile cast iron crankshaft has a difference in stiffness in the web section in close proximity to the critical fillet, as compared to the forged steel crankshaft, which decreases the stress in the fillet, thus decreasing the stress concentration.

According to Shigley and Mitschke [2002], cast iron has very low notch sensitivity, q, ranging in value from 0, or no notch sensitivity, to 0.2. Juvinall and Marshek [1991] also state that cast irons have little to no notch sensitivity. Cast iron has inclusions and porosity which can act as notches. Therefore, these notch effects are

already taken into account in the cyclic material properties obtain from the strain-controlled specimen fatigue testing. Shigley and Mitschke recommend that to be conservative, a value of q = 0.2 be used for all cast irons [2002]. Using q = 0.2 resulted in K_f = 1.42. The results of the life predictions were excessively nonconservative when this approach was used to calculate K_f. The true value for notch sensitivity, therefore, lies somewhere between the values obtained using these two approaches. The life predictions are presented using both values of K_f, however, the approach using the higher fatigue notch factor, K_f = 2.93, is considered the primary approach due to the better agreement with the component fatigue tests data.

The fatigue life at 2 x 10^6 reversals was reduced by K_f. Therefore, for the notched member, one point on the S-N line was S_f / K_f at 2 x 10^6 reversals. The forged steel crankshaft had a notched fatigue strength at 2 x 10^6 reversals of 94.4 MPa. The ductile cast iron is also assumed to have a fatigue limit at 2 x 10^6 reversals [Juvinall and Marshek, 1991]. The notched fatigue strength at 2 x 10^6 reversals for the cast iron crankshaft based on K_f = 2.93 was 89.5 MPa, and based on K_f = 1.42 the notched fatigue strength was 185.0 MPa.

The point at 2 x 10^6 reversals was connected to the stress amplitude, σ_f', at one reversal for each material. This approach assumes that there is no effect of the notch at one cycle due to the presence of gross plastic deformation, or yielding.

The notched S-N line for the forged steel crankshaft is represented by:

$$S_f = 1124 \left(2N_f\right)^{-0.1704} \tag{4.7}$$

and the notched S-N line for the ductile cast iron crankshaft with K_f = 2.93 is represented by:

$$S_f = 927\left(2N_f\right)^{-0.1611} \tag{4.8}$$

The S-N lines obtained above assume R = -1. To account for mean stress which is present in situations where the loading is not completely reversed, the modified Goodman equation is often used. The modified Goodman equation is given by [Stephens et al., 2000]:

$$\frac{S_a}{S_{Nf}/K_f} + \frac{S_m}{S_u} = 1 \tag{4.9}$$

where S_a is the alternating stress, S_m is the mean stress, S_u is the ultimate strength of the material, and S_{Nf} is the fully reversed fatigue strength at 2 x 10^6 reversals.

Dynamic load analysis determined the stress ratio, R, of the crankshafts to be approximately -0.2. The details of the dynamic load analysis are shown in Montazersadgh and Fatemi [2007] and Montazersadgh [2007]. The R-ratio was used to calculate the mean stress. The R-ratio is defined by:

$$R = \frac{S_{\min}}{S_{\max}} \tag{4.10}$$

For R = -0.2 the relationship between S_a and S_m was calculated to be:

$$S_m = 0.667 S_a \tag{4.11}$$

The equation for the notched R = -0.2 condition for the forged steel crankshaft is represented by:

$$S_a = \frac{1124\ MPa}{\left(2N_f\right)^{0.170} + 0.906} \tag{4.12}$$

which results in a fatigue strength of 87.8 MPa at 2 x 10^6 reversals. The equation for the notched R = -0.2 condition and high notch sensitivity (K_f = 2.93) for the ductile cast iron crankshaft is then represented by:

$$S_a = \frac{927\ MPa}{(2N_f)^{0.161} + 0.939} \tag{4.13}$$

which results in a fatigue strength of 82.1 MPa at 2 x 10^6 reversals. For the low notch sensitivity (K_f = 1.42) assumption of ductile cast iron, the S-N curve is represented by:

$$S_a = \frac{927\ MPa}{(2N_f)^{0.111} + 0.939} \tag{4.14}$$

which results in a fatigue strength of 155.8 MPa at 2 x 10^6 reversals.

The unnotched R = -1, notched R = -1, and notched R = -0.2 S-N curves are shown in Figure 4.5 for the forged steel crankshaft and in Figure 4.6 for the ductile cast iron crankshaft. Results of the S-N life predictions for the forged steel and for the ductile cast iron crankshafts are shown in Tables 4.5 and 4.6, respectively.

4.3.2 Comparisons with experimental results

The results of the S-N life predictions along with the crankshaft fatigue test data are summarized in Table 4.7 for the forged steel and ductile cast iron crankshafts. The forged steel predicted S-N line superimposed with the experimental data points is shown in Figure 4.7 for the crack initiation criterion and in Figure 4.8 for the 5% change in displacement amplitude criterion. The figures show a very good agreement between the predictions and the experimental data for both failure criteria.

The ductile cast iron crankshaft predicted S-N lines, using both values of K_f, superimposed with the experimental data points are shown in Figure 4.9 for the crack initiation criterion and in Figure 4.10 for the 5% change in displacement amplitude criterion. When K_f = 1.42 is used, the S-N life predictions for both the crack initiation and 5% displacement amplitude are nonconservative, while the opposite is true if the

value for K_f = 2.93 is used. Based on the S-N lines, the predictions using K_f = 2.93 more closely match the experiment data than when K_f = 1.42 was used. For the S-N approach for the ductile cast iron crankshafts, the most accurate predictions are obtained using K_f = 2.93 and the crack initiation failure criterion as evidenced by the close proximity of the experimental data points to the predicted S-N curve in Figure 4.9. Since the predictions using the low notch sensitivity assumed for cast iron (K_f = 1.42) were not in agreement with the experimental data, further comparisons using this assumption are not presented.

The comparison between experimental results and predicted results are shown in Figure 4.11 for the crack initiation failure criterion for both the forged steel and ductile cast iron crankshafts (K_f = 2.93). In Figure 4.11, the center line with a slope of one (45 degrees) and passing through the origin represents a perfect correlation between the prediction and experimental data. Data points that are above the line represent an over prediction (non-conservative), while points below the line represent an under prediction (conservative). The other lines represent factors of two and three differences. The experimental results versus predicted results are plotted for the 5% change in displacement amplitude criterion in Figure 4.12 for both crankshafts.

Figures 4.11 and 4.12 show that for the forged steel crankshafts, the experimental data fall within a factor of two of the prediction for both the crack initiation and 5% change in displacement amplitude criteria. Comparison of Figures 4.11 and 4.12 reveals that the crack initiation data is in better agreement with the prediction than the 5% change in displacement amplitude criterion. This is expected, as the failure for specimen fatigue tests was based on crack initiation, and data from these tests were used for crankshaft life

predictions. The prediction is more conservative when the 5% change in displacement amplitude criterion is used.

The predictions for the cast iron crankshaft were less in agreement with the predictions for the forged steel crankshaft although the predictions were still reasonably accurate when the higher notch sensitivity was used. The experimental data for the cast iron crankshaft are along the factor of two and factor of three scatter bands when the crack initiation failure criterion is used as shown in Figure 4.11. When the 5% change in displacement amplitude criterion is used, the experimental data are along or slightly outside of the factor of three scatter band as shown in Figure 4.12 with predictions being conservative.

The S-N prediction took into account the stress concentration caused by the crankpin fillet and the mean stress effect. However, the effect of surface finish was neglected for both the forged steel and cast iron crankshafts. The surface of the both crankshafts appeared to be ground and, therefore, a very smooth surface finish with few machining marks, which was approximated as a smooth surface. Had the critical location been in an area that was in the as forged or as cast condition, a surface finish correction factor would have been needed.

The fillets of crankshafts in automotive applications are often rolled to induce compressive residual stresses. The residual stress will, in a long life situation, provide better fatigue performance. However, residual stresses were not considered since the crankshafts were not rolled in this case.

4.4 Stain-Life Approach and Life Predictions

4.4.1 Procedures and predictions

The strain-life approach to life estimation is commonly used in low cycle fatigue applications due to the presence of inelastic strain in the component. In addition, strains can be measured in complex geometries and at stress concentrations, resulting in an easy comparison with data obtained from strain-controlled specimen fatigue tests. Although crankshafts are a high cycle fatigue component, the strain-life approach can still be valuable due the presence of notches in the crankshaft. The strain-life approach is commonly used for notched members, because local plastic deformation often occurs at the root of the notch, even when an elastic loading condition is present. This approach uses the stresses and strains at the root of the notch, as opposed to the S-N approach which uses nominal stresses. In the stress-life approach the nominal stresses are known and, therefore, the life to crack initiation can be directly calculated. However, in the strain-life approach, first the notch stresses and strains must be determined.

There are several methods which can be used to calculate the local stress and strain at the root of the notch given the nominal elastic stress. Analytical methods to calculate the local stress and strain include the linear rule, Neuber's rule, and Glinka's rule. Neuber's rule, the most commonly used model, is presented here. In the case of a plane strain situation, Glinka's rule is more applicable [Stephens et al., 2000]. For comparison the notch stresses and strains were also calculated using Glinka's rule and the results were very similar to those obtained using Neuber's rule.

Neuber's rule assumes that the geometric mean of the stress concentration and strain concentration factors remain constant under plastic deformation and are also equal

to the stress concentration factor. Graphically, the notch stress and strain are determined from the intersection of the stress-strain curve and the Neuber hyperbola. The stress-strain curve is represented by the Ramberg-Osgood equation given by:

$$\varepsilon = \varepsilon_e + \varepsilon_p = \frac{\sigma}{E} + \left(\frac{\sigma}{K}\right)^{1/n} \tag{4.15}$$

while Neuber's hyperbola is represented by:

$$\varepsilon\sigma = K_t^2 eS \tag{4.16}$$

where S and e are the nominal stress and strains, and σ and ε are the stress and strain at the root of the notch. Therefore, the intersection point can be found by solving equations 4.15 and 4.16 simultaneously.

The nominal stress is typically elastic, otherwise there will be gross plastic deformation and the part fails by yielding rather than fatigue crack initiation. In the case where the nominal stress is elastic, the engineering strain, e, is simply the nominal stress divided by modulus of elasticity (S/E). Therefore, Neuber's rule for nominal elastic behavior becomes:

$$\varepsilon\sigma = \frac{(K_t S)^2}{E} \tag{4.17}$$

In the case of cyclic loading, which is the case when using Neuber's rule for fatigue life predictions, the stress-strain curve is replaced with the stable hysteresis loop represented by the equation [Stephens et al., 2000]:

$$\Delta\varepsilon = \frac{\Delta\sigma}{E} + 2\left(\frac{\Delta\sigma}{2K'}\right)^{1/n'} \tag{4.18}$$

Equation 4.18 assumes that the material exhibits a Massing behavior, with a factor of 2, meaning that the hysteresis loop can be obtained by doubling the cyclic stress-strain

curve. For cyclic loading, the stresses and strains are replaced with the stress and strain ranges and Neuber's rule becomes:

$$\Delta\varepsilon\,\Delta\sigma = \frac{\left(K_f\,\Delta S\right)^2}{E} \tag{4.19}$$

It should be noted that in this equation K_t was replaced with K_f which has been shown by Topper et al. [Stephens et al., 2000] to have better agreement with experimental data. For the first cycle $\Delta\varepsilon$, $\Delta\sigma$, and ΔS in equations 4.18 and 4.19 were replaced with ε_{max}, σ_{max}, and S_{max}, respectively. This approach assumes that the maximum stress is reached in the first cycle, whereas in testing the load gradually increased to the maximum values over approximately 100 cycles. Therefore, there could be some differences in lives between using this approach versus performing the analysis based on the test gradually reaching the maximum load.

After the notch stresses and strains are determined, the life to crack initiation can be predicted. The prediction estimates the life to the onset of a crack on the order of 1 mm. Several equations exist for predicting fatigue life in the presence of mean stresses, based on the strain-life approach, including Morrow's mean stress parameter, and the Smith–Watson–Topper (SWT) parameter. Both equations account for the mean stress effects. The SWT parameter has been shown to be applicable to a broad range of materials [Stephens et al., 2000]. Due to its broad applicability, the SWT parameter was used in this study.

The SWT parameter assumes that the product of maximum notch stress and notch strain amplitude ($\sigma_{max}\,\varepsilon_a$) remains constant regardless of the individual contribution of notch strain amplitude, ε_a, and notch mean stress σ_m. The SWT equation is represented by:

$$\sigma_{\max}\varepsilon_a E = (\sigma_f')^2 (2N_f)^{2b} + \sigma_f'\varepsilon_f' E(2N_f)^{b+c} \quad (4.20)$$

Using the material properties for each material and the product of σ_{max} and ε_a for each test level which were determined using Neuber's rule, the fatigue life was predicted using Equation 4.20.

4.4.2 Comparisons with experimental results

The SWT parameter versus reversals to failure for the forged steel crankshaft is shown in Figure 4.13 for the crack initiation criterion and in Figure 4.14 for the 5% change in displacement amplitude criterion. The same plots are shown for the cast iron crankshaft in Figures 4.15 and 4.16. For the cast iron crankshafts only predictions for the higher notch sensitivity (K_f = 2.93) are presented due to the S-N approach showing that the low notch sensitivity predictions were not in agreement with experimental data. The results from the strain-life predictions using the SWT parameter along with the notch stresses and strains obtained from Neuber's rule are summarized in Table 4.5 for the forged steel and in Table 4.6 for the cast iron crankshafts. The predictions along with the crankshaft experimental data are also presented in Table 4.7.

For the forged steel crankshaft, the strain life approach resulted in predictions that reasonably agreed with the experimental data when the crack initiation failure criterion was used, as shown in Figure 4.13. When the 5% change in displacement amplitude failure criterion was used the predictions were also reasonable, as shown in Figure 4.14. The predictions, however, more closely agreed with the data using the crack initiation criterion.

For the cast iron crankshafts, where the high notch sensitivity was assumed, the strain-life predictions under-estimated the fatigue lives. This was true for both the crack initiation failure criterion as shown in Figure 4.15, and the 5% change in displacement amplitude criterion as shown in Figure 4.16. Although the predictions were less accurate than they were for the forged steel crankshaft, the predictions were always conservative.

The predicted cycles to failure using the strain-life approach versus experimental cycles to failure using the crack initiation criterion are shown in Figure 4.17 for the forged steel and ductile cast iron crankshafts, and in Figure 4.18 for the 5% change in displacement amplitude criterion. Figure 4.17 shows that for the forged steel crankshaft, the predictions were reasonably accurate as all of the data points are inside the factor of 3 scatter band based on the crack initiation criterion. Figure 4.18 shows that for the forged steel crankshaft the predictions were more conservative when compared to the 5% change in displacement experimental data. For the cast iron crankshaft, all of the data points were outside of the factor of 3 scatter band, indicating less accurate, although conservative predictions, when compared to experimental data based on both failure criteria. For both the forged steel and ductile cast iron crankshafts, the strain-life predictions were more accurate when compared to the crack initiation failure criterion.

4.5 Discussion of Life Prediction Results

The results of the predictions using the stress-life and strain-life are shown in Table 4.7 along with the component test data. The strain-life approach in this case resulted in shorter fatigue life predictions than the S-N approach, which resulted in the

strain-life approach always under-predicting the fatigue lives of both the forged steel and ductile cast iron crankshafts. Therefore, the strain-life approach always provided conservative fatigue life predictions. Both methods of predictions resulted in more accurate comparisons for the forged steel crankshaft than the ductile cast iron crankshaft.

For the forged steel crankshaft, life predictions using the stress-life and strain-life approaches were reasonable for both the crack initiation and 5% change in displacement amplitude criteria. However, both the S-N and strain-life approaches were more accurate when the crack-initiation failure criterion was used, compared to the 5% change in displacement amplitude criterion. This result is reasonable since the fatigue life for prediction purposes is considered to be the life to the onset of cracks on the order of a millimeter. By the time the change in displacement amplitude was 5%, the crack was already much longer than 1 mm. Therefore, it was expected that the crack-initiation data would better fit the life predictions. The strain-life approach resulted in predictions that were conservative, while the S-N approach did not always result in a conservative predictions. The S-N approach predicted longer lives than the strain-life approach, and in this case the S-N approach sometimes predicted longer lives than what was observed in the crankshaft fatigue tests. The strain-life approach always predicted lives that were less than the actual fatigue lives of the crankshafts when compared to experimental data, making the strain-life approach more conservative.

Table 4.1: Analytical nominal stress results at the critical location and comparison with FEA results for the forged steel and cast iron crankshafts.

	Forged Steel Stress (MPa)			*Cast Iron Stress (MPa)*			
Moment Amplitude (N-m)	**Analytical**	**FEA**		**Analytical**		**FEA**	
	Location a and b	**Location a**	**Location b**	**Location a**	**Location b**	**Location a**	**Location b**
630	134.7	118.9	140.3	206.3	187.5	218.9	185.6
517	110.4	97.6	115.0	169.1	153.7	179.6	152.1
431	92.0	81.4	95.9	141.0	128.1	149.8	126.8
350	74.8	66.1	78.0	114.6	104.2	121.6	103.1

Table 4.2: Comparison between FEA, experimental, and analytical stress results for the forged steel crankshaft in the as-tested condition at the locations shown in Figure 4.2.

At Location a				
Load (N)	FEA (MPa)	EXP (MPa)	% Difference between FEA and EXP	ANALYTICAL (MPa)
-890	-61.6	-59.3	3.80%	-72.4
890	61.5	65.5	6.50%	72.4
At Location b				
Load (N)	FEA (MPa)	EXP (MPa)	% Difference between FEA and EXP	ANALYTICAL (MPa)
-890	86.9	81.4	6.30%	72.4
890	-86.7	-90.3	4.20%	-72.4
At Location c				
Load (N)	FEA (MPa)	EXP (MPa)	% Difference between FEA and EXP	ANALYTICAL (MPa)
-890	-76.4	-71.7	6.10%	-72.4
890	76.3	75.8	0.50%	72.4
At Location d				
Load (N)	FEA (MPa)	EXP (MPa)	% Difference between FEA and EXP	ANALYTICAL (MPa)
-890	75.5	71.7	5.00%	72.4
890	-75.6	-76.5	1.30%	-72.4

Table 4.3: FEA results for the test setup boundary conditions for the forged steel crankshaft for the locations identified in Figure 4.2.

Location	Load (kN)	Stress (MPa)	Moment Arm (cm)
1	4.45	405.08	--
2		539.74	14.26
3		374.74	11.04
4		52.52	14.26
5		76.53	11.04
6		161.48	--
8		155.90	--
9		392.85	--
a		106.22	12.65
b		121.63	12.65

Table 4.4: FEA results for the test setup boundary conditions for the cast iron crankshaft for the locations identified in Figure 4.2.

Location	Load (kN)	Stress (MPa)	Moment Arm (cm)
2	4.45	496.86	12.29
a		159.77	10.34
b		135.31	10.34

Table 4.5: Life prediction results including the S-N and ε-N approaches for the forged steel crankshaft.

Moment Amplitude (N-m)	S_a (MPa)	S-N	ε-N: Neuber's Rule			
		Predicted N_f	$\Delta\sigma$ (MPa)	$\Delta\varepsilon$	$\varepsilon_a\sigma_{max}$	Predicted N_f
630	140.3	49,695	916.2	0.0056	1.580	23,163
517	115.0	182,710	811.1	0.0042	1.116	74,074
431	95.9	585,600	705.0	0.0017	0.828	250,786
350	78.0	$>10^6$	584.7	0.0037	0.592	$>10^6$

Table 4.6: Life prediction results including the S-N and ε-N approaches for the ductile cast iron crankshaft.

Moment Amplitude (N-m)	S_a (MPa)	S-N		ε-N: Neuber's Rule			
		$K_f = 2.93$	$K_f = 1.42$	$K_f = 2.93$			
		Predicted N_f		$\Delta\sigma$ (MPa)	$\Delta\varepsilon$	$\varepsilon_a\sigma_{max}$	Predicted N_f
630	185.6	2,978	149,321	947.2	0.0070	2.022	691
517	152.1	13,219	$>10^6$	840.0	0.0053	1.435	1,946
431	126.8	49,125	$>10^6$	728.2	0.0043	1.072	5,754
350	103.1	210,216	$>10^6$	601.3	0.0034	0.774	24,961

Table 4.7: Experimental data and life prediction results for the forged steel and ductile cast iron crankshafts.

Applied Moment Amp. (N-m)	Crack Initiation	Cycles at 5% Change in Disp. Amp.	S-N Prediction		ε-N Prediction
Forged Steel Crankshaft					
630	29,248	45,568	49,695		23,163
	45,302	69,670	49,695		23,163
	58,236	90,853	49,695		23,163
517	145,000	234,289	182,710		74,074
	98,741	213,885	182,710		74,074
	204,174	396,011	182,710		74,074
431	$>2.09 \times 10^6$	$>2.09 \times 10^6$	585,600		250,786
	$>3.980 \times 10^6$	$>3.980 \times 10^6$	585,600		250,786
350	$>3.24 \times 10^6$	$>3.24 \times 10^6$	$>10^6$		$>10^6$
Cast Iron Crankshaft					
			$K_f = 1.42$	$K_f = 2.93$	$K_f = 2.93$
630	7,132	17,353	149,321	2,978	691
	9,256	17,380	149,321	2,978	691
	8,021	20,957	149,321	2,978	691
517	25,512	47,513	$>10^6$	13,219	1,946
	24,096	52,790	$>10^6$	13,219	1,946
	37,380	54,966	$>10^6$	13,219	1,946
431	75,200	132,877	$>10^6$	49,125	5,754
	78,367	121,866	$>10^6$	49,125	5,754
	82,200	143,259	$>10^6$	49,125	5,754
350	920,783	1,005,665	$>10^6$	210,216	24,900
	301,774	370,216	$>10^6$	210,216	24,900

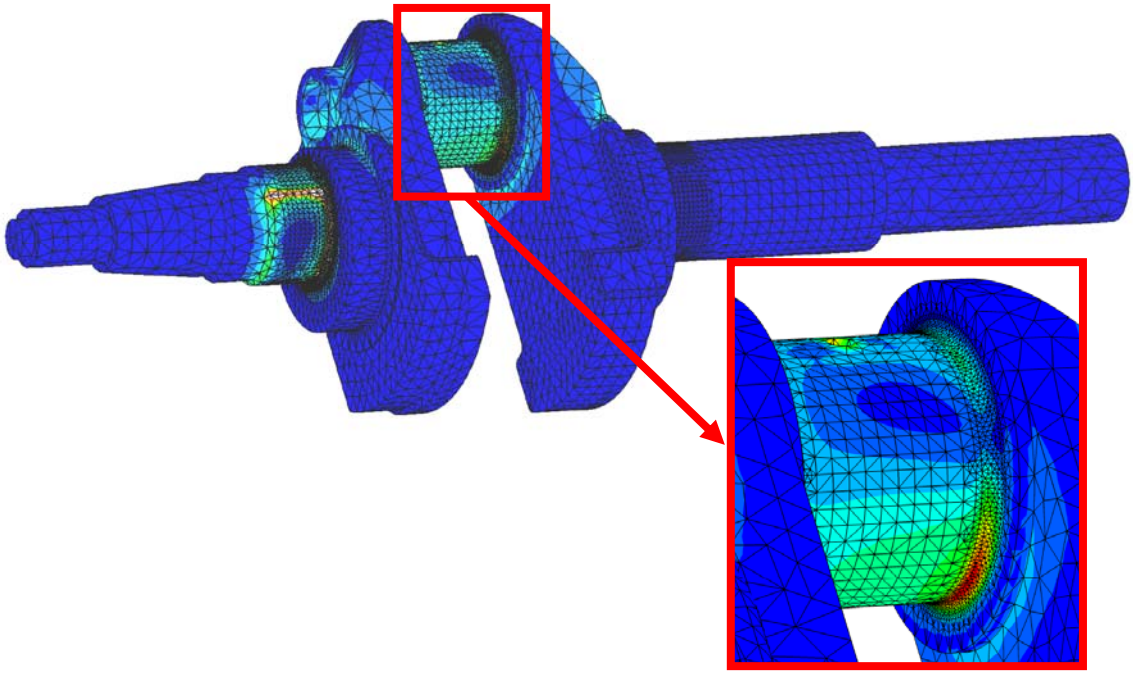

Figure 4.1: Forged steel crankshaft showing FEA stress contour with the crankpin fillet magnified [Montazersadgh, 2007]

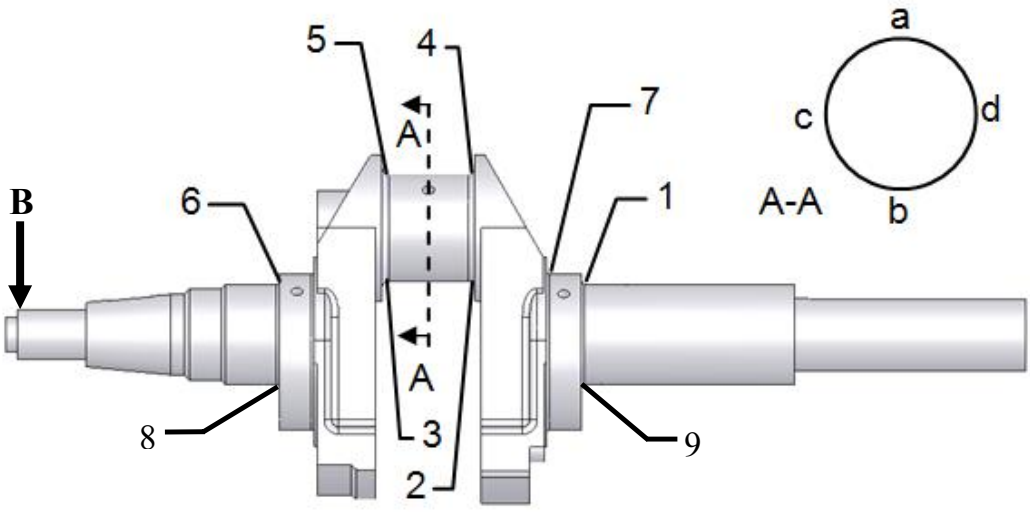

Figure 4.2: Forged steel crankshaft showing the analyzed locations for the dynamic load analysis and dynamic based FEA.

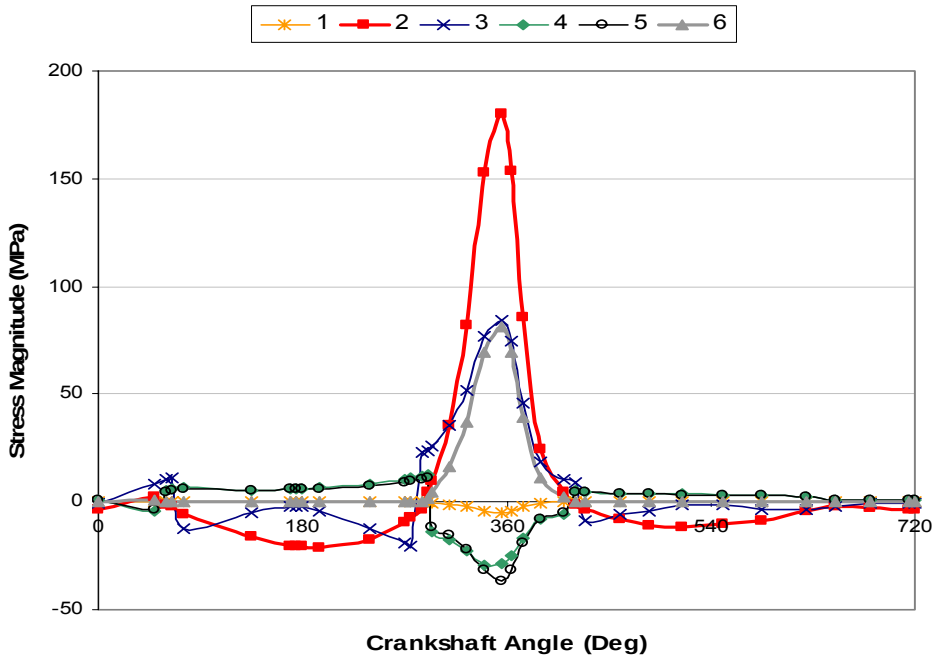

Figure 4.3: Stress magnitude versus crankshaft angle for the locations shown in Figure 4.2 [Montazersadgh and Fatemi, 2007].

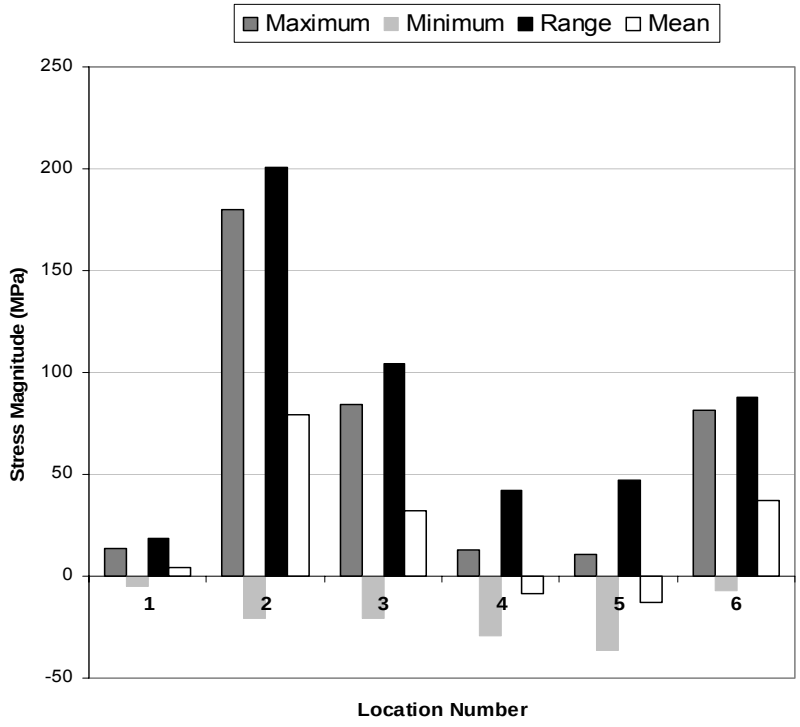

Figure 4.4: Maximum stress, minimum stress, stress range, and mean stress results from FEA for the locations shown in Figure 4.2 [Montazersadgh and Fatemi, 2007].

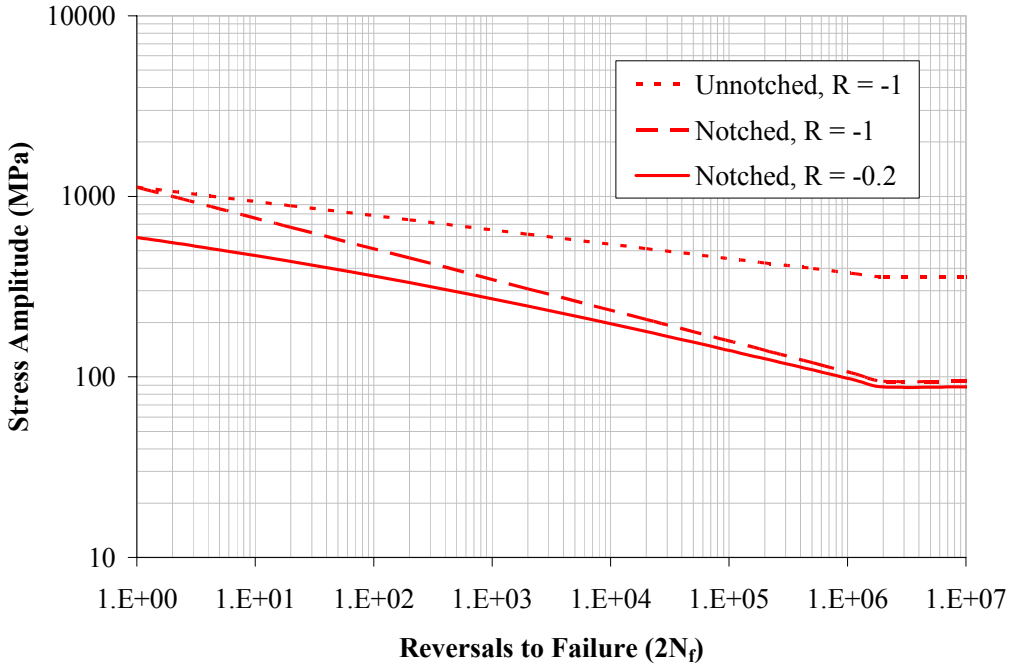

Figure 4.5: Forged steel crankshaft S-N lines for the unnotched, notched, and notched R = -0.2 condition.

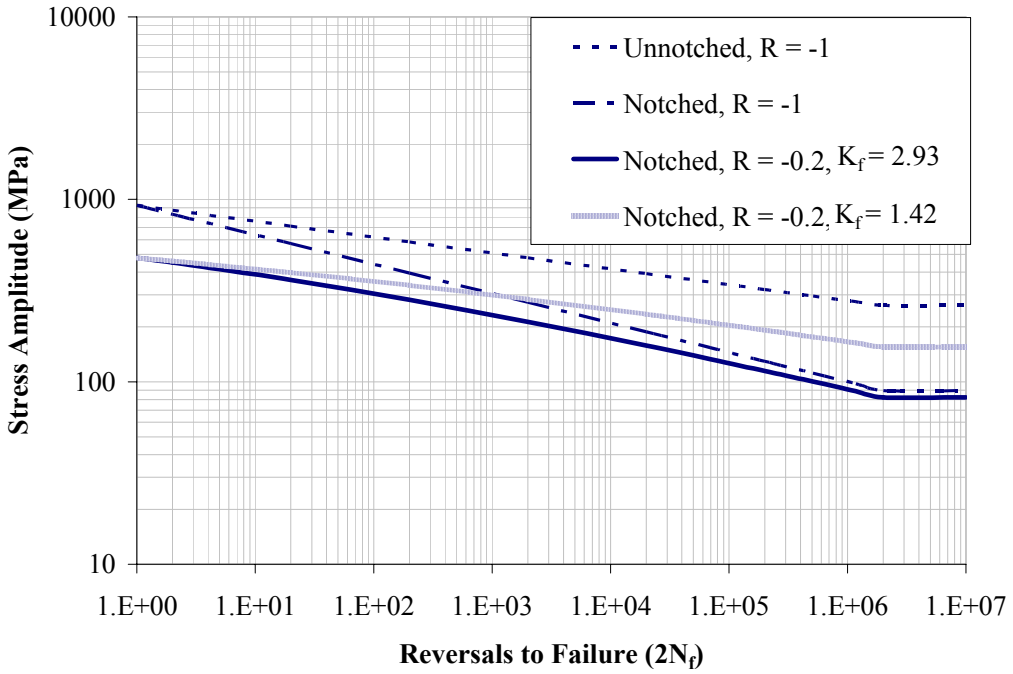

Figure 4.6: Ductile cast iron crankshaft S-N lines for the unnotched, notched, and notched R = -0.2 condition.

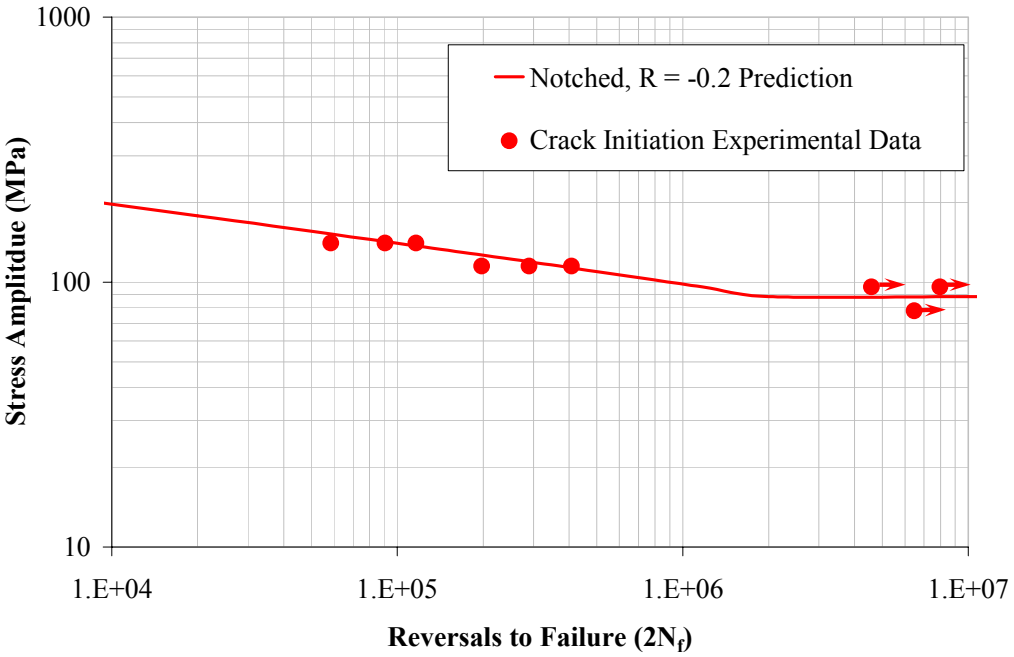

Figure 4.7: Forged steel crankshaft S-N line for the notched R = -0.2 condition superimposed with the crack initiation experimental data.

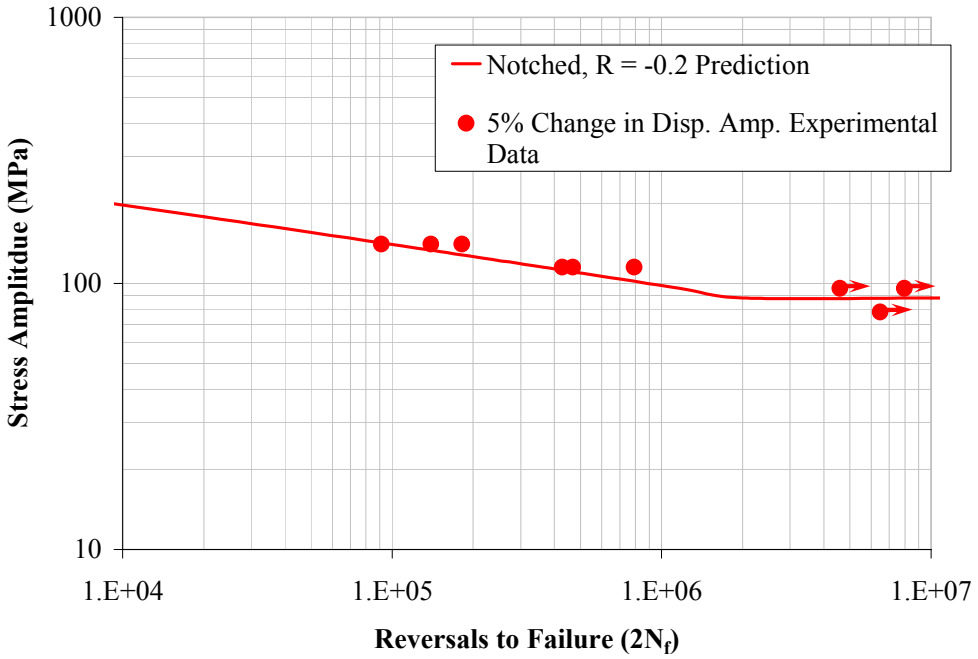

Figure 4.8: Forged steel crankshaft S-N line for the notched R = -0.2 condition superimposed with the 5% change in displacement amplitude experimental data.

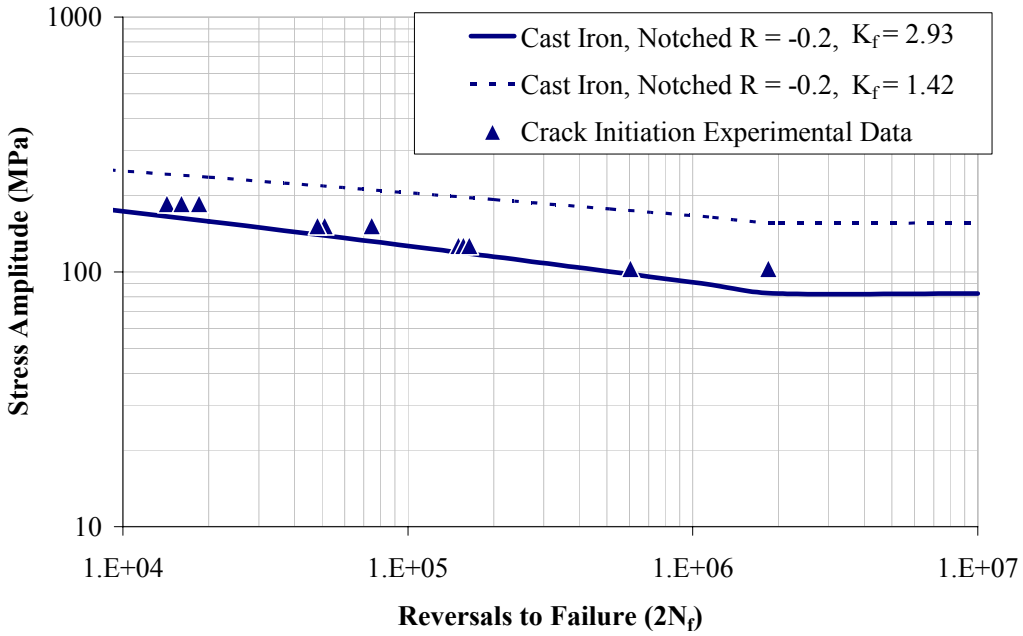

Figure 4.9: Ductile cast iron crankshaft S-N lines for the notched R = -0.2 condition superimposed with the crack initiation experimental data.

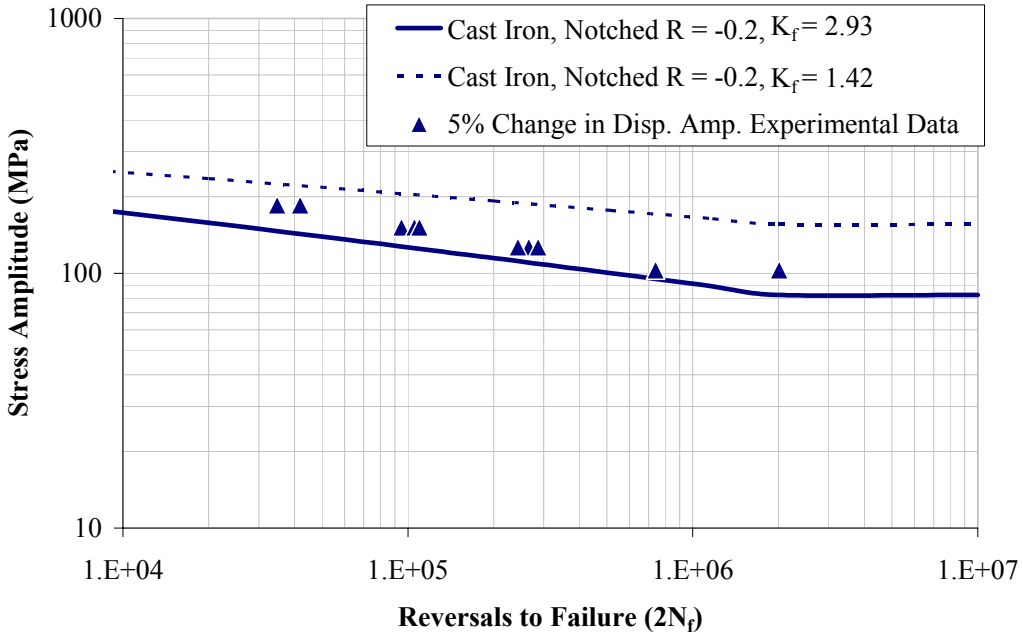

Figure 4.10: Ductile cast iron crankshaft S-N lines for the notched R = -0.2 condition superimposed with the 5% change in displacement amplitude experimental data.

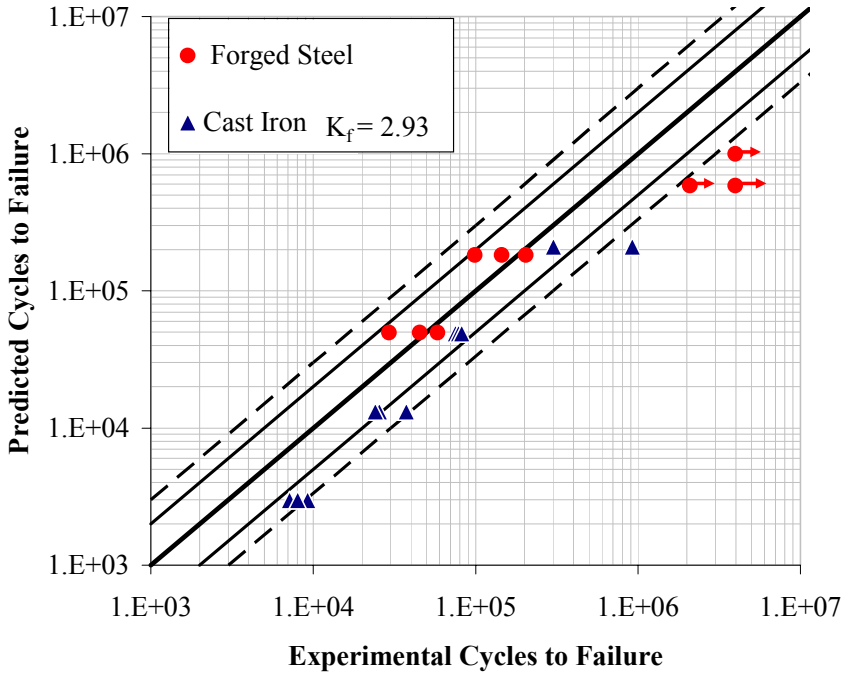

Figure 4.11: Predicted versus experimental cycles to failure using the S-N approach for the forged steel and ductile cast iron crankshafts using the crack initiation failure criterion.

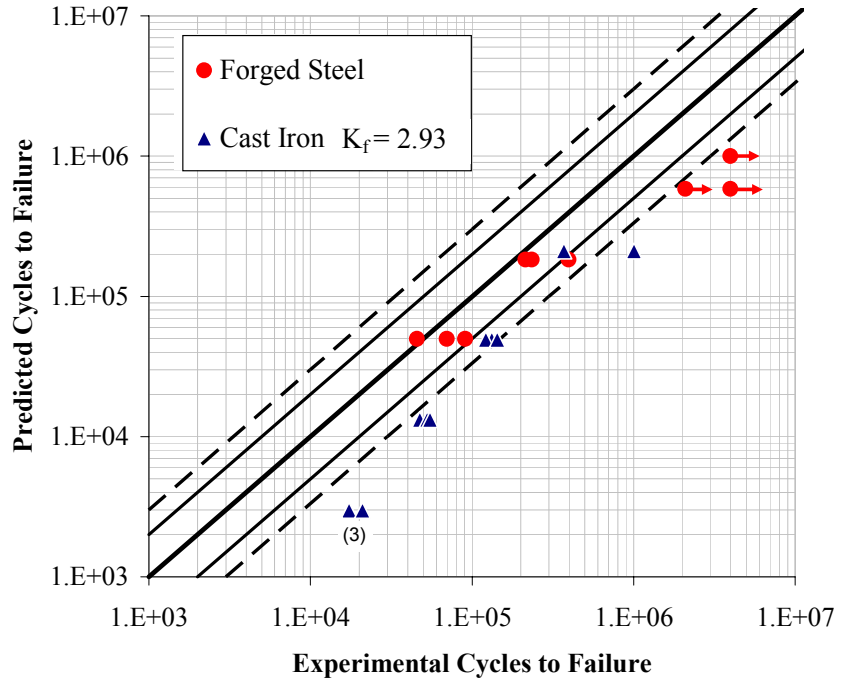

Figure 4.12: Predicted versus experimental cycles to failure using the S-N approach for the forged steel and ductile cast iron crankshafts using the 5% change in displacement amplitude failure criterion.

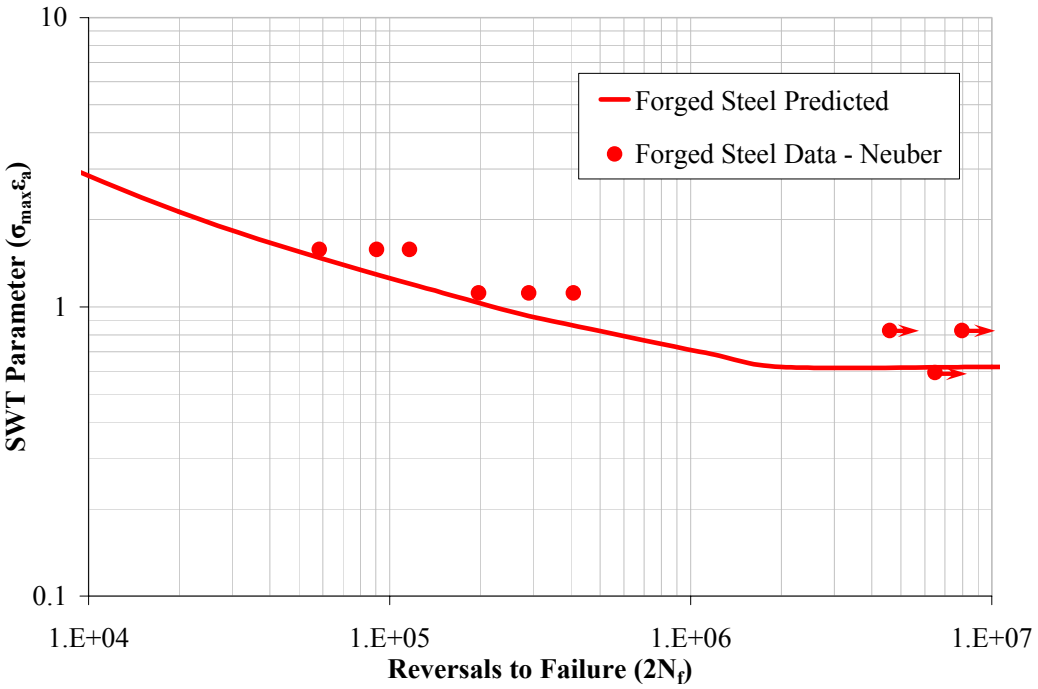

Figure 4.13: SWT parameter versus reversals to failure based on crack initiation with strain-life prediction data superimposed for the forged steel crankshafts.

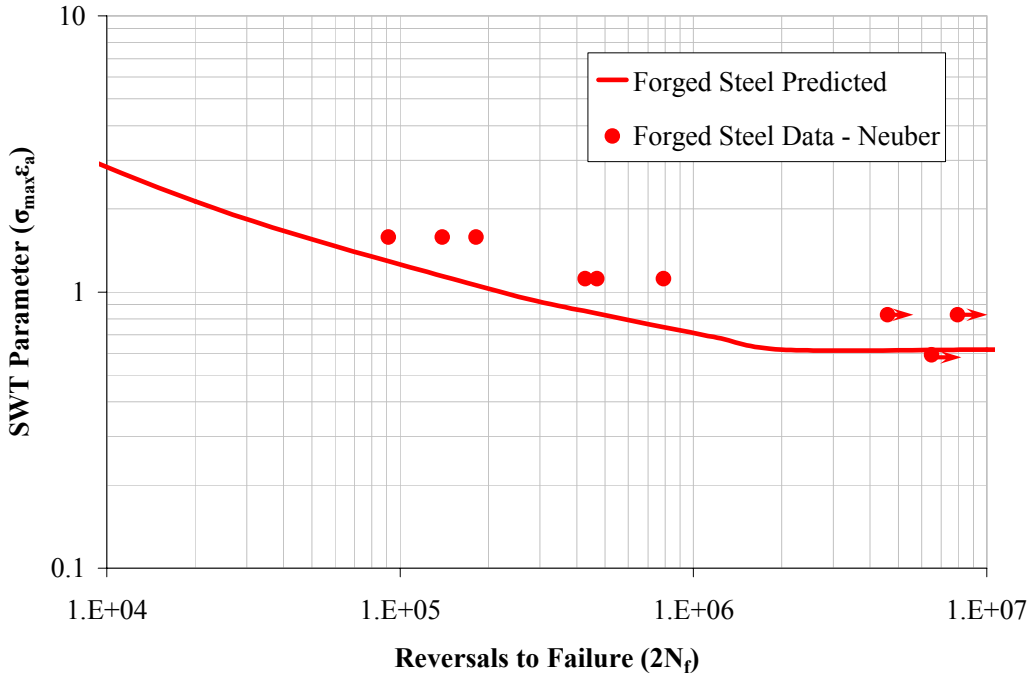

Figure 4.14: SWT parameter versus reversals to failure based on 5% change in displacement amplitude with strain-life prediction data superimposed for the forged steel crankshafts.

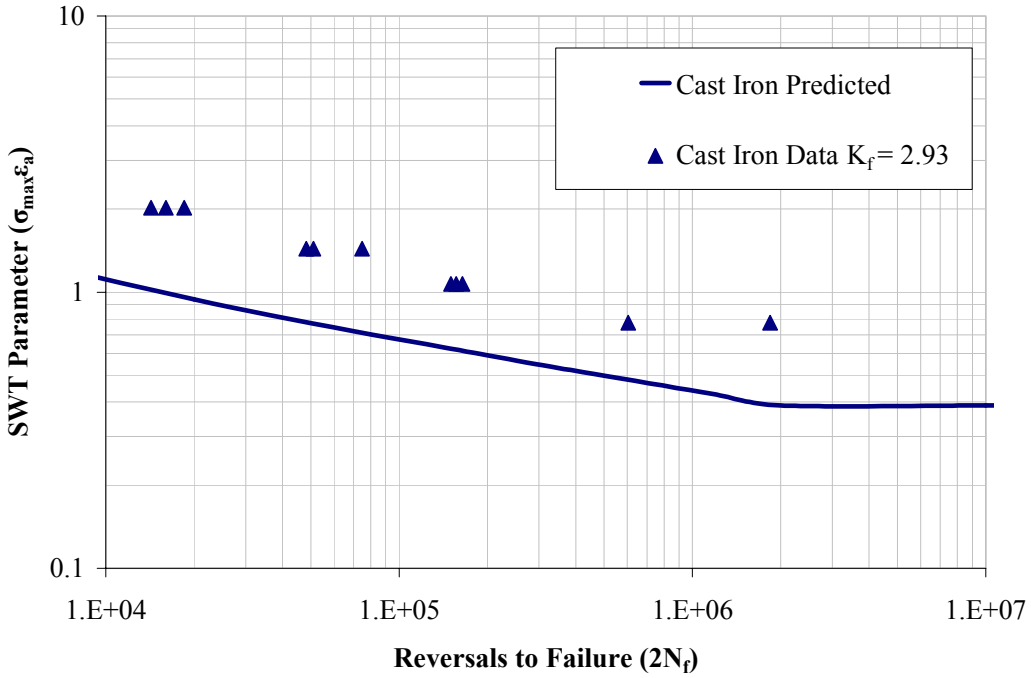

Figure 4.15: SWT parameter versus reversals to failure based on crack initiation with strain-life prediction data superimposed for the ductile cast iron crankshafts.

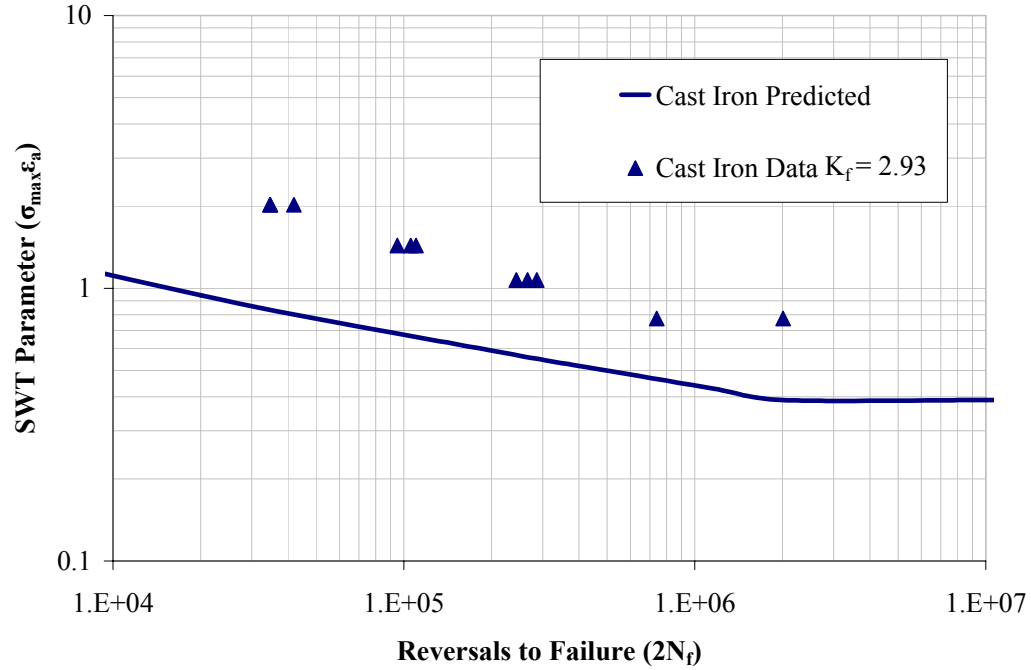

Figure 4.16: SWT parameter versus reversals to failure based on 5% change in displacement amplitude with strain-life prediction data superimposed for the ductile cast iron crankshafts.

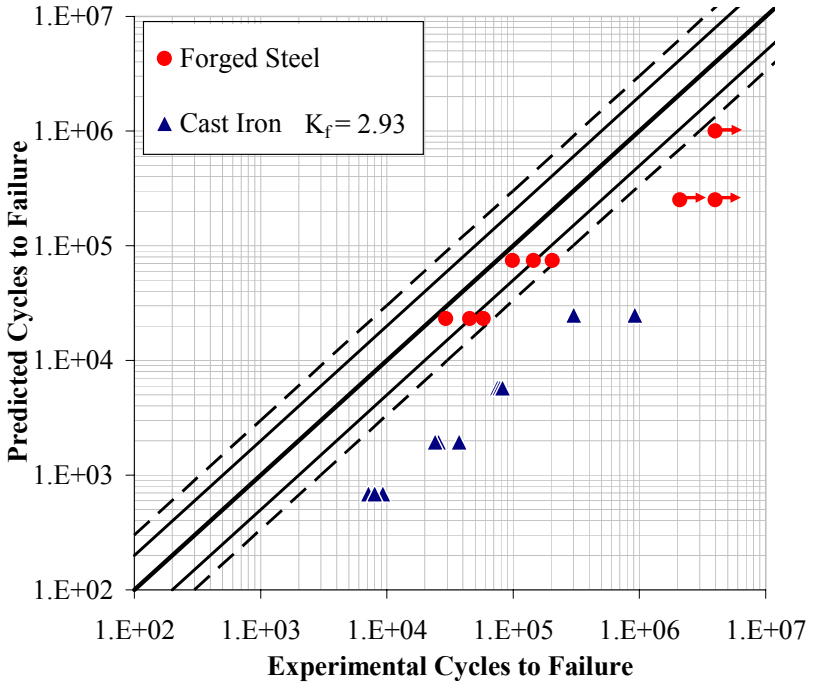

Figure 4.17: Predicted versus experimental cycles to failure using the strain-life approach for the forged steel and ductile cast iron crankshafts based on the crack initiation failure criterion.

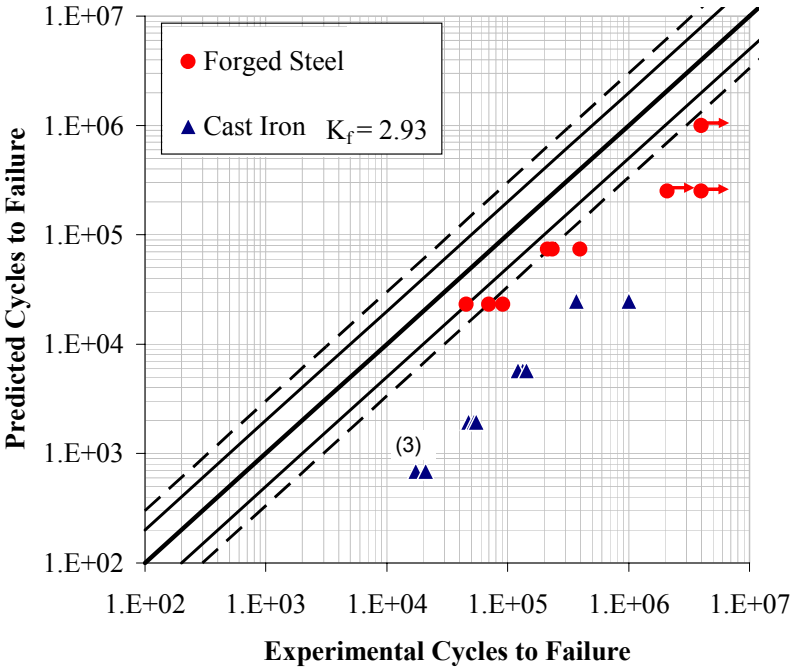

Figure 4.18: Predicted versus experimental cycles to failure using the strain-life approach for the forged steel and ductile cast iron crankshafts based on the 5% change in displacement amplitude failure criterion.

CHAPTER 5

SUMMARY AND CONCLUSIONS

The fatigue behaviors of forged steel and cast iron crankshafts from a one cylinder engine were obtained and compared. In order to compare the two crankshafts, first specimen testing was carried out on specimens machined from the as-forged and as-cast crankshafts. Specimen testing included tensile tests to obtain the monotonic material properties, strain-controlled uniaxial fatigue tests to obtain the cyclic properties of the two materials, and Charpy V-notch impact tests to determine the impact toughness of the materials. Load-controlled bending fatigue tests with R = -0.2 were then performed on the crankshafts. Results from finite element analysis [Montazersadgh and Fatemi, 2007] were used to obtain the stresses in the crankshafts. Fatigue life predictions using the S-N and ε-N approaches were then carried out using the stress results from FEA. Based on the experimental results and the analyses performed the following conclusions were drawn:

1. Based on the monotonic tensile test results, the forged steel has significantly higher strength than the ductile cast iron. The yield strength of the forged steel is 52% higher than that of the cast iron, while the ultimate strength is 26% higher for the forged steel than the ductile cast iron.

2. The forged steel material also has more ductility than the ductile cast iron as shown by the percent reduction in area, which was 58% for the forged steel and 6% for the ductile cast iron.
3. The forged steel Charpy V-notch impact results show that the forged steel in both the L-T and T-L directions have higher impact toughness than the ductile cast iron at all temperature levels investigated. This is important for this application due to the possibility of impact loading condition in the engine if subjected to a sudden stop.
4. The S-N curves for the two materials show that the forged steel has better fatigue resistance than the ductile cast iron. The fatigue strength at 10^6 cycles was 359 MPa for the forged steel and 263 MPa for the ductile cast iron, which results in a factor of 30 longer life for the forged steel in the long life region. The forged steel fatigue strength at 10^6 cycles is 36% higher than the ductile cast iron.
5. The forged steel also shows longer life when subjected to plastic deformation, based on the true plastic strain amplitude versus reversals to failure plot. For a given plastic strain amplitude, the forged steel has a factor of 40 longer life than the ductile cast iron.
6. The Neuber curves for the two materials also show better fatigue performance for the forged steel material, compared to the ductile cast iron. The Neuber curves show that in the long life region the forged steel has a factor of 50 longer life than the ductile cast iron.
7. The crack growth life for both crankshafts was a significant portion of the fatigue life during the crankshaft testing. The crack growth rate of the forged steel crankshaft was slower than the ductile cast iron crankshaft.

8. The failure criterion based on crack initiation is more reasonable in crankshaft applications since an engine would not tolerate the increased deflection caused by the presence of a crack. The 5% change in displacement criterion resulted in a crack that was 10 mm or longer.
9. Based on the crack initiation failure criterion the forged steel crankshaft had a factor of 6 longer life than the ductile cast iron crankshaft at long lives. The 5% change in displacement amplitude also showed better fatigue performance for the forged steel crankshaft, resulting in an order of magnitude longer life than the ductile cast iron crankshaft at long lives.
10. At 10^6 cycles the fatigue strength of forged steel crankshaft was 36% higher than the fatigue strength of the ductile cast iron crankshaft. Specimen fatigue test results also show that the fatigue strength of the forged steel material was 36% higher than the fatigue strength of the ductile cast iron material at 10^6 cycles.
11. During crankshaft fatigue tests, circumferential cracks developed in the rear crankpin fillet of both forged steel and ductile cast iron crankshafts which was identified as the critical location from FEA. These cracks grew and were the ultimate cause of failure for the crankshafts, despite secondary cracks which developed in the opposite crankpin fillet in some crankshafts.
12. Finite element analysis was necessary to obtain the stresses in the crankshafts due to the relatively complex geometry. The geometry led to a lack of symmetry at the top and bottom of the crankpin in the forged steel crankshaft in spite of cross-section symmetry, which could not be accounted for in the analytical stress calculations.

The lack of symmetry at the top and bottom of the crankpin in the forged steel crankshaft was confirmed with experimental strain gage results.

13. The life predictions were more accurate for the forged steel crankshafts than the ductile cast iron crankshafts. The S-N predictions proved to be a more accurate life prediction method, providing reasonable results for both the forged steel and cast iron crankshafts. The strain-life predictions also provided reasonably accurate estimations for the fatigue life of the forged steel crankshafts and less accurate, however conservative, estimations for the ductile cast iron crankshafts.
14. The accuracy of fatigue life predictions using the S-N or the strain-life approach is strongly influenced by an accurate estimation of notch sensitivity of a material. Using a low notch sensitivity for the ductile cast iron crankshaft (q = 0.2) as suggested in the literature resulted in life predictions that did not agree with the experimental data. When low notch sensitivity was assumed the predictions overestimated the results while high notch sensitivity underestimated the results.

REFERENCES

Asi, O., 2006, "Fatigue Analysis of a Crankshaft Made from Ductile Cast Iron," *Fatigue Failure Analysis,* Vol. 13, pp. 1260-1267

ASTM Standard E8-04, 2004, "Standard Test Methods for Tension Testing of Metallic Materials," *Annual Book of ASTM Standards*, Vol. 03.01, West Conshohocken, PA, USA.

ASTM Standard E23-02a, 2004, "Standard Test Methods for Notched Bar Impact Testing of Metallic Materials," *Annual Book of ASTM Standards*, Vol. 03.01, West Conshohocken, PA, USA.

ASTM Standard E83-02, 2004, "Standard Practice for Verification and Classification of Extensometer System," *Annual Book of ASTM Standards*, Vol. 03.01, West Conshohocken, PA, USA.

ASTM Standard E606-92, 2004, "Standard Practice for Strain-Controlled Fatigue Testing," *Annual Book of ASTM Standards*, Vol. 03.01, 2004, West Conshohocken, PA, USA.

ASTM Standard E646-00, 2004, "Standard Test Method for Tensile Strain-Hardening Exponents (n-Values) of Metallic Sheet Materials," *Annual Book of ASTM Standards*, Vol. 03.01, West Conshohocken, PA, USA.

ASTM Standard E739-91, 2004, "Standard Practice for Statistical Analysis of Linear or Linearized Stress-Life (S-N) and Stain-Life (ε-N) Fatigue Data," *Annual Book of ASTM Standards*, Vol. 03.01, West Conshohocken, PA, USA.

Bayrakçeken, H., Tasgetiren, and S., Aksoy, F., 2006, "Failures of Single Cylinder Diesel Engines Crankshafts," *Fatigue Failure Analysis*, Vol. 14, pp. 725-730.

Behrens, B. A., Reinsch, S., Specker, A., and Telkamp, K., 2005, "Further Development in the Precision Forging Technology for High Duty Automotive Parts," In *MPMD Sixth Global Innovations Proceedings Trends in Materials and Manufacturing Technologies for Transportation Industry and Powder Metallurgy Research and Development in the Transportation Industry*, San Francisco, CA, USA, The Minerals, Metals, and Materials Society.

Chatterley, T.C. and Murrell, P., 1998, "ADI Crankshafts - An Appraisal of Their Production Potentials," *SAE Technical Paper No. 980686*, Society of Automotive Engineers, Warrendale, PA, USA.

Chien, W.Y., Pan, J., Close, D., and Ho, S., 2005, "Fatigue Analysis of Crankshaft Sections Under Bending with Consideration of Residual Stresses," *International Journal of Fatigue*, Vol. 27, pp. 1-19.

Damir, A.N., Elkhatib, A., and Nassef, G., 2007, "Prediction of Fatigue Life Using Modal Analysis for Grey and Ductile Cast Iron," *International Journal of Fatigue,* Vol. 29, pp. 499-507.

Fergusen, C. R., 1986, "*Internal Combustion Engines, Applied Thermo Science*," John Wiley and Sons, New York, NY, USA.

Grum, J., 2003, "Analysis of Residual Stresses in Main Crankshaft Bearings after Induction Surface Hardening and Finish Grinding," *Journal of Automobile Engineering,* Vol. 217, pp. 173-182.

Heitmann, W.E., August 14, 2006, Private Communication.

http://www.tpub.com/engine3/en3-53.htm

http://en.wikipedia.org/wiki/Four-stroke_cycle

Jensen, E.J., 1970, "Crankshaft Strength Through Laboratory Testing," *SAE Technical Paper* No. 700526, Society of Automotive Engineers, Warrendale, PA, USA.

Juvinall, R.C. and Marshek, K.M., 1991, "*Fundamentals of Machine Design Components,"* 2nd Edition, John Wiley & Sons, New York, NY, USA.

Laus, L. and Heitmann, W.E., February 15, 2007, Private Communication.

Montazersadgh, F.H., 2007, "Stress Analysis and Optimization of Crankshafts Subjected to Dynamic Loading," Masters Thesis, The University of Toledo, Toledo, OH, USA.

Montazersadgh, F. and Fatemi, A., 2007, "Dynamic Load and Stress Analysis of a Crankshaft," *SAE Technical Paper* No. 2007-01-0258, Society of Automotive Engineers, Warrendale, PA, USA.

Park, H., Ko, Y. S., and Jung, S. C., 2001, "Fatigue Life Analysis of Crankshaft at Various Surface Treatments," *SAE Technical Paper* No. 2001-01-3374, Society of Automotive Engineers, Warrendale, PA, USA.

Pichard, C., Tomme, C., and Rezel, D., 1993 "Alternative Materials for the Manufacture of Automobile Components: Example of Industrial Development of a Microalloyed Engineering Steel for the Production of Forged Crankshafts," In *Proceedings of the 26th ISATA International Symposium on Automotive Technology and Automation*, Aachen, Germany.

Shigley, J.E., and Mitschke, C.R., 2002, *"Mechanical Engineering Design,"* 5th Edition, McGraw-Hill, Inc., Boston, MA, USA.

Silva, F.S., 2003, "An Investigation into the Mechanism of a Crankshaft Failure," *Key Engineering Materials,* Vols. 245-246, pp. 351-358, Trans Tech Publications, Switzerland.

Spiteri, P., Ho, S., and Lee, Y., 2007, "Assessment of a Bending Fatigue Limit for Crankshaft Sections with Inclusion of Residual Stresses," *International Journal of Fatigue,* Vol. 29, pp. 318-329.

Stephens, R.I., Fatemi, A., Stephens, R.R., and Fuchs, H.O., 2000, "*Metal Fatigue in Engineering*," 2nd Edition, John Wiley & Sons, Inc., New York, NY,USA.

Wang, Z., Xu, J., Bao, G., Zhang, J., Fang, X., and Liu, T., 2007, "Fabrication of High-Powered Diesel Engine Crankshafts by Electro-slag Casting Process," *Journal of Materials Processing Technology,* Vol. 182, pp. 588-592.

Williams, J. and Fatemi, A., 2007, "Fatigue Performance of Forged Steel and Ductile Cast Iron Crankshafts", *SAE Technical Paper* No. 2007-01-1001, Society of Automotive Engineers, Warrendale, PA, USA.

Williams, J., Montazersadgh, F.H., and Fatemi, A., 2007, "Fatigue Performance Comparison and Life Prediction of Forged Steel and Ductile Cast Iron Crankshafts," *27th Forging Industry Technical Conference*, Fort Worth, TX.

Zoroufi, M. and Fatemi, A, 2005, "A Literature Review of Durability Evaluation of Crankshafts Including Comparisons of Competing Manufacturing Processes and Cost Analysis," *26th Forging Industry Technical Conference*, Chicago, IL.